Food and Agriculture Organization of the United Nations

Remote sensing techniques for mapping and monitoring mangroves at fine scales

The Nature Conservancy

Remote sensing techniques for mapping and monitoring mangroves at fine scales

by

Steve Schill, Valerie McNulty and Denise Perez
The Nature Conservancy

Kenichi Shono and Kim Friedman
Food and Agriculture Organization of the United Nations

Food and Agriculture Organization of the United Nations
Rome, 2024

Required citation:
Schill, S.R., McNulty, V.P., Perez, D., Shono, K. & Friedman, K. 2024. *Remote sensing techniques for mapping and monitoring mangroves at fine scales*. Rome, FAO. https://doi.org/10.4060/cd0823en

The designations employed and the presentation of material in this information product do not imply the expression of any opinion whatsoever on the part of the Food and Agriculture Organization of the United Nations (FAO) concerning the legal or development status of any country, territory, city or area or of its authorities, or concerning the delimitation of its frontiers or boundaries. The mention of specific companies or products of manufacturers, whether or not these have been patented, does not imply that these have been endorsed or recommended by FAO in preference to others of a similar nature that are not mentioned.

The views expressed in this information product are those of the author(s) and do not necessarily reflect the views or policies of FAO.

ISBN 978-92-5-138796-2
© FAO, 2024

Some rights reserved. This work is made available under the Creative Commons Attribution-NonCommercial-ShareAlike 3.0 IGO licence (CC BY-NC-SA 3.0 IGO; https://creativecommons.org/licenses/by-nc-sa/3.0/igo/legalcode).

Under the terms of this licence, this work may be copied, redistributed and adapted for non-commercial purposes, provided that the work is appropriately cited. In any use of this work, there should be no suggestion that FAO endorses any specific organization, products or services. The use of the FAO logo is not permitted. If the work is adapted, then it must be licensed under the same or equivalent Creative Commons licence. If a translation of this work is created, it must include the following disclaimer along with the required citation: "This translation was not created by the Food and Agriculture Organization of the United Nations (FAO). FAO is not responsible for the content or accuracy of this translation. The original [Language] edition shall be the authoritative edition."

Disputes arising under the licence that cannot be settled amicably will be resolved by mediation and arbitration as described in Article 8 of the licence except as otherwise provided herein. The applicable mediation rules will be the mediation rules of the World Intellectual Property Organization http://www.wipo.int/amc/en/mediation/rules and any arbitration will be conducted in accordance with the Arbitration Rules of the United Nations Commission on International Trade Law (UNCITRAL).

Third-party materials. Users wishing to reuse material from this work that is attributed to a third party, such as tables, figures or images, are responsible for determining whether permission is needed for that reuse and for obtaining permission from the copyright holder. The risk of claims resulting from infringement of any third-party-owned component in the work rests solely with the user.

Sales, rights and licensing. FAO information products are available on the FAO website (www.fao.org/publications) and can be purchased through publications-sales@fao.org. Requests for commercial use should be submitted via: www.fao.org/contact-us/licence-request. Queries regarding rights and licensing should be submitted to: copyright@fao.org.

Cover photograph: Mangrove forest in Tyrell Bay, Grenada. ©TNC

CONTENTS

Acknowledgements vii
Abbreviations viii

1. INTRODUCTION 1
   1.1 The purpose of the manual 1
   1.2 The importance of mangroves 3
   1.3 Global commitments and efforts to protect and restore mangroves 4
   1.4 Types of mangroves 5
   1.5 Approach to mangrove mapping 7

2. REMOTE SENSING DATA CONSIDERATIONS 9
   2.1 Spatial, spectral and temporal resolution 10
   2.2 Types of remotely sensed data 14
   2.3 Aerial photography for mapping mangrove change over time 17
   2.4 Optical high resolution satellite imagery (< 5 m) 22
   2.5 Synthetic Aperture Radar for defining mangrove structure 26
   2.6 Light Detection and Ranging for defining mangrove height and structure 27
   2.7 Uncrewed aerial systems 29
      2.7.1 Platforms and sensors 29
      2.7.2 Mission planning and data collection 35
      2.7.3 Data processing 40

3. MANGROVE MAPPING TECHNIQUES 45
   3.1 Visual interpretation method 45
   3.2 Automated classification method 47
   3.3 Remote sensing-derived indicators and methods for feature extraction 49
      3.3.1 Vegetation indices 49
      3.3.2 Change detection using Normalized Difference Vegetation Index 50
      3.3.3 Change detection using other indices 53

4. ONLINE RESOURCES FOR MANGROVE MAPPING 55
   4.1 Existing mangrove maps 58
      4.1.1 Global Mangrove Watch 58
      4.1.2 Ocean Data Viewer 59
      4.1.3 WorldCover 10-m mangrove class 59
   4.2 Open-source imagery data, software and tools for mangrove managers 60
      4.2.1 Imagery 60
      4.2.2 Software 60
      4.2.3 Tools 61

5. CONCLUSIONS AND FUTURE DIRECTIONS 65

References 67

APPENDIX 71

Case study 1 Parque Nacional Manglares Del Bajo Yuna, the Dominican Republic 71
Case study 2 Caracol and Fort-Liberté, Three Bays National Park, Haiti 74
Case study 3 Ashton Lagoon, Union Island, Saint Vincent and the Grenadines 76
Case study 4 Tyrrel Bay, Carriacou, Grenada 78

TABLES

1. General mangrove typologies based on their sedimentary, geomorphic and habitat settings 5
2. Types and examples of optical and active satellite data sources with advantages and limitations 16
3. Available high spatial resolution (< 5 m) satellite imagery options for mangrove mapping and monitoring 22
4. Advantages and disadvantages of mapping mangroves using a UAS 29
5. Advantages of multi-rotor vs. fixed-wing UAS 30
6. Widely used multirotor and fixed-wing UAS and technical specifications 31
7. Popular multispectral sensors used on fixed-wing and heavy-lift UAS platforms 34
8. Flying heights and resulting spatial resolution and area mapped using a DJI Phantom Pro v2 using 70 percent front and side overlap 37
9. Examples of available UAS mission planning apps 39
10. Options for postprocessing UAS data into photogrammetric products 41
11. Common vegetation indices and their corresponding formulas 49
12. Formulas for MSAVI and NDMA both useful for detecting changes in mangrove forests 53
13. Directory of online resources for mangrove maps and tools 55
14. List of mangrove datasets 56

FIGURES

1. A case study in Bajo Yuna National Park, Dominican Republic from TNC's Esri Story Map "Mapping Mangroves" showing how UAS can be used to detect mangrove change 2
2. Fine-scale mangrove classifications based on local geographic descriptions 6
3. Examples of different mangrove growth patterns on Andros Island, Bahamas 9
4. Near-infrared image composites of mangroves in Ashton Lagoon, Saint Vincent and the Grenadines showing varying spatial resolutions captured by different remote sensing platforms 10
5. Multispectral imagery of mangroves acquired with a UAS in Ashton Lagoon, Saint Vincent and the Grenadines displayed using various band combinations 11
6. Satellite images acquired over Guadeloupe on different dates that depict varying cloud cover percentages Image 11
7. Differences between three mangrove classifications using different satellite data and methods in Andros Island, Bahamas 13
8. SkySat imagery over a mangrove area in west Andros Island, Bahamas 14

9. Synthetic Aperture Radar (SAR) data acquired over mangrove areas from two different SAR satellites and combined into false colour composites 14
10. Point cloud and vertical profile of a mangrove forest derived from LiDAR data 15
11. Three types of aerial photography (left to right: panchromatic; natural colour; and colour infrared) 17
12. Vertical, low oblique and high oblique aerial photos over a mangrove forest providing different perspectives 17
13. Examples of historical aerial photos of the U.S. Virgin Islands taken in 1954 18
14. Historical aerial photos collected in January 1954 over Saint Thomas, the United States Virgin Islands 19
15. Example of the selection of GCPs for georeferencing an aerial photo 19
16. Appearance of mangrove forests in Jamaica in historical panchromatic and colour infrared aerial photos 20
17. Historical aerial photography and mangrove change detection in Saint Thomas East End Reserve, the United States Virgin Islands 20
18. Comparison of multiple remote sensing data showing mangrove die-off and growth due to alternation of hydrology by a causeway near Salt River, Jamaica 21
19. Examples of different high resolution satellite data displayed using different band combinations. 25
20. Different radar wavelengths penetrate and record canopy characteristics at different depths of the forest canopy. 26
21. Comparison of global digital elevation models (AW3D30 and CoastalDEM®) for mangroves in Bajo Yuna National Park, Dominican Republic 27
22. Estimates of mangrove above-ground biomass and maximum canopy height in Manglares de Estero Balsa, Dominican Republic 28
23. Examples of a multi-rotor (left) and a fixed-wing (right) UAS 30
24. A GNSS base station collecting position correction data during a UAS mission 32
25. Two cost-effective UAS platforms with supplementary infrared sensors attached for assessing mangrove extent and health 33
26. A DJI Mavic 3 Multispectral with a 20 MP RGB camera and integrated 4-band multispectral sensors (green, red, red-edge and NIR) for calculating vegetation indices 34
27. Two UAS platforms for mapping mangroves 35
28. Examples of UAS mission plans and the area mapped at varying flight altitudes 36
29. UAS imagery acquired over mangroves at different times of the day (solar noon and early morning) in Ashton Lagoon, Saint Vincent and the Grenadines 37
30. Comparison of UAS images acquired using a fast vs slow shutter speed. 38
31. User interface examples of mission planning apps include Pix4Dcapture (top left), DroneDeploy Flight (top right), DJI GS Pro (bottom left) and Map Pilot Pro (bottom right) 39
32. UAS products of a mangrove area created from 85 overlapping stereo images taken at different perspectives and processed using photogrammetry software 40
33. The rayCloud camera positions showing the location where each stereo image was taken 42
34. Comparison of the original image of a mangrove and a 3D point cloud generated from stereo images using Agisoft Metashape photogrammetry software 43

35. Example of mangrove digitization in QGIS with multiple basemaps 45
36. Tracking the impacts of marina development on a mangrove forest in Playa de Maimon, Dominican Republic using the timeline tool in Google Earth..... 46
37. Tracking the change in mangrove forests at the mouth of the Barracote River in Bajo Yuna National Park, Dominican Republic using the timeline tool in Google Earth..... 46
38. Segmenting a satellite image means creating objects around pixels that have similar spectral properties and reflectance values 47
39. Using a DJI M300RTK multi-rotor UAS with a Micasense RedEdge MX to capture and compute NDVI to track mangrove recovery following a hurricane 50
40. TNC's Blue Carbon Explorer showing an example of NDVI change analysis in eastern Grand Bahama between 2015 and 2021 using Planet NICFI Dove imagery 51
41. Examples of using natural colour (RGB) UAS imagery to calculate VARI to inform mangrove change detection in Bajo Yuna National Park, Dominican Republic 52
42. The GMW online platform provides remote sensing data and tools for monitoring mangroves 58
43. The ESA WorldCover online portal that provides access to global 10-m data for land cover and forest types..... 59
44. The Blue Carbon Explorer's example of mangrove restoration prioritization in eastern Grand Bahama, 2015–2021..... 62
45. TNC's Mapping Ocean Wealth platform includes maps of mangrove restoration potential and blue carbon storage 63

ACKNOWLEDGEMENTS

This manual was developed through collaboration between the Food and Agriculture Organization of the United Nations (FAO) and The Nature Conservancy (TNC).

The authors are grateful to our partners and collaborators for their valuable contributions to this publication. We especially thank the following reviewers from The Nature Conservancy for their insights and feedback: Mark Spalding; Lindsey Smart; Stefanie Simpson; Kate Longley-Wood; and Fain McGough. We also appreciate the direction and support of Rob Brumbaugh, Shenique Albury-Smith, and Marcia Musgrave from The Nature Conservancy. External reviewers who provided helpful editing include George Raber from the University of Southern Mississippi, Tom Worthington from Cambridge University, and Ryan Moyer from TerraCarbon LCC.

We also appreciate the guidance and feedback provided by FAO colleagues, including Sara Casallas Ramirez; Frederic Castell; Simon Funge-Smith; Thomas Hofer; Pablo Martin; Maria Nuutinen; Aurelie Shapiro; and Tiina Vähänen.

Robin Leslie provided copyediting and Kate Ferrucci designed the publication.

ABBREVIATIONS

3BNP	Three Bays National Park, Haiti
3D	three-dimensional
AGB	above-ground biomass
ALOS	Advanced Land Observing Satellite
AW3D30	ALOS World 3D-30m
BGB	below-ground biomass
CBD	Convention on Biological Diversity
COP	Conference of the Parties
CMRI	Combined Mangrove Recognition Index
DBH	diameter at breast height
DEM	digital elevation model
dpi	dots per inch
DSM	digital surface model
ESA	European Space Agency
ExGI	Excess Green Index
EVI	Enhanced Vegetation Index
FAO	Food and Agriculture Organization of the United Nations
GBF	Global Biodiversity Framework
GCPs	ground control points
GEDI	Global Ecosystem Dynamics Investigation
GEE	Google Earth Engine
GEEMMM	Google Earth Engine Mangrove Mapping Methodology
GIS	geographic information system
GLAS	Geoscience Laser Altimeter System
GMA	Global Mangrove Alliance
GMW	Global Mangrove Watch
GNSS	Global Navigation Satellite System
GPS	global positioning system
GSD	ground sampling distance
IDL	Interactive Data Language
ISO	International Standards Organization
ICESat	Ice, Cloud, and land Elevation Satellite
IUCN	International Union for Conservation of Nature
JPEG	Joint Photographic Experts Group
KML	keyhole markup language
KNN	K-Nearest Neighbours
KOMPSAT	Korea Multi-Purpose Satellite
L8MI	Landsat 8 Mangrove Index
LAANC	Low Altitude Authorization and Notification Capability

LiDAR	Light Detection and Ranging
PALSAR	Phased Array type L-band Synthetic Aperture Radar
MPA	marine protected area
MQI	Mangrove Quality Index
MVI	Mangrove Vegetation Index
NASA	National Aeronautics and Space Administration
NDC	nationally determined contributions
NDMI	Normalized Difference Mangrove Index
NDVI	Normalized Difference Vegetation Index
NDWI	Normalized Difference Water Index
NGO	non-governmental organization
NICFI	Norway's International Climate and Forests Initiative
NIR	near-infrared
OTB	Orfeo ToolBox
PPK	Post Processed Kinematic (GPS correction technology technique)
QGIS	Quantum-GIS
RADAR	Radio Detection and Ranging
REDD+	Reducing Emissions from Deforestation and forest Degradation, plus the sustainable management of forests, and the conservation and enhancement of forest carbon stocks
RGB	red, green, blue natural colour composite
RMSE	root mean square error
RTK	Real Time Kinematic (GPS correction technology technique)
RVI	Ratio Vegetation Index
SAR	Synthetic Aperture Radar
SAVI	Soil-Adjusted Vegetation Index
SDGs	Sustainable development goals
SIDS	Small Island Developing States
SPOT	Satellite pour l'Observation de la Terre
SRTM	Shuttle Radar Topography Mission
SWIR	shortwave infrared
TGI	Triangular Greenness Index
TIFF	Tag Image File Format
TNC	The Nature Conservancy
UAS	uncrewed aerial system
UAV	unmanned aerial vehicle
UNFCCC	United Nations Framework Convention on Climate Change
VARI	Visible Atmospherically Resistant Index
VCI	Vegetation Condition Index
VIs	vegetation indices
VTOL	vertical take-off and landing technology

©TNC

1. INTRODUCTION

1.1 THE PURPOSE OF THE MANUAL

Achieving food security and improved nutrition for the world's population depends on preserving biodiversity and ecosystem services for sustainable production across the agriculture, forestry, aquaculture and fisheries sectors. However, despite efforts spanning several decades, biodiversity continues to be degraded. Recent global assessments confirm that biodiversity and ecosystem services are declining at an unprecedented rate and the pressures driving the decline are intensifying (Leal and Spalding, eds., 2022; Waldron *et al.*, 2020; Waltham *et al.*, 2020; Friess *et al.*, 2019). Several of these pressures are directly or indirectly associated with agrifood systems, including land-use change, overexploitation, pollution and unsustainable consumption patterns. These pressures are exacerbated by climate change impacts including sea level rise, increased and more intense storms, and altered precipitation and temperature regimes that influence mangrove vulnerability (Ward *et al.*, 2016).

Mangrove ecosystems play a critical role in harbouring biodiversity and providing a variety of ecosystem services. The need for developing better techniques for classifying and monitoring mangroves is increasing, especially with the growing demand in blue carbon markets as mangrove forests are massive carbon sinks capable of storing up to four to ten times as much carbon per hectare as terrestrial forests (Alongi, 2020; Sanderman *et al.*, 2018). Mangrove systems provide critical habitats for aquatic species of economic importance to coastal communities (e.g. crabs, shrimps, molluscs and many fish) and enhance fisheries in adjacent systems, such as coral reefs and seagrass beds, which also serve as recognized nursery environments. Lastly, mangroves play a significant role in climate change adaptation, providing coastal resilience and disaster risk reduction through shoreline protection, particularly in reducing the impacts of storm surge.

Given the critical importance of mangroves to resilience and livelihoods, the need for robust information on the status and changes in mangroves to inform decision-making processes related to sustainable coastal development is increasingly recognized. In response, several global tools have been developed for mapping and monitoring mangroves. However, most of these datasets have been derived using 30-m spatial resolution imageries (e.g. Landsat) that make it difficult to identify mangrove patches smaller than 60 m in their smallest dimensions. Despite recent improvements, for example, the free WorldCover 10 m global land cover datasets produced by the European Space Agency (ESA) developed using Sentinel-1 and Sentinel-2 satellite data (Zanaga *et al.*, 2022), these global datasets typically fail to detect many of the narrow and fringing mangroves common on small islands. In addition, many local resource managers lack the resources or technical capacity to map and monitor at a local scale using modern technologies, including higher resolution satellite imagery or uncrewed aerial systems (UAS), including drones. Many countries are challenged by the need to improve their mangrove cover estimates to inform decision-making on coastal land use and to guide local conservation efforts including restoration planning.

This manual was developed to help overcome this problem by providing guidance, specifically targeted to build capacity for mangrove resource managers on how to use and take advantage of the latest technologies in mapping and monitoring mangroves. Each remote sensing data source has unique spatial, spectral and temporal characteristics that need to be appropriately matched to a research question. The plethora of remote sensing data can be overwhelming. This manual helps the reader make the best decision based on project needs and available budget. Before embarking on any mapping project, it is important to evaluate practical accuracy requirements and available skillsets. Where possible, low-cost options for obtaining data, as well as open-source software for analysis can be used. There are many options for assessing mangrove change using historical aerial photos and archives of optical and active satellite datasets. As UAS are becoming a popular tool for local scale monitoring, this manual also provides a current inventory of available platforms and sensors as well as the latest choices for mission planning applications and postprocessing solutions. A review of pertinent vegetation indices provides guidance for assessing mangrove condition and change. Options for online data resources and relevant open-source software offer solutions for low-budget projects.

This manual enables collection of data that informs conservation decision-making, guiding the planning of mangrove restoration and protection activities that will ultimately lead to enhanced management and conservation of mangroves. Case studies are presented on estimating mangrove extent, structure, condition and change, using a range of remote sensing-derived sources that are focused on < 5-m spatial resolution. This includes historical aerial photography, current high resolution optical and active satellite imagery, locally acquired UAS imagery and an inventory of existing mangrove sources and software. We also share TNC's new Google Earth Engine application, the Blue Carbon Explorer[1] that permits users to detect spatiotemporal changes in mangroves using derived vegetation indices that are computed using archived satellite data and an instructional web-based Esri StoryMap[2] that summarizes the results of this manual and includes instructional field-based videos (**Figure 1**).

Figure 1. *A case study in Bajo Yuna National Park, Dominican Republic from TNC's Esri Story Map "Mapping Mangroves" showing how UAS can be used to detect mangrove change*

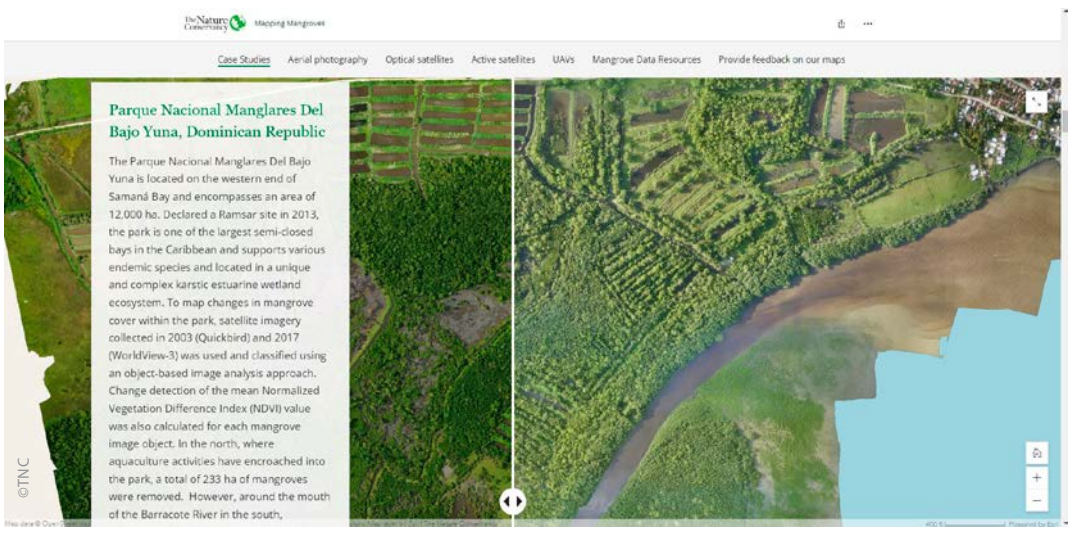

Source: TNC & FAO. 2022. Mapping mangroves. Building data for coastal resilience and ecosystem-based climate adaptation planning. https://storymaps.arcgis.com/stories/75615bb17fcd4704940b97fea318ad59

[1] https://bluecarbon.tnc.org/
[2] https://arcg.is/1WHqC5

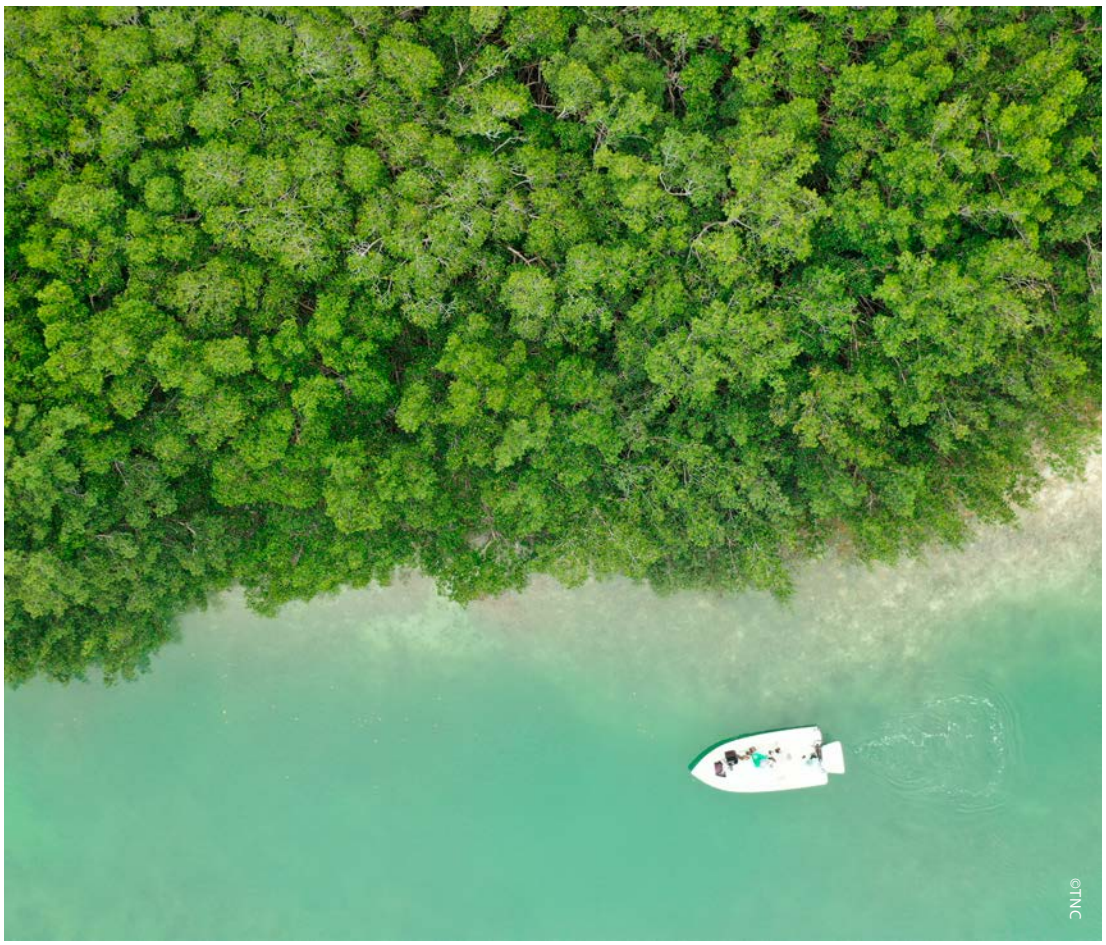

1.2 THE IMPORTANCE OF MANGROVES

Mangrove forests provide multiple benefits for people and the Earth. Mangroves serve as a biodiversity hotspot and these forests are critical for sustaining local fisheries, with 4.1 million of the world's marine small-scale fisheries primarily located in mangrove areas (Zu Ermgassen *et al.*, 2020).

Mangroves serve as natural buffers along coastlines reducing damage from storms, with global estimates of USD 65 billion in avoided property damage and the protection of 15 million people from flooding (Menéndez *et al.*, 2020). Mangrove forests can be up to four times more efficient than some other forest systems at converting carbon dioxide (CO_2), a greenhouse gas, to stored organic carbon or blue carbon. This is due to the soils being waterlogged, which slows down the rate of decomposition (Donato *et al.*, 2011). Global estimates suggest mangrove forests store some 22.86 gigatonnes of CO_2, with 87 percent of this figure being soil carbon (Leal and Spalding, eds., 2022). Degradation of mangroves contributes to climate change through loss of stored blue carbon as CO_2 is released (Spalding and Leal, 2021).

Conversion of mangroves to produce agricultural commodities (aquaculture, oil palm and rice) accounted for 43 percent of the global mangrove losses between 2000 and 2020 (FAO, 2023). Other anthropogenic threats to mangroves include unsustainable extraction of mangrove resources, conversion to various forms of agriculture, coastal development and pollution. Natural retraction of mangroves, including from sea level rise and coastal erosion exacerbated by the impacts of climate change, accounted for 26 percent of mangrove losses during the same period. The climate-change-driven loss of mangroves further exposes vulnerable communities, including in Small Island Developing States, to disasters such as storm surges, floods and tsunamis, against which healthy mangroves provide a certain level of protection (FAO, 2023).

1.3 GLOBAL COMMITMENTS AND EFFORTS TO PROTECT AND RESTORE MANGROVES

Over the past 40 years, we have lost approximately 30 percent of the world's mangroves (FAO, 2007; FAO, 2020). Eleven of the world's 70 mangrove species (16 percent) are at an elevated threat of extinction based on an assessment of IUCN Red List data, and mangrove habitats often represent primary target areas for conversion to aquaculture and other forms of agriculture, as well as coastal development projects (Polidoro *et al.*, 2010). Although the rate of mangrove loss has declined in recent decades, continuing loss and degradation of mangroves remain a global concern (FAO, 2023).

This situation has motivated governments to increase protection and restoration activities to preserve and enhance critical ecosystem services. Currently, 42 percent of mangrove areas is in protected areas (Spalding and Leal, 2021). Many countries have also recognized the vital role of mangroves in mitigating and enhancing resilience to climate change. As of October 2021, 71 countries have included marine and coastal nature-based solutions in their nationally determined contributions (NDCs) under the Paris Agreement of the United Nations Framework Convention on Climate Change (UNFCCC) (Lecerf *et al.*, 2021).

Under the 2030 Agenda for Sustainable Development, Sustainable Development Goal (SDG) 14 "Life below water" aims to conserve and sustainably use the oceans, seas and marine resources for sustainable development. Mangroves are closely linked with and make strong contributions to SDG 14 as they support fisheries and associated coastal communities. In addition, mangroves are also covered under Target 14.2 to sustainably manage, protect and restore marine and coastal ecosystems.

The Global Mangrove Alliance[3] (GMA), a collaboration of non-governmental organizations (NGOs), governments, scientists, industry, local communities and donors working towards a common goal of conserving and restoring mangrove ecosystems, has announced its own 2030 goals to help with climate adaptation and mitigation in support of the Paris Agreement (Leal and Spalding, eds., 2022). At the 27th Conference of the Parties of the UNFCCC (COP27), the GMA, in collaboration with the United Nations Climate Change High-level Champions, called for signatories to a "Mangrove Breakthrough", a unified global approach towards mangrove conservation (Climate Champions, 2022). This includes halting loss of mangroves (an estimated 168 km^2 of avoided loss), restoring half of what had been lost since 1996 (some 4 092 km^2 of mangroves restored) and doubling protection of an additional 61 000 km^2 managed for conservation benefits (Leal and Spalding, eds., 2022).

There are many other global and regional initiatives and commitments to restoration that offer opportunities to further bolster mangrove restoration efforts. These include: the United Nations Decade on Ecosystem Restoration 2021-2028;[4] Target 2 under the recently adopted Kunming-Montreal Global Biodiversity Framework[5] (GBF) to place 30 percent of degraded areas under effective restoration; the Bonn Challenge[6] to bring 350 million hectares of degraded and deforested landscapes into restoration by 2030; AFR100 (the African Forest Landscape Restoration Initiative);[7] and the Initiative 20x20[8] in Latin America and the Caribbean. Recent studies (FAO, 2023; Leal and Spalding, eds., 2022) highlight the dynamic nature of mangroves as coastal ecosystems transition from one to another with changes in the environmental conditions. Mangroves have high potential for natural recovery where suitable habitat conditions can be restored. These dynamics should be considered when planning for restoration interventions.

[3] www.mangrovealliance.org
[4] www.decadeonrestoration.org
[5] www.cbd.int/gbf/targets/2
[6] www.bonnchallenge.org
[7] https://afr100.org/
[8] https://initiative20x20.org/restoring-latin-americas-landscapes

Remote sensing techniques, which are validated with field data, play a key role in identifying the spatial extent and condition of mangrove forests, which are key information when considering biodiversity value and ecosystem service benefits, such as carbon sequestration. This can support the identification of suitable mangrove restoration sites as well as the development of an appropriate technical approach to restoration.

1.4 TYPES OF MANGROVES

Mangroves are salt-tolerant evergreen forests that grow within intertidal regions along coastlines, where waters are calm enough and there is enough sediment for roots to take hold (Leal and Spalding, eds., 2022). Globally, there are approximately 70 mangrove species that occur in tropical to warm temperate regions, growing within deltas, estuaries, lagoons or fringing areas along shorelines. Nutrient availability, salinity and elevation can greatly influence the species composition and structure of mangroves. Worthington *et al.* (2020) provide a broad-scale biophysical typology for classifying mangroves based on their sedimentary substrate (carbonate or terrigenous) and geomorphic setting (deltaic, estuarine, lagoonal or open coast) (**Table 1**). Mangroves growing in carbonate sediments occur in areas where limestone deposits predominate,

Table 1. *General mangrove typologies based on their sedimentary, geomorphic and habitat settings*

SEDIMENTARY SETTINGS	GEOMORPHIC SETTINGS	DEFINITION OF GEOMORPHIC SETTINGS	HABITAT SETTINGS
Carbonate	Lagoonal	Shallow coastal waterbodies, intermittently separated from ocean inputs, usually formed parallel to the shore	Sand/shingle barriers
	Open coasts	Sheltered environments on oceanic islands behind coral reefs and carbonate banks	Low-energy coasts
Terrigenous	Deltaic	Shoreline protuberances typified by a wide fan-shaped alluvial plain derived from large volumes of river transported sediment	River-dominated, allochthonous
	Estuarine	Funnel-shaped main channels with bidirectional tidal flows, characterized by large catchment areas and high precipitation input	Tide-dominated, allochthonous
	Lagoonal	See above	Wave-dominated barrier lagoons
	Open coasts	Sheltered embayments such as drowned bedrock valleys	Drowned bedrock valleys

Source: Worthington T.A., zu Ermgassen P.S.E., Friess D.A., Krauss K.W., Lovelock C.E., Thorley J., Tingey R., Woodroffe C.D., Bunting P., Cormier N., Lagomasino D., Lucas R., Murray N.J., Sutherland W.J. & Spalding, M. 2020. A global biophysical typology of mangroves and its relevance for ecosystem structure and deforestation. *Scientific Reports*, 10:14652.

Figure 2. *Fine-scale mangrove classifications based on local geographic descriptions*

Overwash (tide-dominated)	Found on small and narrow elevated islands that may be an extension of a larger landmass and can have little organic matter due to the frequent movement of the tides. 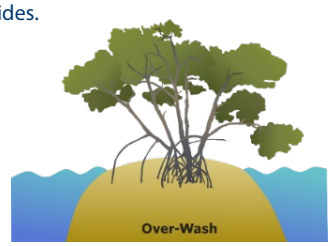	
Fringe (river- and tide-dominated)	Grow as a relatively thin fringe along the coastlines due to the topography or nutrient availability. 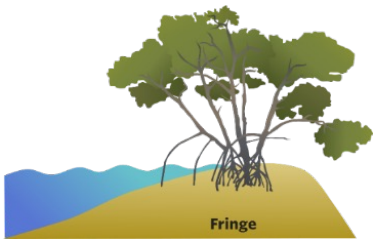	
Riverine (river-dominated)	The tallest mangroves found in sheltered floodplains along flowing waters such as tidal rivers and creeks that are bolstered by fluvial nutrient influx and the daily flushing tides. 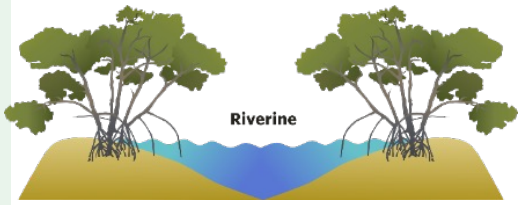	
Basin (interior)	Grow in partially impounded depressions that are flooded occasionally during the dry season and regularly during the wet season. As a result of the stagnant or slow flowing regime, these forests are often stunted in growth. 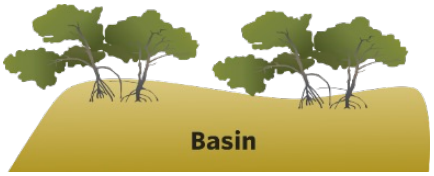	
Scrub (dwarf) (interior and tide-dominated)	Scrub (dwarf) mangroves are more common in broad flat tidal areas found in arid or cooler climates with low nutrient availability. 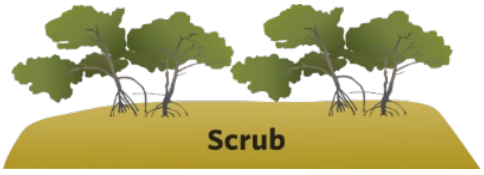	

Source: TNC & FAO. 2022. *Mapping mangroves. Building data for coastal resilience and ecosystem-based climate adaptation planning.* https://storymaps.arcgis.com/stories/75615bb17fcd4704940b97fea318ad59

Graphic credit: Tracey Saxby, Integration and Application Network. https://ian.umces.edu/media-library

including islands and carbonate banks constructed by coral reefs, while mangroves growing on terrigenous sediments (soil derived from land) can be dominated by rivers, tides, waves or a combination of river and wave influence.

Mangroves can be further categorized into finer classifications based on local geographic descriptions (**Figure 2**). *Overwash* mangroves are stands that are not contiguous with any dry land – on the highest tides they are entirely flooded. *Fringe* mangroves grow narrowly alongside shorelines and islands due to topography or nutrient availability and can be sensitive to erosion from waves and tides. *Riverine* mangroves grow in tidal brackish waters along the banks of creeks and rivers. They typically receive large amounts of freshwater and nutrients and can have some of the tallest canopies. *Basin* mangroves are found in low-lying areas located in interior settings, away from the water's edge where there is minimal wave activity and, in some cases, only rare tidal flooding. *Scrub* or *dwarf* mangroves can be found in many different mangrove environments and have very stunted growth and sparse biomass due to low nutrient availability, high salinity or colder climates.

1.5 APPROACH TO MANGROVE MAPPING

To protect mangroves and the extensive ecosystem services they provide, it is critical to understand their extent, scale and condition. Global mangrove monitoring tools, such as Global Mangrove Watch (GMW), can be used to determine the general distribution or trends of mangroves at a broad scale, however finer-scale mapping and monitoring is often needed to inform national-scale and local-scale conservation and management decision-making. Three critical aspects to consider in designing a mangrove mapping approach are 1) the research question, 2) the scale of the area of interest and 3) available capacity for field data collection and image processing.

For monitoring mangrove health at small sites, such as a restoration area or a local marine protected area, UAS monitoring is likely to be the most appropriate approach as it provides high resolution insights and the ability to monitor changes at regular intervals over time. For monitoring larger areas, it would be more appropriate to collect images and species information via UAS imagery and photos at a few representative sites, then use satellite imagery to scale up that information to a larger scale (e.g. national) map that is re-evaluated every few years.

Ready-to-use map products and decision-support tools may also be available from local NGOs or forestry departments depending on the region of interest. It is important to consider the scale of datasets and the training data that were used to generate them; global datasets are generally not useful for planning at the national scale but can give an indication of global mangrove trends and drivers of degradation. Regional datasets can be useful at the national scale, depending on where the training data were collected. To map carbon content, more field data are required beyond drone imagery and species information. Tree counts, height, diameter at breast height (DBH), and canopy density need to be collected to estimate above-ground biomass (AGB), while soil cores need to be collected and processed to estimate below-ground biomass (BGB). With enough field data, allometric equations can be developed for estimating carbon content more broadly using remote sensing.

2. REMOTE SENSING DATA CONSIDERATIONS

Given the various growth patterns and corresponding appearance, mangrove forests can be difficult to map at fine scales using remote sensing techniques. Although all mangrove forests consist of the primary components of leaves, stems and branches, the reflectance patterns can vary based on age, health, species, season, soil type, water quality, leaf density and leaf geometry. The mixing of these components and corresponding reflectance is greater in remote sensing datasets with coarser spatial resolution, which adds another layer of complexity. Mangrove mapping is also inherently biased being based on the analyst because both manual digitization and automated classifications involve some level of visual interpretation. For these reasons, mapping efforts can be difficult to transfer across teams or applications (Kuenzer *et al.*, 2011). In addition, species and growth patterns vary greatly across different parts of the world, between neighbouring islands, and even on a single island, so a one-size-fits-all interpretation process and analysis technique can be problematic (**Figure 3**). Therefore, field data are essential for interpreting these patterns and improving classification accuracy.

Figure 3. *Examples of different mangrove growth patterns on Andros Island, Bahamas*

Notes: These mangroves grow on different substrates and in different spatial patterns, which makes them difficult to map at a fine scale. ***Top left:*** Scrub/dwarf mangroves growing on elevated black algal mats with low nutrient availability. ***Top right:*** Expansive scrub/dwarf mangroves across a tidal flat with taller and denser fringing mangroves growing along tidal creeks where nutrient availability is higher. ***Bottom left:*** A coppice ridge elevated area where a broadleaf and palm forest grow separated from the low-lying mangrove forest. ***Bottom right:*** Very sparse scrub/dwarf mangroves growing near a blue hole on a sandy substrate.

2.1 SPATIAL, SPECTRAL AND TEMPORAL RESOLUTION

Although some countries have developed their own national-scale datasets, many developing countries do not have the resources and expertise to conduct their own mapping and have relied on global remote sensing-derived datasets as their principal source for documenting mangrove extent. Such global datasets are often based on medium resolution satellite data (i.e. 30-m pixel) and miss much of the narrow, fringing and scrub/dwarf mangroves that often exist across small islands. When deciding on an image data source to use for mapping mangroves, it is important to evaluate three fundamental remote sensing resolutions:

1. **Spatial resolution** is the actual area covered on the Earth's surface within a pixel dimension (Figure 4). This influences the ability to recognize and map features within an image. This is also called ground sampling distance (GSD). The highest spatial resolution that can be obtained from a satellite image is a 0.3-m pixel while UAS sensors can record detail down to centimetre (cm) per pixel.

Figure 4. *Near-infrared image composites of mangroves in Ashton Lagoon, Saint Vincent and the Grenadines showing varying spatial resolutions captured by different remote sensing platforms*

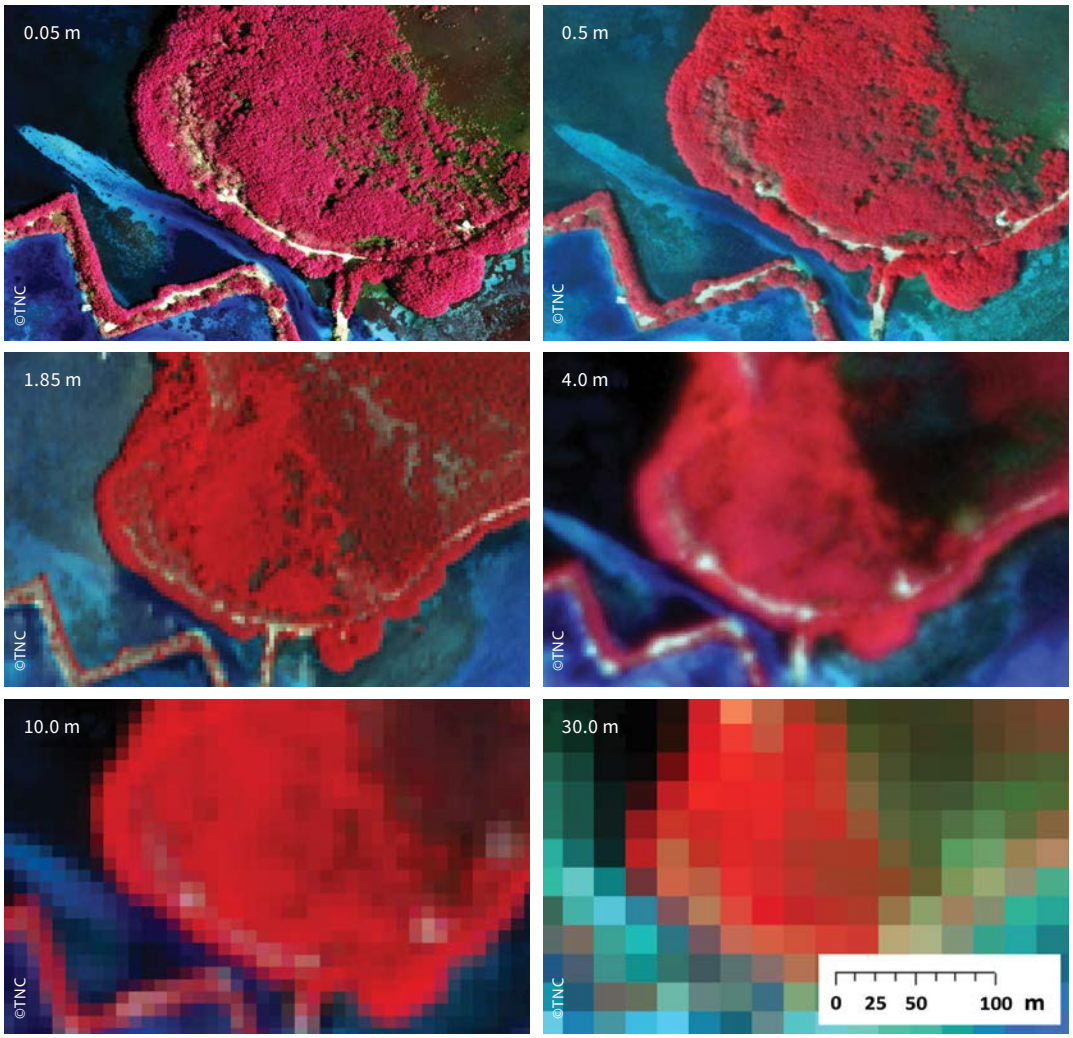

Notes: The spatial resolution of a remote sensing dataset indicates the resolving ability per pixel. The drawback of having better clarity in an image is that the footprint of the scene covers a smaller geographic area. These false colour composites show vegetation as red and are useful for detecting stress levels in plants as healthier vegetation reflects higher levels of near-infrared energy. Examples shown here are: Altum multispectral data acquired from a UAS (0.05 m) and SkySat (0.5 m) (top row left to right); WorldView-2 (1.8 m) and PlanetScope SuperDove (4 m) (middle row); and Sentinel-2 (10 m) and Landsat 9 (30 m) (bottom row).

2. **Spectral resolution** refers to the way light is recorded on the sensor, both in the number of bands but also the narrowness of how light is being recorded (Figure 5). It can be a simple three-band (RGB = red, green, blue) natural colour image from a UAS, an eight-band satellite image from the WorldView-3 satellite or a hyper-spectral image acquired from an airplane with hundreds of bands. Multispectral sensors record wavelengths beyond the visible spectrum and into the infrared wavelengths that do a much better job of detecting vegetation health. The absorption of red light and reflection of infrared light provides critical information related to the health of a plant. The more spectral bands that are recorded, the greater the ability increases to separate features based on their reflectance patterns.
3) **Temporal resolution** refers to how often the sensor records imagery of a particular area, or the data collection revisiting frequency (Figure 6). Some satellites can take days to revisit an area while a UAS can be deployed on demand provided the environmental conditions are appropriate.

Figure 5. *Multispectral imagery of mangroves acquired with a UAS in Ashton Lagoon, Saint Vincent and the Grenadines displayed using various band combinations*

Notes: Variations in spectral resolution can be seen in this multispectral imagery collected with a Micasense Altum multispectral sensor mounted on a WingtraOne fixed-wing transitional UAS over a mangrove forest located at Ashton Lagoon in Union Island, Saint Vincent and the Grenadines. This payload captures five bands of data (red, green, blue, red edge and NIR spectrums) at spatial resolutions down to 3.4 cm/pixel and thermal down to 54 cm/pixel. The left image is in natural colour (RGB), the middle and right images are false NIR colour composites (RGB = red-edge, red and green and RGB = NIR, red-edge and red). The displayed colours will change based on what bands are assigned to the different colour channels (e.g. red, green, blue). These infrared bands permit a much broader evaluation of plant health and vegetation stress detection.

Figure 6. *Satellite images acquired over Guadeloupe on different dates that depict varying cloud cover percentages*

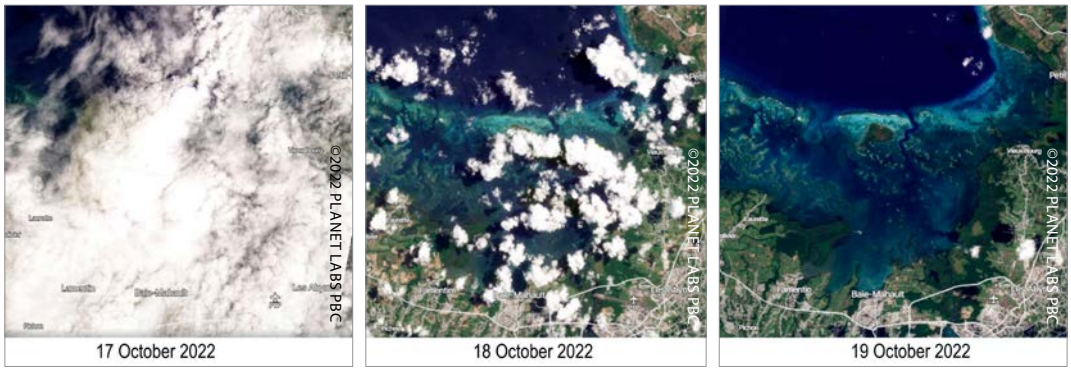

Notes: Temporal resolution addresses the ability to revisit a site to collect data when needed. One of the advantages of the PlanetScope satellite constellation is that it has a very high temporal resolution that makes available a selection of daily scenes to choose from. This can be particularly useful in the tropics where a cloud-free day is rare. These PlanetScope SuperDove scenes were acquired over the same mangrove area in Guadeloupe but collected over three consecutive days with different cloud cover results.

Each remote sensing data source has unique spatial, spectral and temporal characteristics that need to be appropriately matched to the research question, while considering the available budget and size of the project area. Matching datasets appropriately can better support decision-making around improved management, conservation and restoration of mangroves.

Regarding spatial resolution, a general rule of thumb is that the spatial resolution of the imagery should be less than one-half the size of the feature of interest measured in its smallest dimension. For example, identifying a fringing mangrove of 2-m width will require an imagery with a spatial resolution of 1-m pixel or less. National forest definitions also need to be considered when determining the appropriate spatial resolution. The highest spatial resolution is not always the best option because it results in significantly larger data volume to process and there may be an overload of information to deal with (e.g. shadows, more features that need to be classified). In addition, higher spatial resolution datasets from satellites will have narrower imaging swaths, so this may not be practical for mapping large areas.

In terms of spectral resolution, more spectral bands will generally provide a greater ability to discriminate between features. For example, it would be difficult to distinguish different mangrove species using only three visible bands (RGB), however, a WorldView-3 satellite scene with eight bands that include a red edge and two near-infrared (NIR) bands, would improve the likelihood of species separation when combined with field data.

Figure 7. *Differences between three mangrove classifications using different satellite data and methods in Andros Island, Bahamas*

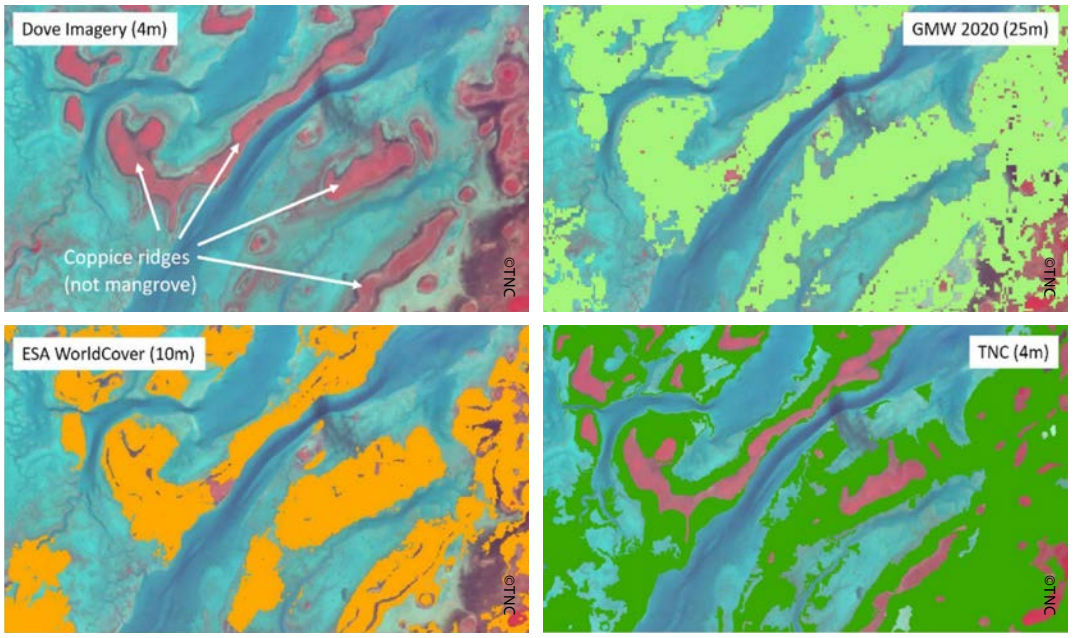

Notes: Three classifications of mangroves using different satellites and methods that produced different results. ***Top left:*** A high resolution (4-m pixel) infrared composite of a PlanetScope Dove scene over a mangrove area in western Andros Island, the Bahamas. Through field verification, the identified coppice ridges indicated on the image are elevated land features that consist of broadleaf forests and palms, not mangroves. ***Top right:*** The mangrove extent as mapped by the Global Mangrove Watch 2021 dataset (25-m pixel). ***Bottom left:*** The mangrove extent as mapped by the ESA WorldCover 2021 dataset (10-m pixel). ***Bottom right:*** The classification by TNC using PlanetScope Dove imagery (4-m pixel) which excludes the coppice ridges and includes much of the scrub/dwarf mangrove areas that are absent in the other two datasets. When coupled with field data and higher resolution satellite imagery, more accurate boundaries can be mapped for mangrove extent.

The temporal resolution of a sensor is important when mapping mangroves in areas with persistent cloud cover. A significant advantage of using the Planet Dove satellite constellation is the near daily cadence of data collection that provides more options for selecting the best possible (cloud-free) scene. UAS can have a very high temporal resolution because they can be deployed whenever suitable environmental conditions prevail.

Finally, the image swath or footprint (i.e. image area of a scene) varies between data sources so the size of the project area will dictate the most appropriate data source to use. Mapping using multiple image swaths that were acquired at various times, seasons and environmental conditions can be problematic for achieving consistency in mapping across seamlines. National-scale mangrove inventories are typically conducted using satellite imagery where each scene covers a larger geographic extent. For mapping larger areas (e.g. > 10 km^2), the use of UAS is often not practical because of the limited area that can be mapped per battery, difficulty in achieving consistency in environmental conditions, and the volume of data produced. In these instances, airplane or satellite imaging is often more appropriate.

Figure 7 shows examples of three different mangrove classifications based on different satellite datasets that produced varying levels of accuracy. When combined with field data, higher spatial resolution satellite imagery, such as Planetscope Dove (4-m pixel), can help separate out elevated areas, such as coppice broadleaf ridges that are not mangroves, and identify sparse scrub mangroves. Compared to global products, such as the Global Mangrove Watch 2021 dataset (25-m pixel) and the ESA WorldCover 2021 dataset (10-m pixel), finer scale imagery can achieve higher accuracy in mapping mangrove extent. Field validation is important as higher spatial resolution datasets often overestimate mangrove extent.

2.2 TYPES OF REMOTELY SENSED DATA

Remote sensing data can be classified into optical and active systems.

Most Earth observation satellites are optical remote sensing systems that record reflected electromagnetic energy. Optical satellite imagery that has a spatial resolution of less than 5 m provides adequate level of detail for mapping at the local scale and some systems can be tasked to acquire data over a user-defined area (**Figure 8**).

Figure 8. *SkySat imagery over a mangrove area in west Andros Island, Bahamas*

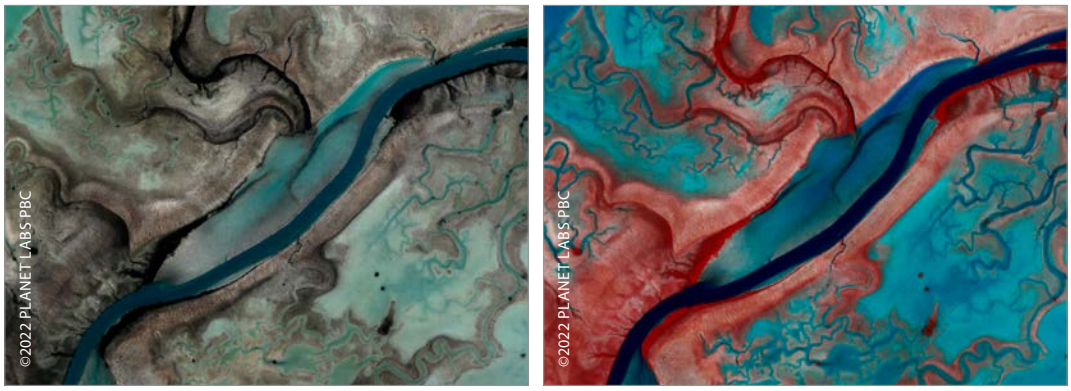

Notes: SkySat optical four-band satellite imagery (1-m MS/0.5-m PAN) shows a natural colour composite (RGB) on the left and a false colour infrared composite on the right. Because healthy plants reflect much more infrared energy, the detection of vegetation is much clearer in the infrared composite, and denser plant growth (i.e. more biomass) appears in darker shades of red.

Active systems, such as Radio Detection and Ranging (RADAR) and Light Detection and Ranging (LiDAR) emit and record the backscatter of their own energy (e.g. microwave, infrared) and are not dependent on the Sun's energy. Active sensing systems can be used to detect mangrove forest structure, map individual trees and stand diameters, and predict volume and biomass (**Figure 9**).

Figure 9. *Synthetic Aperture Radar (SAR) data acquired over mangrove areas from two different SAR satellites and combined into false colour composites*

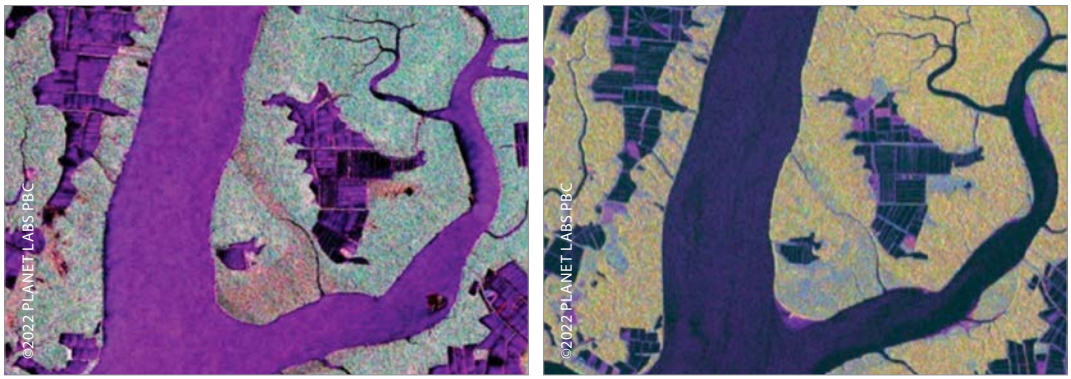

Left: ALOS PALSAR-1 (L-band, 23-cm) data. ***Right:*** Sentinel-1 (C-band, 5.5-cm) data. Dark colours represent smooth surfaces where radar signals are reflected away from the sensor, and brighter surfaces indicate roughness where signals bounce back and are recorded by the sensor. The different wavelengths and polarizations provide insight into mangrove height and canopy structure with stronger backscatter in taller mature canopies and weaker backscattering recorded in younger, low-density forests.

Adapted from: Simard, M. 2019. Radar remote sensing of mangrove forests. In: A. Flores, K. Herndon, R. Thapa & E. Cherrington, eds. *NASA SAR Handbook: Comprehensive methodologies for forest monitoring and biomass estimation.* NASA. DOI: 10.25966/33zm-x271

One of the main advantages of RADAR is that it can penetrate cloud cover and be acquired at different wavelengths, with each band capable of characterizing different forest stand parameters. LiDAR data can be used to generate detailed three-dimensional point clouds that can be used to visualize, quantify and classify vegetation characteristics (**Figure 10**).

Figure 10. *Point cloud and vertical profile of a mangrove forest derived from LiDAR data*

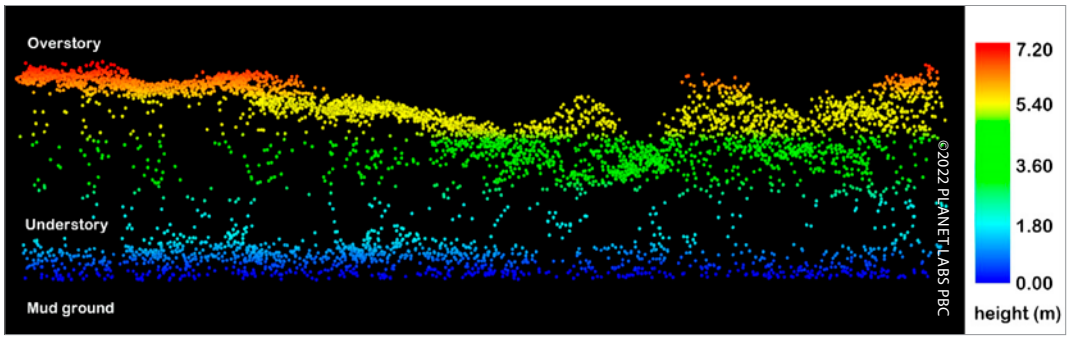

Notes: The different colours represent the height of the laser return and are classified into different canopy height levels, which provide information on the canopy structure.

Source: Li, Q., Wong, F.K.K. & Fung, T. 2019. Classification of mangrove species using combined WordView-3 and LiDAR data in Mai Po nature reserve, Hong Kong. *Remote Sensing*, 11(18): 2114.

Table 2 provides a summary of the widely adopted optical and active remote sensing data sources for mapping and monitoring mangroves along with their associated advantages and limitations. There are various optical satellite image providers to choose from and each satellite has different spatial, spectral and temporal characteristics that should be considered, depending on the mapping objectives. Higher resolution datasets can be more expensive (not in the public domain), cover a smaller area and scene availability may be lower due to the smaller scene footprint.

Table 2. *Types and examples of optical and active satellite data sources with advantages and limitations*

TYPES	SENSOR / RESOLUTION	EXAMPLES	APPLICATIONS	ADVANTAGES	LIMITATIONS
Optical	Aerial: high spatial resolution (< 0.5 m)	Aerial photography, UAS imagery	Local-scale mapping, species identification, 3D modelling	Ultra-detail, can be acquired below cloud cover, often historical imagery available allowing for long-term monitoring	Impractical to use for larger areas, data volume
	Satellite: high spatial resolution (0.5 m to 5 m)	WorldView-3, PlanetScope, Pléiades, SkySat, KOMPSAT-5, SPOT-7	Broader-scale mapping applications, canopy modelling, species level with multispectral data, DSM generation	Can be tasked to image a particular area (higher temporal resolution), multispectral, broader area than UAS	Smaller footprint than medium resolution, cost, scene availability, data collection after year 2000
	Satellite: medium spatial resolution (5 m to 30 m)	Sentinel-2 (10 m), Landsat (30 m)	National or regional scale, monitoring of large-scale changes and condition assessments	Public domain Landsat is available for longer time periods than newer, high-resolution satellite data, which is important for longer term change detection	Coarser spatial resolution that misses narrow and fringing mangroves
	Hyper-spectral	Airborne/ UAS	Species discrimination and plant health assessments	Powerful classification potential, user-defined spatial and spectral resolution based on the research question	Limited availability, expensive, large data volume, requires extensive analytical skills to process
Active	Synthetic Aperture Radar (SAR)	Sentinel-1, ICEYE SAR, TerraSAR-X/ PAZ, Capella	Invaluable asset for canopy modelling and moisture detection, useful when combined with optical data, DSM generation	Sentinel-1 C-band can image down to 5 m. High frequency X-band provides better user-defined detail, weather and daylight independent, flexible area coverage, complements optical data	Requires advanced processing capabilities, higher costs, requires optical data integration
	LiDAR	Often airborne, GEDI, ICESat (space-based)	3D canopy modelling, point cloud and DSM generation	Very high accuracy, speed, versatile, automated functionality, cost-effective over large areas	Requires advanced processing capabilities, higher costs, large data volume

Adapted from: Kathiresan, K. & Bingham, B.L. 2001. Biology of mangroves and mangrove ecosystems. *Advances in Marine Biology*, 40: 81–251; Kuenzer, C., Bluemel, A., Gebhardt, S., Quoc, T.V. & Dech, S. 2011. Remote sensing of mangrove ecosystems: A review. *Remote Sensing*, 3(5): 878–928.

2.3 AERIAL PHOTOGRAPHY FOR MAPPING MANGROVE CHANGE OVER TIME

While medium resolution (e.g. 30-m pixel) satellite image products have been available since the 1980s, high resolution satellite technology (< 5-m pixel) has only existed since the early 2000s. In contrast, aerial photography provides an invaluable, high-resolution record of land cover conditions that dates back as early as the 1930s. Aerial photos are used for a variety of applications including the creation of topographic maps, generation of contour lines, land-use change analysis and photogrammetric measurements. Aerial photos can be extremely valuable for determining the spatial extent of historical mangrove cover. Early aerial photos were typically acquired using two types of black and white film: *panchromatic* and *infrared*. Starting in the 1950s, colour film became more widely used in both natural colour (RGB) and colour infrared formats (**Figure 11**). As vegetation reflects much more infrared energy, infrared film offers better contrast between forest types and greater ability to distinguish between healthy and diseased vegetation, delineate bodies of water and penetrate atmospheric haze (Avery, 1969).

Figure 11. *Three types of aerial photography (left to right: panchromatic; natural colour; and colour infrared)*

Aerial photos acquired for mapping purposes are typically captured vertically, with the camera pointed straight down (**Figure 12**). The rate of photo capture is sequenced so that each photo will have at least 60 percent overlap between each sequential photo and 30 percent photo overlap between flightlines. Because each photo is captured at a slightly different perspective, paired stereo photos can be used to visualize the landscape in three dimensions. Stereo photos can be processed into *orthophoto* mosaics which composite all photos into a single file, removing all distortion so they are planimetrically correct and measurements can be taken. This is done using photogrammetric methods, capturing key points among overlapping photos which generates a relief model. This in turn is then used to transform the aerial photos into a perspective, making them appear to have been taken vertically above at an infinite distance.

Figure 12. *Vertical, low oblique and high oblique aerial photos over a mangrove forest providing different perspectives*

Another important aspect of vertical aerial photos is *photo scale* which is the ratio of the distance between two points on a photo to the actual distance between the same two points on the ground. One way to calculate photo scale is to divide the focal length of the camera by the flying height above the ground. If a standard lens focal length of 15 cm is assumed, photo scales will range from about 1:2 000 (very large scale) to approximately 1:135 000 (very small scale). Most aerial photos are acquired in scales ranging from 1:12 000 to 1:20 000. The higher the flying altitude, the smaller the scale (less detail). Other helpful information often found on the frame of an aerial photo includes the date and time, roll and frame number, and altimeter.

Aerial photos can also be collected at oblique angles with the camera tilted at various angles between the horizon and the ground. A *low oblique* photo is where the horizon is not visible and a *high oblique* photo is taken at a higher angle, where the horizon can be seen (**Figure 12**). Oblique photos cover a larger area and are often easier to interpret. However, it is not possible to take accurate measurements from them as they have significant scale distortions due to the varying distances.

Historical aerial photos that have been digitized, and even georeferenced, can often be found in public web-based mapping libraries and archives. Another option is to query government agencies as historical photos are often archived and stored by planning, survey or forestry departments. Originally delivered as hard copy 9 x 9-inch (23 x 23-cm) photos or transparencies, these can be scanned and georeferenced for use in geographic information system (GIS) software. Photos or transparencies can be scanned using a large-format scanner and a user-defined dot-per-inch (dpi) analogue to the digital conversion rate (Jensen, 1996). For example, a 1:20 000 scale photograph scanned at 500 dpi would result in a digital file with each pixel representing 1 x 1 m on the ground. Scanning rates greater than 2 000 dpi are not recommended because this exceeds the resolution of the emulsion properties of the film; moreover, the file size becomes exponentially larger with higher scan rates (Ruzgienė, Bagdžiūnaitė and Ruginytė, 2012). Transparencies can be scanned using a scanner that has a special hood that allows light to pass through the transparency and record the value on the top part of the scanner.

Figure 13. *Examples of historical aerial photos of the United States Virgin Islands taken in 1954*

Left: A panchromatic photo taken on 29 January 1954 of the eastern end of Saint Thomas, the United States Virgin Islands at a scale of 1:28 400. ***Right:*** A colour infrared photo taken in April 1971 of Portland Bight, Jamaica. Mangroves are much more discernible in the colour image. These photos can be scanned and georeferenced, then used in a GIS to digitize historical mangrove extent for change detection purposes.

Once the aerial photos are scanned and in a digital format (TIFF or JPEG), they can be georeferenced to a coordinate system by selecting ground control points (GCPs) that match an existing georeferenced base map, such as a high-resolution satellite image, using open-source GIS software (e.g. QGIS). It is important to select GCPs that represent permanent positions such as roads and other artificial features (not soft coastlines which are dynamic and change over time). There are many online tutorials[9] that describe how to do this.

Once sufficient GCPs (a minimum of four) have been identified across the image as uniformly as possible, a resampling (i.e. warping) algorithm is applied to reproject the image into the defined coordinate system. The reported root mean square error (RMSE) will indicate the resulting geometric accuracy of the georeferenced image. Once the image is georeferenced, GIS software and image interpretation can be used to digitize polygon boundaries around the interpreted mangrove extent (**Figures 13 to 18**).

Figure 14. *Historical aerial photos collected in January 1954 over Saint Thomas, the United States Virgin Islands*

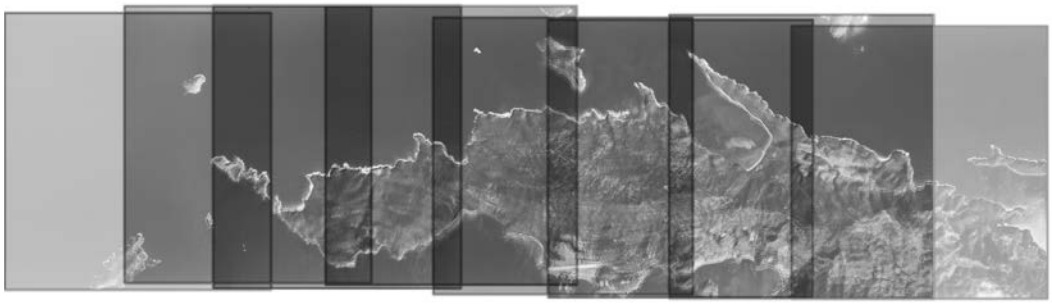

Notes: These photos were acquired in an overlapping (stereo-pair) format, with at least 60 percent overlap between each photo capture and 30 percent sidelap between flightlines. The collection of stereo photos permits stereo viewing and the creation of an orthophoto mosaic in which all geometric distortions are removed (GIS ready). This is identical to the way a UAS mission is planned, however the overlap is generally higher (e.g. 70 percent) because the UAS is flying in closer proximity to the ground.

Figure 15. *Example of the selection of GCPs for georeferencing an aerial photo*

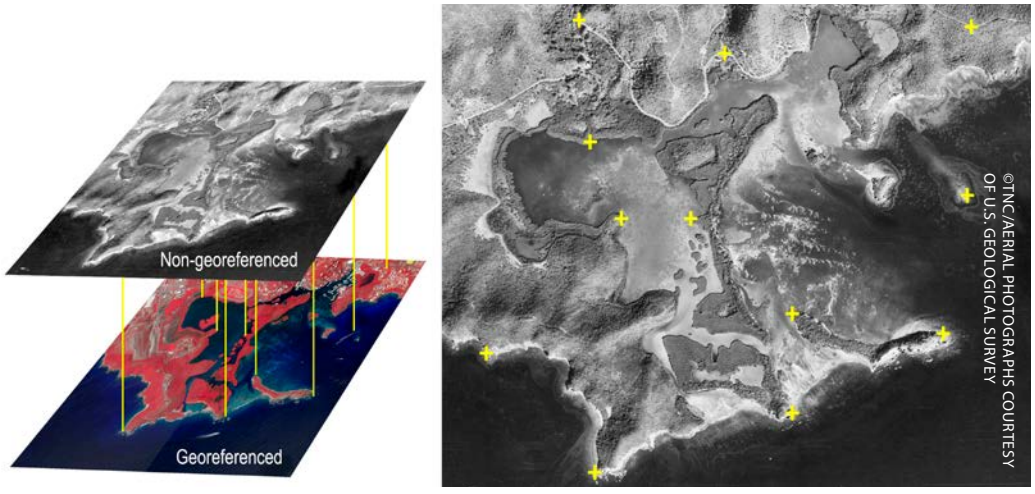

Notes: These photos were acquired in an overlapping (stereo-pair) format, with at least 60 percent overlap between each photo capture and 30 percent sidelap between flightlines. The collection of stereo photos permits stereo viewing and the creation of an orthophoto mosaic in which all geometric distortions are removed (GIS ready). This is identical to the way a UAS mission is planned, however the overlap is generally higher (e.g. 70 percent) because the UAS is flying in closer proximity to the ground.

[9] https://docs.qgis.org/3.22/en/docs/user_manual/working_with_raster/georeferencer.html

Figure 16. *Appearance of mangrove forests in Jamaica in historical panchromatic and colour infrared aerial photos*

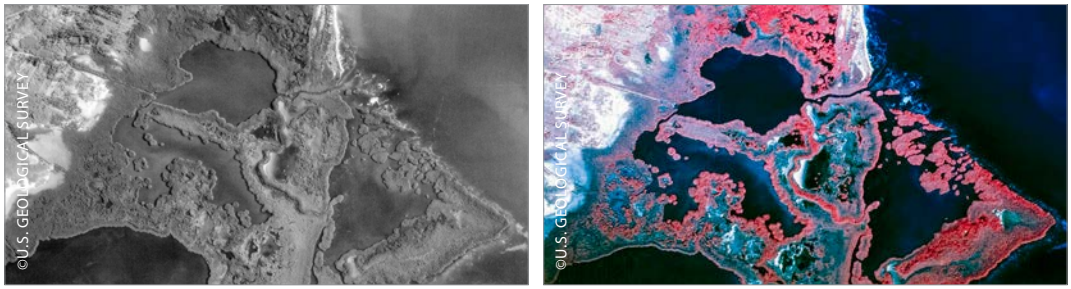

Note: It is much easier to identify mangroves using colour clues, but canopy texture is also helpful when interpreting imagery.

Figure 17. *Historical aerial photography and mangrove change detection in Saint Thomas East End Reserve, the United States Virgin Islands*

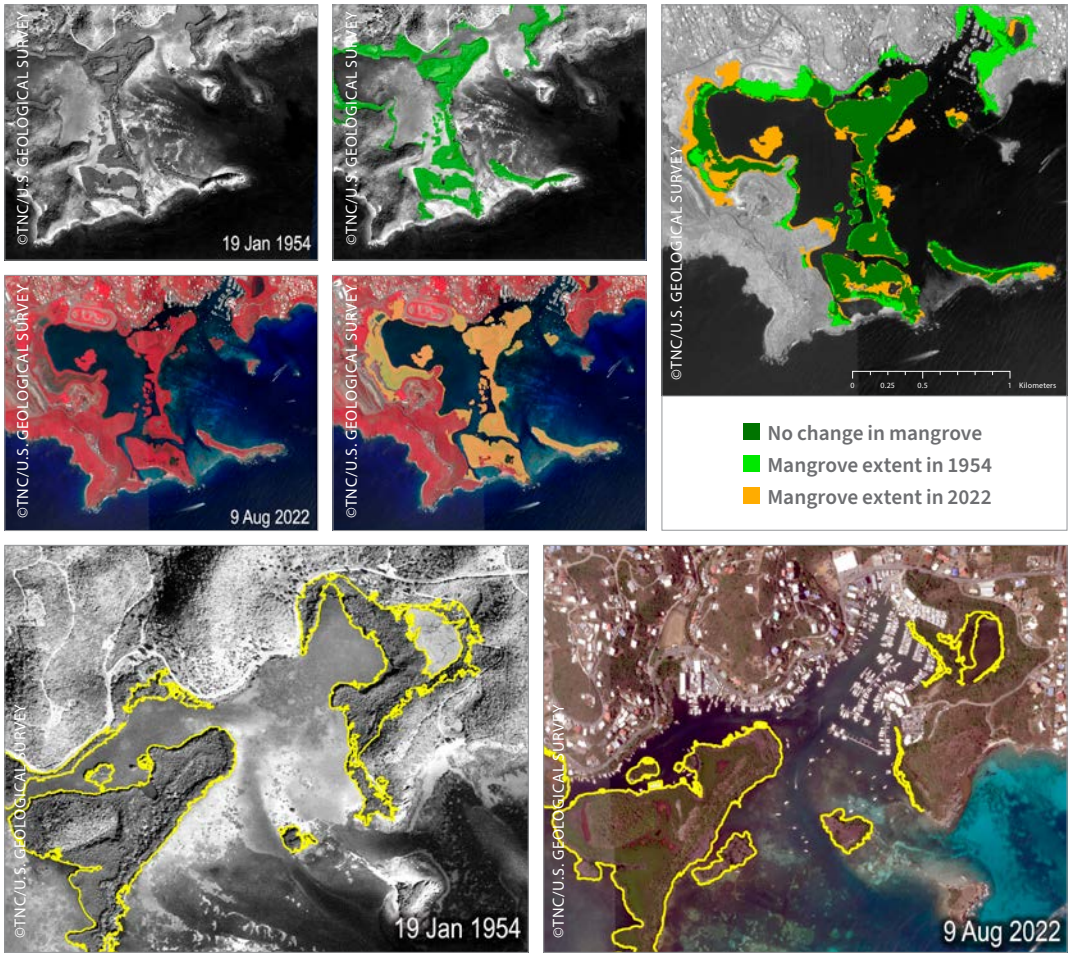

Note: Using historical aerial photography in Figure 17, mangrove change was detected over a 68-year period. The construction of a marina resulted in the removal of several hectares of mangrove, however, mangroves have expanded into other areas.

Figure 18. *Comparison of multiple remote sensing data showing mangrove die-off and growth due to alternation of hydrology by a causeway near Salt River, Jamaica*

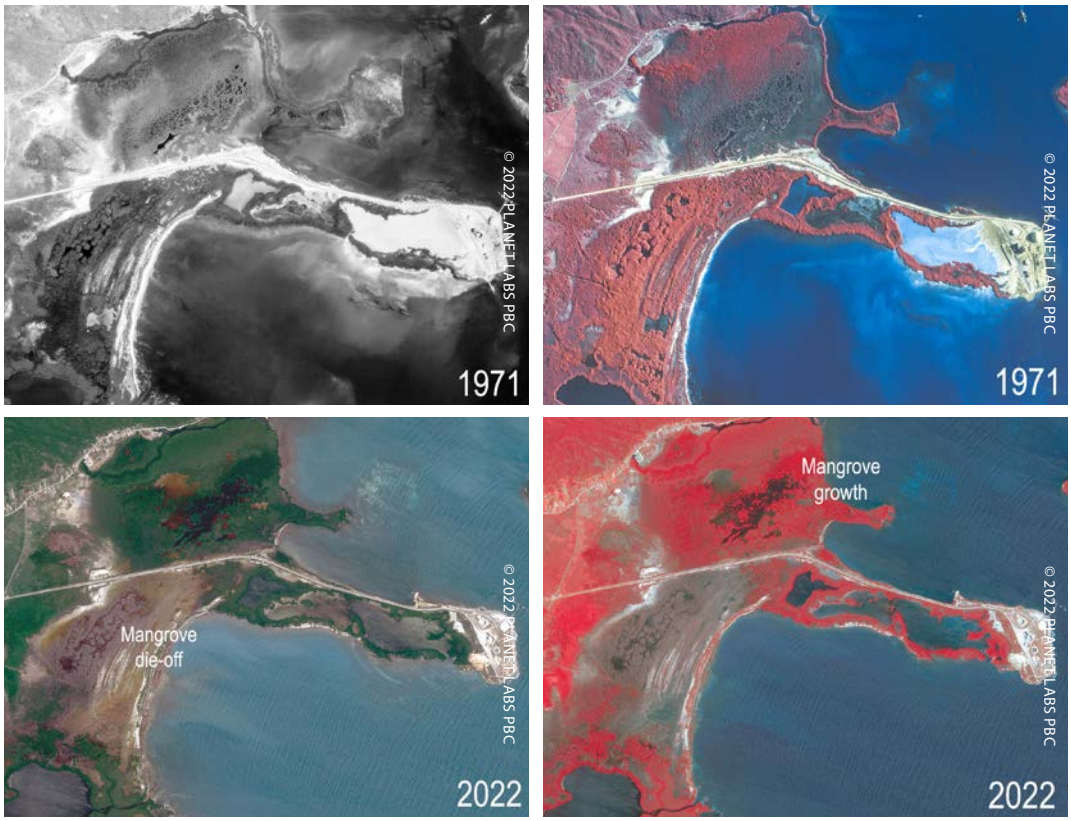

Notes: The top images are panchromatic and colour infrared aerial photos acquired in 1971. The bottom images are from SkySat acquired on 26 May 2022 and are shown in both natural colour (RGB) and colour infrared composites. Aerial photographs courtesy of U.S. Geological Survey/Image

2.4 OPTICAL HIGH RESOLUTION SATELLITE IMAGERY (< 5 M)

There are many choices of high-resolution satellite imagery for mapping and monitoring mangroves at less than 5-m spatial resolution (Table 3). The options and price structures are constantly changing as satellite technology continually improves and new satellite constellations are launched.

Table 3. *Available high spatial resolution (< 5 m) satellite imagery options for mangrove mapping and monitoring*

SATELLITE	SPECTRAL BANDS	SPATIAL RESOLUTION (m)	SCENE SWATH (km)	MIN. ORDER AREA (km^2)	PRICE/KM^2 * (USD)	ACQUISITION DATES
AIRBUS						
Pléiades Neo	Pan	0.3	14	25	20–25	May 2021 to present
	6-band MS	1.2				
Pléiades 1A/1B	Pan	0.5	20	25	10–15	Dec 2011 to present
	4-band MS	2				
SPOT-6/7	Pan	1.5	60	100	< 5	2012/2014 to present
	4-band MS	6				
MAXAR						
World-View-4	Pan	0.31	13	25	20–25	Nov 2016 to Jan2019
	4-band MS	1.24				
World-View-3	Pan	0.31	13	25	20–25	Aug 2014 to present
	8-band MS	1.24				
	8-band SWIR	3.71				
World-View-2	Pan	0.46	16.4	25	15–20	Oct 2009 to present
	8-band MS	1.85				
World-View-1	Pan	0.5	17.7	25	10–15	Sep 2007 to present
GeoEye-1	Pan	0.5	15	25	15–20	Sep 2008 to present
	4-band MS	1.84				
Quickbird	Pan	0.6	17	25	15–20	Oct 2001 to Dec 2014
	4-band MS	2.4				
IKONOS	Pan	1	11.3	25	10–15	Sep 1999 to Dec 2014
	4-band MS	4				
PLANET						
PlanetScope Dove/ SuperDove	4-band MS 8-band MS	~4	24 32.5	25	On request	Jul 2014 to Apr 2022 Mar 2020 to present
SkySat	Pan	0.5	11	On request	5–10	Nov 2013 to present
	4-band MS	1				
ADDITIONAL OPTIONS						
BlackSky	Pan	1	26–59	On request	On request	Nov 2018 to present
	3-band MS					
EROS B	Pan	0.7	7	25	5–10	Apr 2006 to present
GaoFen-2 (GF-2)	Pan	0.8	45	25	< 5	Aug 2014 to present
	4-band MS	3.2				

SATELLITE	SPECTRAL BANDS	SPATIAL RESOLUTION (m)	SCENE SWATH (km)	MIN. ORDER AREA (km^2)	PRICE/KM^2 * (USD)	ACQUISITION DATES
ADDITIONAL OPTIONS (continued)						
GEOSAT-2 (Formerly Deimos-2)	Pansharpened	0.75	12	25	5–10	Jun 2014 to present
	Pan	1				
	4-band MS	4				
Jilin-1	Pan	0.5	11.6	25	5–10	Oct 2015 to present
	4/5-band MS	2				
	Colour night-time	1				
	Colour video	1				
KazEOSat-1	Pan	1	20	100	< 5	Apr 2014 to present
	4-band MS	4				
KOMP-SAT-3A	Pan	0.5	12	25	10–15	Aug 2014 to present
	4-band MS	2				
KOMPSAT-3	Pan	0.5	16	25	5–10	Aug 2014 to present
	4-band MS	2				
OVS-3	Natural colour	0.9 (OVS-1, 1.9; OVS-2, 0.9)	22.5	131	5–10	Aug 2014 to present
SuperView-1	Pan	0.5	12	25	10–15	Aug 2014 to present
	4-band MS	2				
TripleSat	Pan	0.8	23.8	25	5–10	Aug 2014 to present
	4-band MS	3.2				
TeLEOS-1	Pan	1	12	100	< 5	Sep 2008 to present

* Estimated prices as of April 2023. Discounts may be available for NGOs and non-commercial applications.
Source: Authors' elaborations.

This section provides a general (non-exhaustive) overview of available remote sensing data options and technical specifications that may fit certain budgets and project requirements. The five main considerations in selecting satellite imagery are 1) spatial resolution in both panchromatic and multispectral images; 2) the number of available bands; 3) the swath dimension for each scene (footprint); 4) the dates of available imagery; and 5) cost.

Airbus[10] operates the Pléiades satellite constellation that has been collecting imagery since December 2011 and offers more affordable 0.5-m panchromatic (pan) and 1-m multispectral (colour) data options with one of the largest swaths (20 km). The company recently launched the Pléiades Neo (0.3-m pan/1.2-m colour), a constellation of four identical satellites and along with WorldView-3, it has the highest spatial resolution available from space. Costing about the same as WorldView-3, the Neos have a slightly larger swath, but fewer spectral bands (6 vs 8 bands). However, the 8-band WorldView-3 data archive goes back to 2014. In addition to Pléiades, Airbus operates and distributes the TanSAR-X/TanDEM-X high resolution radar products, the KazEOSat-1 (1-m pan/4 m-colour) and SPOT-6/7 (1.5-m pan/6-m colour) which have been operating since 2014 and have the largest imaging swath of 60 km. Airbus imagery can be searched, browsed and purchased through the GeoStore[11] and custom tasking of a satellite can be scheduled.

[10] www.intelligence-airbusds.com/imagery/constellation
[11] www.intelligence-airbusds.com/en/4871-ordering

MAXAR[12] (formerly DigitalGlobe) is a pioneer in high resolution satellite imaging, going back to the first 1-m satellite, IKONOS (1-m pan/4-m colour), that was launched in 1999 and continued operating until March 2015. This was followed by the launching of Quickbird (0.6 m-pan/2.4 m-colour) in 2001, the first submeter satellite that operated until December 2014. GeoEye-1 (0.5-m pan/1.8-m colour) was launched in 2008, followed by WorldView-2 (0.5 m pan/1.8 m colour) in 2009 with a much larger swath (25 km) and the first 8-band multispectral imaging system (coastal blue, blue, green, yellow, red, red-edge, near-IR, near-IR2). WorldView-3 was launched in 2014 and was the first satellite to image below 0.5-m spatial resolution (0.3-m) with eight 1.2-m multispectral bands. WorldView-4 was similar to WorldView-3, but only collected data between November 2016 and January 2019 due to mechanical failure. Maxar also distributes C-band Radarsat-2 imagery that has been collected since 2008. The new WorldView Legion six satellite constellation is scheduled to launch in 2023 and will provide 0.3-m resolution imagery with up to 15 revisits per day. Imagery for Maxar's constellation can be searched, browsed and purchased through the Discover[13] portal and custom tasking of a satellite can be scheduled.

Planet[14] is a company that started in 2010 and now manages the largest constellation of satellites with over 200 currently in orbit. They operate the PlanetScope Dove and SuperDove nanosatellites (5 kg each) that collect daily 4-band scenes and 8-band scenes at 4-m spatial resolution. These are most likely to be the most affordable high resolution image products unless one qualifies for the Norway's International Climate and Forest Initiative (NICFI) satellite data programme that provides free imagery to partners working to curb deforestation in tropical areas of the world. Researchers and educators can also apply to access free imagery. Planet also operates the SkySat satellites (0.5-m pan/1-m colour) which collect 4 bands at an 11-km swath and can be tasked. In 2023, Planet will upgrade their 21 SkySat satellites and start launching their 32 Pelican satellites that will offer 0.3-m imagery with up to 30 revisits per day. Planet[15] is a searchable database of archived scenes and global basemaps mosaics that are available monthly or quarterly. Other plans include the development of a hyperspectral fleet of satellites called Tanager which will be of great benefit for mangrove mapping and change detection.

BLACKSKY[16] operates a constellation of satellites that provide 1-m pan scenes that are up to 60-km wide as well as radar images down to 0.25-m resolution with a structured pricing system. Other options include the Chinese-operated 4-band satellites, the Jilin-1 (0.5 m-pan/2-m colour) launched in 2015 and the SuperView-1/2 (0.5-m pan/2-m colour) that was launched in 2016. Two Jilin-1 hyperspectral satellites were launched in January 2019 and provide 28 bands at 5-m spatial resolution. Three Jilin-1 Smart Video satellites were launched in November 2017 and provide 4K video for real-time monitoring at a 1 m spatial resolution. A new SuperView Neo 28 satellite constellation was launched in 2022 and will provide 0.3 m-pan and 1.2-m 4-band multispectral imagery. Another Chinese operated satellite is the Gaofen-2 (0.8-m pan/3.2-m colour) that was launched in August 2014 and has a 45-km swath.

The Korea Aerospace Research Institute[17] (KARI) launched the four-band Kompsat-3A (0.5-m pan/2-m colour) in March 2015 which is a sister spacecraft to the previously launched Kompsat-3 (0.7-m pan/2.8-m colour). The OVS-3 satellite offers 0.9-m RGB imagery and 120-second video. The TripleSat/DMC3 (0.8 m-pan/3.2-m colour) is an Indian constellation launched on 10 July 2015, with a

[12] www.maxar.com
[13] https://discover.maxar.com/
[14] http://planet.com/
[15] www.planet.com/products/explorer
[16] www.blacksky.com
[17] www.kari.re.kr/eng.do

23-km swath. More affordable options are the EROS B (0.7-m pan) launched in 2006, the TeLEOS-1 with 1 m pan imagery launched in 2016 and the GEOSAT-2 (formerly Deimos-2) (1-m pan/4-m colour) launched in 2014 that has a 12-km swath.

An exciting new future satellite is the Albedo constellation, which will deliver 10 cm pan and 40 cm colour and is anticipated to be launched in 2024. Satellogic is an Argentine-owned company that has launched 17 NewSat satellites since 2013, with plans to develop over 300+ microsatellites by 2025. These microsatellites provide submeter resolution multispectral imagery and 29 bands, 25-m hyperspectral imagery and a 1-m resolution full-motion video capability with daily updates.

Before ordering satellite imagery, the area-of-interest will need to be defined as a polygon file that will be used to search for suitable imagery acquired in the past, or to make a tasking request to acquire new imagery. Data collection parameters such as tide windows, maximum shooting angle and acceptable cloud cover levels can be specified. Typically, there is a minimum area required for placing an order (larger areas when making new tasking requests). Older archived scenes (e.g. > 6 months old) are often less expensive with smaller minimum order areas. Companies typically have different product options in terms of radiometric and geometric accuracy. For classifying the imagery, it is important to order the calibrated percent reflectance product, or radiometric corrections will need to be run. Likewise, higher levels of geometric accuracy will cost more, so it is important to understand the project accuracy requirements

Figure 19. *Examples of different high resolution satellite data displayed using different band combinations*

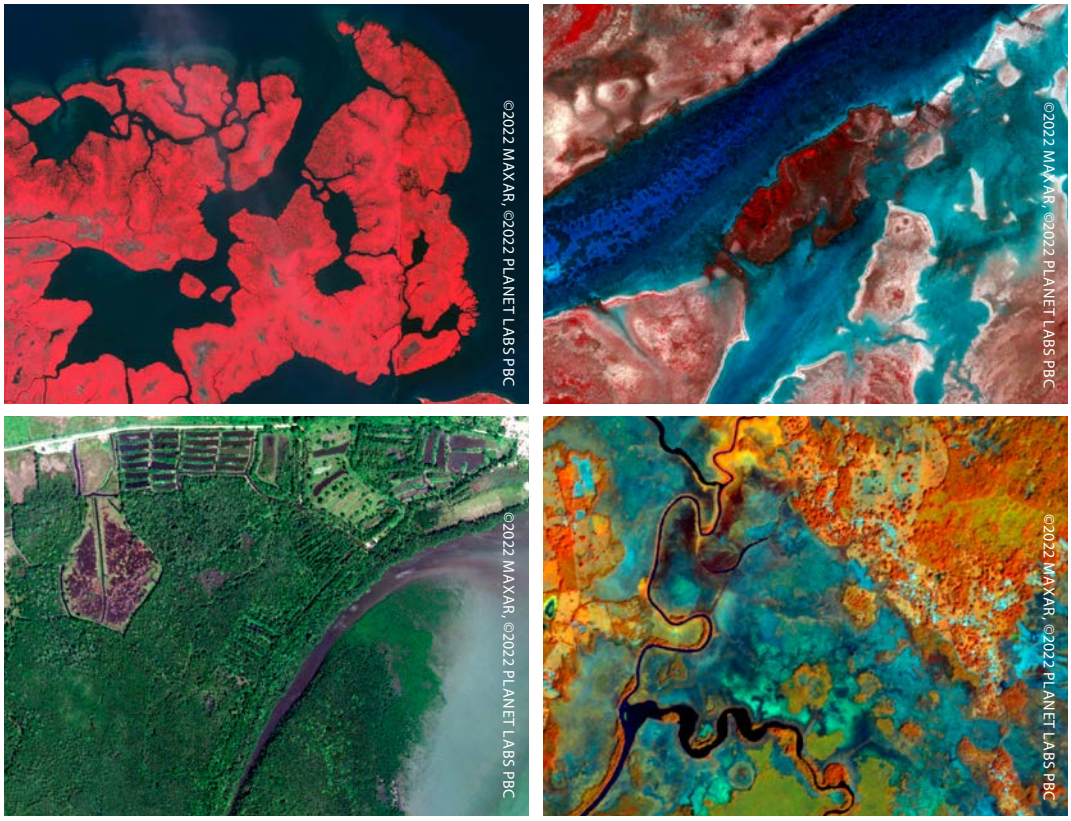

Top left: A WorldView-2 infrared colour composite (2-m pixel) of the mangroves of Caracol Bay, Haiti acquired on 3 September 2011. ***Top right:*** SkySat infrared colour composite (1-m pixel) of mangroves recovering from Hurricane Dorian in eastern Grand Bahama (16 November 2022). ***Bottom left:*** A GeoEye-1 pan-sharpened natural colour composite (1-m pixel) of mangrove reforestation taking place in former aquaculture areas in Bajo Yuna National Park, the Dominican Republic (10 September 2022). ***Bottom right:*** A Planet SuperDove infrared colour composite of the Black River Morass mangroves in Jamaica (3 November 2022). The different band combinations provide insight for various ecological investigations.

and the available budget. One option that is often offered by satellite companies is to *pan-sharpen* the image. This is a radiometric transformation that fuses the high spatial resolution pan band with the lower spatial resolution multispectral bands to produce a high spatial resolution colour image. For example, a 0.3-m pan image is fused with the 1.85-m multispectral (colour) bands to produce 0.3-m colour. Although pan-sharpening delivers higher colour resolution, the process degrades valuable spectral information contained in multispectral imagery that can be important for classifying features when mapping or deriving information that relies on calculated percent reflectance values (**Figure 19**).

2.5 SYNTHETIC APERTURE RADAR FOR DEFINING MANGROVE STRUCTURE

SAR sends measured microwave energy and records the backscatter signal, which is proportional to the size, shape and water content of the leaf (Simard, 2019). One of the main advantages of SAR is that it can penetrate cloud cover, making it particularly useful in tropical areas of the world, and operates both during the day and at night. High spatial resolution SAR data are not widely available in the public domain, however these data can be purchased and used as an effective tool to measure forest structure, such as canopy height, estimate AGB, and identify canopy crown (Pham *et al*., 2019a).

SAR can be acquired at different wavelengths, with each band characterizing different forest stand parameters. Shorter wavelengths (e.g. X-band, 3-cm wavelength) strongly interact with the surface of the canopy (low penetration), while longer wavelengths (e.g. L-band, 23.5-cm wavelength) penetrate further into the canopy and reflect information on branches and stem structure (**Figure 20**). While shorter wavelengths can provide estimations for canopy height, the longer wavelengths are more strongly correlated with forest biomass, structure and other biophysical parameters. The polarization (e.g. HH or horizontal transmit and horizontal receive and HV or horizontal transmit and vertical receive) of the radar (the way the radar is transmitted and received) can reveal moisture content and the geometry of the mangrove canopy.

High resolution X-band SAR datasets that can be purchased include ICEYE SAR[18], TerraSAR-X/TanDEM-X[19] and Capella Space[20] systems. Each SAR system typically has different observation modes, each with a different swath and spatial resolution to address a specific mapping purpose. Radarsat-2 is operated by the Canadian Space Agency and has been operating since 2007, collecting data at a spatial resolution of 3 m in spotlight mode.

Figure 20. *Different radar wavelengths penetrate and record canopy characteristics at different depths of the forest canopy*

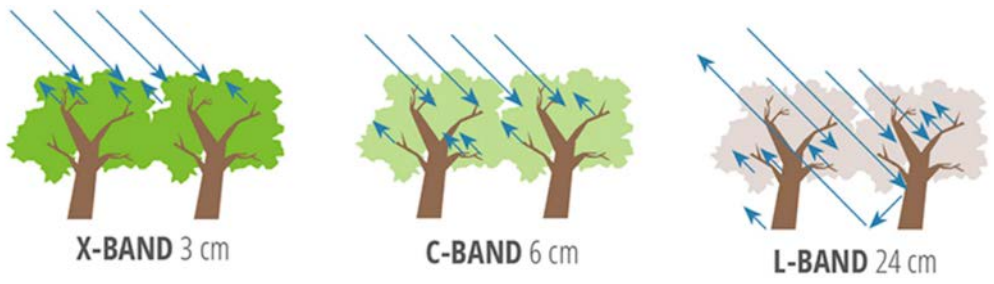

Source: Simard, M. 2019. Radar remote sensing of mangrove forests. In: A. Flores, K. Herndon, R. Thapa & E.. Cherrington, eds. *NASA SAR Handbook: Comprehensive methodologies for forest monitoring and biomass estimation.* NASA. DOI: 10.25966/33zm-x271

[18] www.iceye.com/sar-data
[19] www.intelligence-airbusds.com/en/8694-terrasar-x-tandem-x
[20] www.capellaspace.com

Lower spatial resolution SAR datasets (30 m) available in the public domain include the ESA's Sentinel-1,[21] a medium wavelength C-band (5.6-cm) sensor operated by the ESA and the Japanese Advanced Land Observing Satellite (ALOS PALSAR[22]), a longer L-band sensor that produced 25-m data from 2006 to 2011 and the ALOS-2 PALSAR-2[23] which was launched in 2014 with upgrades and can operate in a 3 m spotlight mode with a 25-km swath.

SAR global products (**Figure 21**) that have been used for estimating tree canopy height and structure include NASADEMHGT,[24] the latest version of the Shuttle Radar Topography Mission (SRTM) data that is a global 30-m C-band-derived DSM product and AW3D30,[25] a DSM derived from the stereo-mapping PRISM sensor on board the Advanced Land Observing Satellite (ALOS). Climate Central's CoastalDEM®[26] is a commercial 30-m global product based on SRTM data which uses machine learning and ICESat-2 LiDAR data to remove vegetation/buildings to create a more accurate "bare earth" digital elevation model. These data are most widely used for coastal flood risk modelling but can also be used as a screening tool to model where mangroves are most likely to grow based on defined elevation ranges (i.e. a habitat suitability model). AGB can be estimated by combining the modelled bare earth product with DSMs.

2.6 LIGHT DETECTION AND RANGING FOR DEFINING MANGROVE HEIGHT AND STRUCTURE

LiDAR is another active remote sensing system that can collect data from space, airplanes, UAS or terrestrial platforms. Unlike SAR that transmits microwave energy, a LiDAR sensor sends thousands of infrared laser pulses and records each individual return in very precise x, y, z coordinates that can be much more accurate than SAR. These LiDAR point clouds can be used to visualize, quantify and classify three-dimensional (3D) vegetation characteristics. However, space-based LiDAR is not well suited for local-scale mapping projects due to the coarse spatial resolution and sensitivity to clouds.

Figure 21. *Comparison of global digital elevation models (AW3D30 and CoastalDEM®) for mangroves in Bajo Yuna National Park, Dominican Republic*

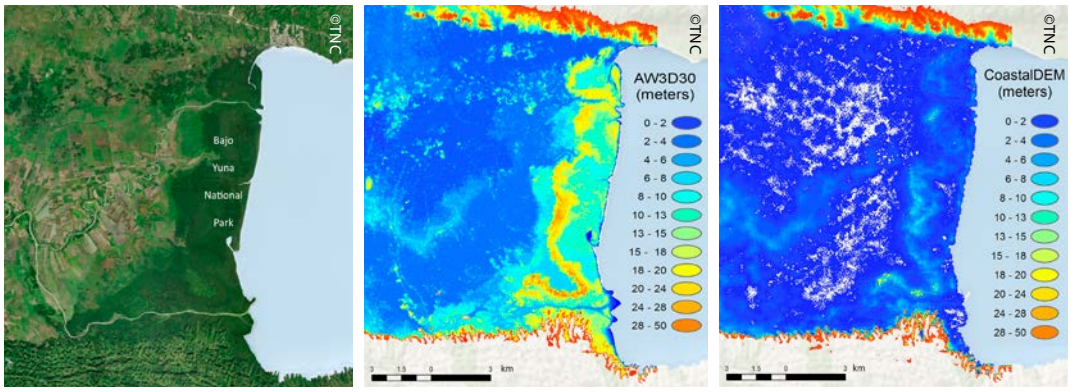

Adapted from: Acosta-Morel, M., McNulty, V.P., Lummen, N., Schill, S.R. & Beck, M.W. 2021. Shoreline solutions: Guiding efficient data selection for coastal risk modelling and the design of adaptation interventions. *Water*, 13(6): 875.

Notes: For assessing mangrove height and canopy structure using SAR, there are several freely available global datasets. Left: The mangrove forest in Bajo Yuna National Park, the Dominican Republic. Centre: The surface elevation as measured by AW3D30, a global 30-m DSM derived from the stereo-mapping PRISM sensor on board ALOS. Right: The CoastalDEM® model representing "bare earth" elevations.

[21] https://sentinels.copernicus.eu/web/sentinel/missions/sentinel-1
[22] https://asf.alaska.edu/data-sets/sar-data-sets/alos-palsar/
[23] www.eorc.jaxa.jp/ALOS-2/en/about/palsar2.htm
[24] https://lpdaac.usgs.gov/products/nasadem_hgtv001/
[25] www.eorc.jaxa.jp/ALOS/en/dataset/aw3d30/aw3d30_e.htm
[26] https://go.climatecentral.org/coastaldem/

Figure 22. *Estimates of mangrove AGB and maximum canopy height in Manglares de Estero Balsa, Dominican Republic*

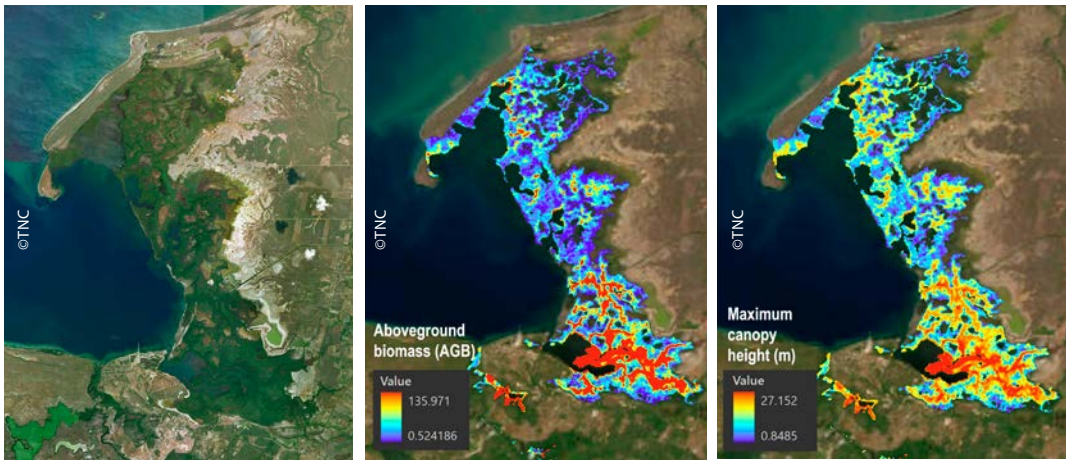

Source: Simard, M., Fatoyinbo, T., Smetanka, C., Rivera-monroy, V.H., Castaneda, E., Thomas, N. & Van der stocken, T. 2019. *Global mangrove distribution, aboveground biomass, and canopy height*. Oak Ridge, Tennessee, USA, ORNL DAAC. doi.org/10.3334/ORNLDAAC/1665

Notes: These data were modelled by Simard *et al.* (2019) and were derived using a 30-m resolution global mangrove ecotype extent map and canopy height measurements from SRTM radar data with LiDAR data from the GLAS on board the ICESat-1 satellite.

LiDAR data are used to capture mangrove forest structure, map individual trees, and predict volume and biomass that can be used to estimate forest carbon stocks. When combined with SAR data, even more accurate mangrove canopy height and structural information can be calculated (**Figure 22**). The University of Maryland has developed a global forest canopy height layer, interpolated from Global Ecosystem Dynamics Investigation[27] (GEDI) data, a full-waveform LiDAR instrument that is operated from the International Space Station and measures the vertical distribution of vegetation by recording the amount of laser energy reflected by plant material (stems, branches and leaves) at different heights above the ground. From GEDI waveforms, four types of structure information can be extracted: surface topography; canopy height metrics; canopy cover metrics; and vertical structure metrics. A global forest canopy height model is freely available from the Global Land Analysis and Discovery (GLAD) laboratory, University of Maryland[28] and in the Google Earth Engine (Potapov *et al*., 2020).

Other global mangrove models (30 m) include: the use of SRTM data to measure canopy height and new mangrove distribution (Aslan and Aljahdali, 2022); and AGB and canopy height models created by integrating SRTM data with LiDAR data from the Geoscience Laser Altimeter System (GLAS), the primary instrument aboard NASA's Ice, Cloud and land Elevation Satellite (ICESat-1) satellite (in orbit from 2003 to 2009) (Simard *et al.*, 2019). In 2018, NASA launched ICESat-2[29] which measures the height of the Earth's surface using multiple laser altimeter beams and satellite LiDAR. Future mangrove products can be improved using LiDAR data from GEDI and ICESat-2 with radar data from the TerraSAR-X that will be calibrated based on field measurement data.

[27] https://gedi.umd.edu/
[28] https://glad.umd.edu/dataset/gedi
[29] https://icesat-2.gsfc.nasa.gov/

2.7 UNCREWED AERIAL SYSTEMS

The advancement of UAS technology and the growing availability of low-cost consumer models provides an emerging monitoring tool for collecting remotely sensed data at a local scale that were previously difficult to acquire. This adaptable "personal remote sensing" platform permits highly customizable and cost-effective data collection on demand (Klemas, 2015), bridging the gap between microscale field measurements and macroscale satellite imagery. Typically flown at altitudes below 120 m, UAS can be rapidly deployed below cloud cover, capturing detailed data using specialized sensors and payloads to map and analyse ecological spatial patterns at custom temporal scales (Joyce, Fickas and Kalamandeen, 2023). Being able to map predetermined areas at precise times offers a distinct advantage for environmental monitoring, such as tracking mangrove restoration success at regular intervals. UAS technology has been used to spatially document and quantitatively track mangrove patterns at multiple levels for investigating vegetation health, estimating biomass, assessing storm damage and detecting deforestation (Navarro *et al.*, 2020; Ayub *et al.*, 2021; Jiang *et al.*, 2021; Zimudzi *et al.*, 2021). Some of the limitations of UAS include inability to map large areas due to battery life and flying altitude/distance constraints, disturbance by rain and wind, and national and local regulations that prevent UAS data collection. Table 4 summarizes the advantages and disadvantages associated with the use of UAS for mangrove mapping.

Before purchasing a UAS, it is important to consider the desired end products (e.g. mangrove extent, biomass, health, change) and match the most appropriate platform and payload sensor based on the project area and budget, as well as the software that will be used to plan the mission to capture the data, then process the data into the end products.

2.7.1 Platforms and sensors

Key considerations in choosing the most appropriate platform include: the spatial extent of the area to be surveyed; conditions and location of operation; and the type of sensor(s) the platform needs to carry to collect the required data. When purchasing an UAS, it is also important to consider the maximum flight time per fully charged battery and maximum radio transmission range (km). Some companies offer protection packages for a limited time that cover any damage to the UAS hull, gimbal or camera sustained during normal use.

Table 4. *Advantages and disadvantages of mapping mangroves using a UAS*

ADVANTAGES	DISADVANTAGES
Cost-effective and easier to deploy than crewed aircraft	Flight limited by battery life and flying altitude which results in mapping of smaller areas only
Quick generation of high-resolution data over a small area – orthophotos and point clouds	Launch area can be limiting
Can be launched on demand as weather permits – below clouds – with minimal staff	Limited by radio connection distance and affected by magnetic deviations
Interchangeable payloads and sensors	Regulations that limit use
Increasing availability of UAS models and software/apps for data collection and processing	Easily affected by weather (e.g. rain, wind)
Continuing advancements in functionality, flight time and payload capabilities	Photogrammetry-derived point cloud limited by canopy
Use of RTK/PPK for precise geolocation	Can cause damage to property and injury to people

Source: Authors' elaborations.

Figure 23. *Examples of a multirotor (left) and a fixed-wing (right) UAS*

Notes: Multirotor UAS are more widely adopted, can be launched from tight spaces, have increased manoeuvrability and easier portability. Fixed-wing UAS are more energy efficient, covering longer distances and mapping larger areas on a single battery.

Table 5. *Advantages of multirotor vs. fixed-wing UAS*

MULTIROTOR	FIXED-WING
Increased manoeuvrability – ability to hover	Longer flight times and ability to cover a much larger area in a single flight
Size and portability for smaller platforms	Increased flight stability in windy conditions
Increased payload capacity for heavy lift multi-rotors (e.g. LiDAR)	Easier to safely land and recover from motor power loss
Generally less expensive	Larger platforms can carry increased payload
More widely adopted with wider selection of models	More suitable for mapping at higher altitudes
Launching and landing in confined places	VTOL UAS can land and take off in more confined spaces
Better camera control – rotation around the x-axis	Ideal for vertical (i.e. nadir) mapping operations

Source: Authors' elaborations.

There are two broad categories of UAS: multirotor and fixed-wing, each having its own advantages and limitations (Figure 23, Table 5).

Multirotor drones are more widely adopted and often less expensive as there are more commercial products. The advantages of this type of UAS include the ability to launch from tight spaces, increased manoeuvrability such as hovering, rotation on its own axis, good camera control (cameras in fixed-wings are not typically mechanically gimballed) and more portability. Some of the limitations include shorter flight times, more moving parts to maintain (or serve as potential fail points), increased noise and smaller payload capacity (unless more expensive and larger heavy-lift multirotor systems are used).

Fixed-wing UAS fly like an airplane and are more energy efficient; they can cover longer distances and map larger areas on a single battery. Due to their larger size, they are more stable in wind and can carry more payload. Some limitations include larger size, low manoeuvrability, higher cost, lack of hovering capacity, less camera control, and the need for larger areas for take-off and landing. New developments in Vertical Take Off and Landing (VTOL) technology have overcome the problem of requiring large open spaces for take-off and landing of fixed-wing UAS.

Table 6 contains a listing of popular UAS platforms for mapping.

Table 6. *Widely used multirotor and fixed-wing UAS and technical specifications*

MAKE	MODEL	PRICE (USD)*	MAX FLIGHT TIME (min)	WEIGHT (Kg)	MAX RANGE (km)	SHUTTER	SENSOR SIZE (inch)	MAX RESO-LUTION (MP)	MAX VIDEO RESO-LUTION (fps)
MULTIROTOR (fixed payload)									
Autel	EVO Max 4T	9 000	42	1.6	20	Electronic	0.8	50	8K/30
Autel	EVO II Pro	3 590	42	1.11	13	Electronic	1	20	6K/30
Autel	EVO Lite+	1 200	40	0.835	12	Electronic	1	20	4K/30
Autel	EVO Nano	825	28	0.249	10	Electronic	1/2	48	4K/30
Autel	EVO Nano+	800	28	0.249	10	Electronic	0.8	50	4K/30
DJI	Mavic 3E	4 000	45	0.915	15	Mechanical	4/3	20	4K/30
DJI	Mavic 3M (Multispectral)	5 000	45	0.951	15	Mechanical Multispectral	4/3	20 G,R, RE,NIR	4K/30
DJI	Air2S	999	31	0.595	12	Electronic	1	20	5.4K/30
DJI	Mini 3**	469	38	0.249	18	Electronic	1/1.3	12	4K/30
DJI	Mini 3 Pro**	759	34	0.249	18	Electronic	1/1.3	48	4K/60
Parrot	Anafi Ai	4 500	32	0.898	4	Electronic	1/2	48	4K/30
Parrot	Anafi USA	7 000	32	0.496	5	Electronic	1/2	21	4K/30
Yuneec	H520E/E90X		25	1.86	7	Electronic	1	20	4K/30
HEAVY-LIFT MULTIROTOR (interchangeable payloads)									
DJI	Inspire 3/ X9-8K Air	16 500	28	4 (can lift 1.3)	15	Mechanical	Full frame	42	8K/75
DJI	Matrice 300 RTK/ Zenmuse H20	17 000	55	6.3 (can lift 2.7)	8	Electronic	1/1.7	20	4K/30
DJI	Matrice 350 RTK /Zen-muse P1	19 000	55	6.5 (can lift 2.7)	20	Mechanical	Full frame	45	4K/60
FIXED-WING									
AgEagle (non- VTOL)	SenseFly eBee X/S.O.D.A.	10 995	90	1.6	8	Mechanical	1	20	N/A
Censys Technologies	Sentaero 5/ Sony A7R IV	95 100	70	10.8	80	Mechanical	Full frame	61	4K/30
Delair	UX11	16 000	59	1.5	53	Mechanical	1	21.4	N/A
Deltaquad	Deltaquad Pro #Map/ Sony A7R IV	24 200	110	6.2	50	Mechanical	Full frame	61	4K/30
Event 38	E400/Sony RX1R II	18 900	90	9	6	Mechanical	Full frame	42	N/A
FIXAR	007/ Sony A7R IV	20 400	59	5	60	Mechanical	Full frame	61	4K/30
Quantum Systems	Trinity Pro/ Sony RX1R II	29 000	90	5.75	7.5	Mechanical	Full frame	42	N/A
Sentera (non- VTOL)	PHX/Double 4K	8 000	59	1.9	3.2	Electronic	1/2.3	12 B,G, R,RE,NIR	N/A
Wingtra	WingtraOne (Gen II)/RGB61	29 900	59	3.7	10	Mechanical	Full frame	61	N/A

*Prices as of December 2023. Heavy-lift multirotors and fixed-wing platforms have interchangeable payloads and may not reflect the listed price.

**For those with limited budgets, these less expensive drones can be used for mapping but may not be compatible with most mission planning apps. These models can be programmed to fly using subscriptions to Dronelink, Map Pilot Pro, or Drone Harmony. Due to their smaller size, the sensors will not provide the same level of detail that more expensive drones can deliver at the same flying altitude. Low-cost post-processing options for creating orthomosaics include OpenDroneMap (local processing) and cloud-based subscriptions to WebODM Lightning or Map Pilot Pro.

Source: Authors' elaborations.

As UAS technology continues to improve, the sensor payload is becoming more compact and sophisticated regarding the data that can be collected. Most consumer UAS come with a built-in optical RGB (visible range) camera. In multirotor versions this primary camera is mounted on a three-axis (tilt, roll, pan) gimbal that provides stability during flight and precise control during data capture. Cameras vary in terms of the size of the sensor, the maximum image resolution (i.e. megapixels), dynamic range and shutter type (i.e. global mechanical vs rolling electronic). The size of the sensor, quality of the lens and the image resolution dictate the spatial resolution achieved at a set flying height. Holding other camera parameters constant (particularly focal length), a 42-megapixel camera flying at a height of 120 m will be able to achieve a similar spatial resolution (1.5 cm/pixel) as a 20-megapixel camera flying at 55 m. When travelling at similar speeds, mapping at the higher altitude would cover almost double the area. A larger detector (e.g. 2.5 cm) will collect imagery of higher quality or fidelity. Image classification can be done using JPEG image format, however, RAW and TIFF formats are uncompressed and produce higher quality images.

The type of shutter will affect the amount and type of distortion in each image. A global mechanical shutter opens and closes at the predefined shutter speed, ensuring that each image on the image sensor is exposed to light at the same time. This helps to minimize distortion compared to a rolling electronic shutter. A rolling electronic shutter, on the other hand, exposes pixels on the image sensor in a line-by-line order so it will introduce distortion effects as it moves forward depending on the rate at which each line is exposed to the scene.

In most modern systems, images are geotagged as they are collected with the location coordinates embedded in the file header. The accuracy of the coordinates is dependent on the quality of the Global Navigation Satellite System (GNSS) receiver in the UAS. Several governments or multinational groups have launched satellite positioning systems, the first of which is maintained by the United States of America and is called the Global Positioning System (GPS). Other systems include GLONASS (the Russian Federation), Galileo (the European Union) and BeiDou (the People's Republic of China). The position reported by a GNSS receiver can be improved to centimetre level when it is corrected using GNSS data collected at a known location called a "base station" (**Figure 24**). This also requires a special receiver installed in the UAS that acts as a "rover" and makes it capable of recording the raw GNSS satellite signals, not just the position of the UAS. When this is done in real time with a data link between the base and the GNSS system in the UAS, it is said to be supplying Real-Time Kinematic (RTK) "live" corrections.

Figure 24. *A GNSS base station collecting position correction data during a UAS mission*

Notes: An Emlid Reach RS2+ multiband GNSS receiver with centimetre precision can be used to collect GCPs or act as a base station for PPK corrections to geotagged UAS images. This is especially critical for change detection of UAS products when pixels need to line up with centimetre accuracy.

When the raw satellite data on the base and rover are stored and then processed after the UAS flight, it is said to provide Post Processed Kinematic (PPK) corrections. The primary advantage of RTK is that the positions are known when they are recorded, and no postprocessing is required. However, it requires a data link between the base and the UAS (e.g. cellular, radio connection). PPK does not require this connection, can be more accurate and will also tolerate a greater distance between the base station and the rover (< 30 km).

If mapping objectives require assessment of mangrove health, a camera capable of recording NIR reflectance is essential. A healthy plant reflects high levels of NIR and as the amount of chlorophyll produced in a plant decreases, less NIR is reflected. The Normalized Difference Vegetation Index (NDVI) equation can be used to detect plant stress by comparing the relationship between reflected intensities of NIR and red light. More information can be found in the vegetation indices section of this manual. There are lower cost NIR camera options that can be mounted on smaller consumer drones, such as those made by MAPIR[30] and Sentera[31] that offer single and multi-sensor cameras and come in a variety of filter transmission options (**Figure 25**). The multirotor DJI Mavic 3 Multispectral has an integrated RGB camera and 4-band multispectral

Figure 25. *Two cost-effective UAS platforms with supplementary infrared sensors attached for assessing mangrove extent and health*

Top row: A Parrot Sequoia multispectral 4-band sensor attached to a DJI Phantom 4 Pr. ***Bottom row:*** a MAPIR Survey 3 NIR camera attached to a DJI Mavic 2 Pro. On each UAS there is a sunshine sensor attached to the top that is used for automatic adjustment of readings to ambient light. Both sensors can be used to compute NDVI used to detect plant stress by comparing the relationship between reflected intensities of NIR and red light.

[30] www.mapir.camera
[31] https://sentera.com

system (Figure 26). More precise and advanced cameras can be operated from fixed-wing and/or heavy-lift multirotors (Figure 27). AgEagle[32] and Agrowing[33] offer a variety of compact options including five multispectral bands (blue, green, red, red-edge and infrared) as well as panchromatic and thermal sensors. Adapted lenses compatible with the Sony A6100 and A7R/4 camera bodies can produce ~ 1.6 cm pixel multispectral imagery flying at 100 m. The DUAL lens (the NDVI and Red-edge) can generate 4 bands at 10 MP and the QUAD lens can generate 12 bands at 12 MP. Many companies offer cloud-based services that use artificial intelligence to automatically detect and identify plant health and diseases based on a variety of vegetation indices.

Figure 26. *A DJI Mavic 3 Multispectral with a 20 MP RGB camera and integrated 4-band multispectral sensors (green, red, red-edge and NIR) for calculating vegetation indices*

Table 7. *Popular multispectral sensors used on fixed-wing and heavy-lift UAS platforms*

	SENSOR	WEIGHT (g)	SPECTRAL BANDS	RGB OUTPUT	GSD AT 120-M FLYING HEIGHT (cm)	PRICE (USD)*
	Sony A7R-IV with QUAD multispectral lens	835	10 narrow bands (405;430;450; 550; 560;570;650; 685;710;850)	12 MP per band Mechanical shutter	1.65	14 500
	Micasense RedEdge P	350	Blue, green, red, red-edge, NIR	5.1 MP per band Mechanical shutter	7.7 (MS) 3.98 (Pan)	10 000
	Micasense Altum PT + DLS 2	406.5	Blue, green, red, red-edge, NIR	3.2 MP per band 12.4 MP (Pan) Mechanical shutter 320 × 256 thermal	5.28 (MS) 33.5 thermal	16 000

*Prices as of December 2023.

Source: Authors' elaborations.

[32] https://ageagle.com
[33] https://agrowing.com

Figure 27. *Two UAS platforms for mapping mangroves*

Top row: A Parrot Sequoia multispectral 4-band sensor attached to a DJI Phantom 4 Pr. ***Bottom row:*** a MAPIR Survey 3 NIR camera attached to a DJI Mavic 2 Pro. On each UAS there is a sunshine sensor attached to the top that is used for automatic adjustment of readings to ambient light. Both sensors can be used to compute NDVI used to detect plant stress by comparing the relationship between reflected intensities of NIR and red light.

2.7.2 Mission planning and data collection

It is important to note that the mission planning takes much longer than the actual flying time. A variety of factors needs to be considered and planned prior to the launch, such as finding a safe launch area, planning for weather and suitable environmental conditions, and having adequate mission approval flying. Data from a UAS can be collected manually or in autonomous mode where the GPS coordinates (i.e. waypoints) of flight lines are uploaded wirelessly and the UAS follows the flight lines, capturing each image at a predetermined overlap setting. When flying in autonomous mode, good planning is the key to collecting accurate data that meet the research objective. This involves the use of a mission planning app where key data collection parameters (such as area boundary with an adequate buffer, camera type and gimbal angle, flying altitude, front and side overlap, and shutter speed) are specified. Most mission planning apps stream high resolution satellite image base maps to enable accurate specification of the mapping area. Some apps even permit the importing of Keyhole Markup Language (KML) files that are designed in Google Earth or GIS vector layers. Flight mission planning will also reveal the amount of time needed to execute the mapping task over the area of interest. Most mission planning apps allow for planning of multiple battery missions within a large area, where the UAS will automatically return to home

Figure 28. *Examples of UAS mission plans and the area mapped at varying flight altitudes*

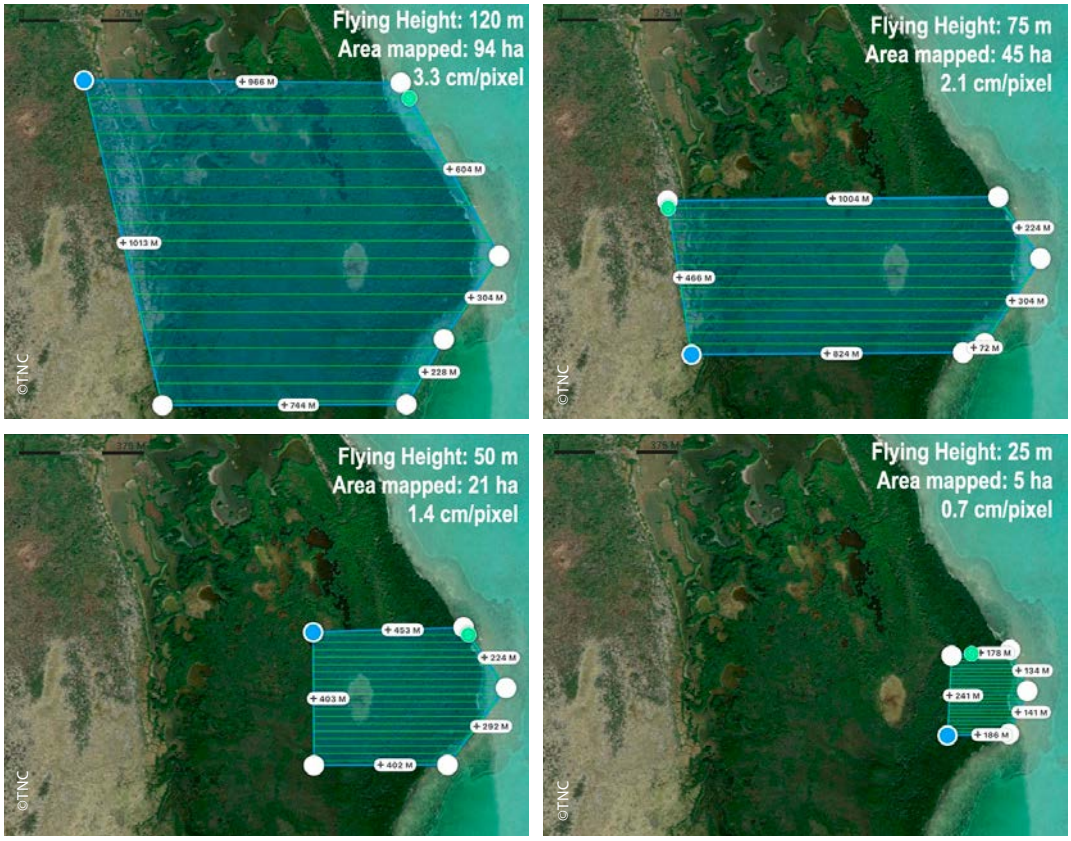

Notes: When planning a UAS mission, the flying height and sensor will dictate the imagery spatial resolution and area that can be mapped. These maps show the spatial extent of single-battery flight missions planned at different flying heights (120 m, 75 m, 50 m and 25 m) using a DJI Phantom 4 Pro. Each mission was planned with 70 percent front overlap and 70 percent sidelap settings and a maximum flying time of 25 minutes.

when battery levels are low. The pilot can then put in a fresh battery and the UAS will return to the last data collection point and resume the mission.

It is best practice to plan flight missions in the office where the area and flight parameters can be carefully assessed and reviewed. This makes field execution much more efficient and timelier. During mission planning, the camera or the sensor to be used need to be specified as this influences the predicted overlap requirements and the calculated spatial resolution (i.e. the GSD). A vertical gimbal angle (i.e. the camera points straight down, 90°) is commonly used, however, more oblique angle settings can be used for capturing the sides of features when a more accurate 3D model needs to be created. More information on UAS best practices is available from the World Wildlife Fund.[34]

In setting the flying height, a balance between the area coverage and the desired spatial resolution needs to be struck. Flying higher will cover more area, but the data will have poorer spatial resolution (**Figure 28**). To determine the appropriate flying height, it is recommended to first acquire test data at varying heights (e.g. 50 m, 75 m, 100 m) under the same environmental and solar conditions to assess the resulting spatial resolution and the ability to discriminate and identify features of interest. Sun angle and weather can have significant influence on the data quality. Ideally, the flight height should be set as high as possible to map a larger area, while still maintaining sufficient spatial resolution.

Specifying adequate forward overlap (along a flight line) and side overlap (between flight lines) is extremely important for the generation of

[34] https://space-science.wwf.de/drones/WWF_CT_Drones_2020_web.pdf

Table 8. *Flying heights and resulting spatial resolution and area mapped using a DJI Phantom Pro v2 using 70 percent front and side overlap*

FLYING HEIGHT (ABOVE-GROUND LEVEL) (m)	SPATIAL RESOLUTION (cm)	AREA MAPPED ON ONE FULLY CHARGED BATTERY (ha)
25	0.7	5
50	1.4	21
75	2.1	45
100	2.7	78
120	3.3	94

Source: Authors' calculated values.

Figure 29. *UAS imagery acquired over mangroves at different times of the day (solar noon and early morning) in Ashton Lagoon, Saint Vincent and the Grenadines*

Notes: Time of day can produce significantly different illumination patterns when acquiring UAS data over mangroves. The imagery on the left was acquired at high solar noon when sun glint on water and sunspots over the canopy was at the highest intensity. The imagery on the right was collected early morning when the sun angle was low to minimize the glint on the water.

high-quality point cloud and orthophoto mosaic. Insufficient overlap will result in data gaps and outputs are likely to have artefacts or errors in image alignment. There should be at least 70 percent forward overlap and side overlap (Table 8). To produce accurate terrain models, a minimum of 80 percent forward overlap and 75 percent side overlap is recommended. Lower flying altitude may require greater percentage overlap (as well as a faster shutter speed), but this depends on the type of sensor used.

Time of day (i.e. sun angle) and tidal cycles are important factors to consider when mapping mangroves. Collecting data within two hours of local solar noon can minimize shadowing, which can significantly affect high resolution multispectral data and cause problems with classification. However, if there is a water surface in the study area, glint may result from the higher sun angles and cause issues with postprocessing. Therefore, flying at high solar noon under sunny conditions should be avoided as this can result in bright sunspots appearing in the data (Figure 29). Data collection during overcast conditions can result in soft, diffuse lighting with minimal shadowing.

Calibrated reflectance panels can be used to create radiometrically calibrated data and should be measured immediately before and after each

Figure 30. *Comparison of UAS images acquired using a fast vs slow shutter speed*

Notes: A slow shutter speed (right) during data capture will result in image motion blur which will affect the image clarity and the ability of the photogrammetry software to recognize features and identify key points. Minimum shutter speeds of at least 1/2 000 (left) are recommended (i.e. shutter priority) with the ISO and aperture set to automatic to adjust to ambient light conditions. The likelihood for image blur is greater with lower flight altitudes (e.g. < 80 m).

mission flight. It is best to avoid capturing data when there are rolling clouds which will intermittently change illumination conditions throughout the flight. Under these conditions, it is best to not set the camera's white balance setting to automatic, as this will cause non-uniform exposures in the data. Instead, set it to cloudy or sunny depending on the prevailing conditions. For optimal data collection, it is recommended to use the fastest shutter speed possible based on light conditions (e.g. 1/2 000 sec) and let the aperture and the ISO float to minimize image blur and facilitate feature detection (**Figure 30**).

When planning missions, it is important to check the airspace restrictions and regulations in the area or the country where the mission will take place. Some countries prohibit drone flights altogether, while others require remote pilot licences and/or permits from the local aviation authority prior to collecting field data. To operate UAS in restricted airspaces, special authorizations (e.g. Low Altitude Authorization and Notification Capability or LAANC) may be required. Many of the mission planning apps will indicate when such authorizations are required and recommend steps to obtain permission. Relevant local and national laws should always be consulted and obeyed, and priority placed on safety.

The mission should be planned based on what detail and spectral information are needed in the data to answer the research question. There are various mission planning apps to choose from along with their supported operating systems and estimated prices (**Table 9**). Examples of a few user interfaces are shown in **Figure 31**. It is important to review the supported platforms and features of each app. Apps, such as Dronelink and Drone Harmony, employ a virtual stick approach and can be used with more affordable drones (e.g. Mavic Mini and Mavic Air series) that previously have not been available for autonomous mapping. All mission planning apps allow for flight missions to be saved, exported and recalled for repeat use, ensuring consistency in data collection between time periods. Some apps have a companion online account that enables synchronization of different devices so that missions can be easily retrieved

Table 9. *Examples of available UAS mission planning apps*

SOFTWARE	OS	PRICE*
Pix4Dcapture Pro	iOS and Android	Free
DJI Pilot 2	iOS and Android	Free
DJI GS Pro	iOS tablets only	Free
DroneDeploy Flight	iOS and Android, desktop	Free, integrated with paid version of postprocessing app
Map Pilot Pro	iOS and Android	Free
PrecisionFlight	iOS and Android	Free
Autel Explorer	iOS and Android for Autel drones	Free
Spexi	iOS and Android	Free
Mission Planner	Windows desktop only for drones using ArduPilot-Pixhawk	Free
Copterus	iOS, supports most DJI drones	USD 5 one time
Litchi	iOS and Android	USD 25 one time
DJIFlightPlanner	iOS and Android	USD 99 one time
dronelink	Windows	USD 50 one time & tiered subscription
drone harmony	Windows	Tiered subscription
UgCS photogrammetry tool	Windows, iOS and Linux	Starting at USD 830
Site Scan for ArcGIS	Windows	Contact Sales

*Prices as of December 2023.

Source: Authors' elaborations.

Figure 31. *User interface examples of mission planning apps include Pix4Dcapture (top left), DroneDeploy Flight (top right), DJI GS Pro (bottom left) and Map Pilot Pro (bottom right)*

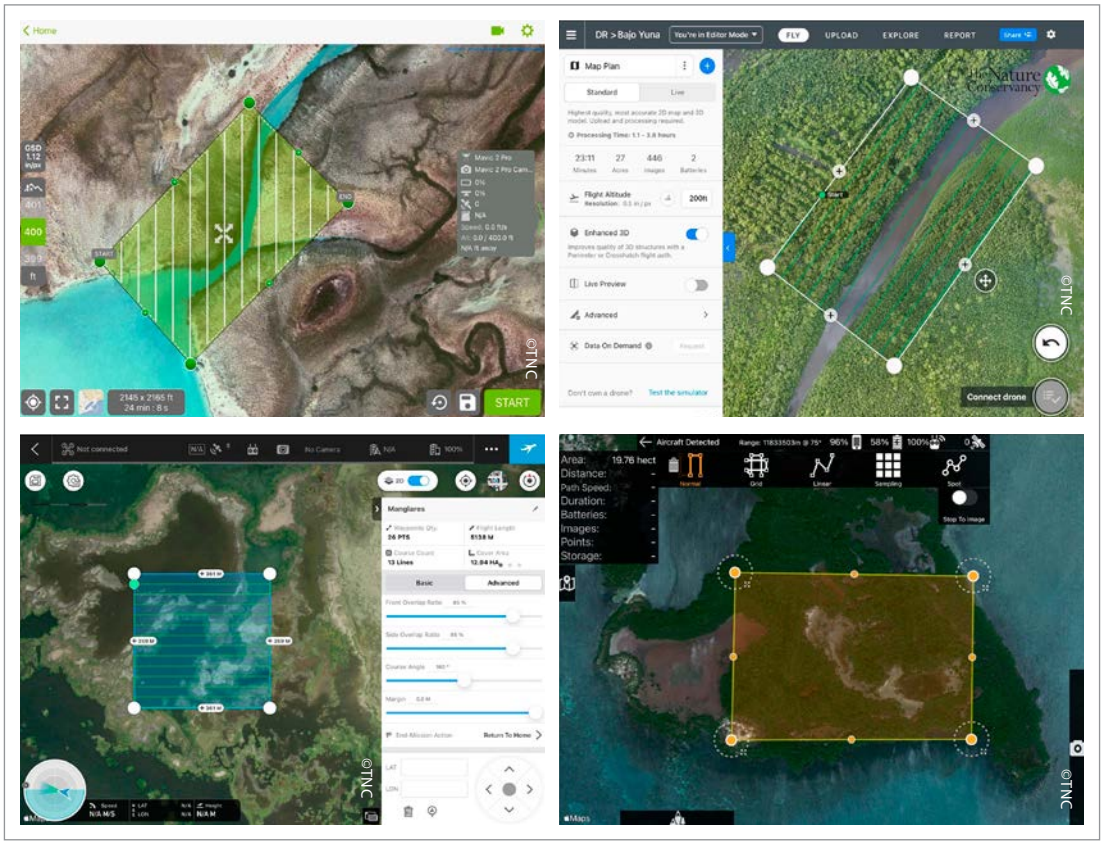

in the field. A few apps (DJI Pilot 2, Map Pilot Pro, DroneDeploy, DroneHarmony) have a feature called "Terrain Awareness" that integrates global elevation products to adjust flightline flying altitude so the UAS maintains sufficient altitude above the terrain and reduces the risk of collision in high topographic areas.

There are several companion apps that can assist in preparing for field data collection. These include: AirMap and AirHub Launch (for reviewing airspace and restrictions); Aloft (LAANC authorization and flight tools); UAV Forecast (weather forecasts specific to remote pilots); Sun Surveyor (planning for sun angles during the missions); Measure Ground Control (drone deployment and management); and GPSdiagnostic (GPS planning tools). There are also some insurance apps such as SkyWatch and Verifly offering protection plans that can be purchased by the hour, month or year with limits up to USD 5 000 000.

2.7.3 Data processing

Once data have been collected in the field and downloaded to a computer, photogrammetry software can be used to process individual images into three primary output products: point clouds, Digital Surface Models (DSMs) and orthophoto mosaics (**Figure 32**). A point cloud is a set of millions of georeferenced points in 3D space that is generated from surface matching and triangulation within overlapping stereo images. The location accuracy of each point is based on the precision of the GPS that was used in the geotagging of the images. A DSM is a georeferenced surface that is created from the point cloud and represents a solid plane connecting all the points. The DSM will represent all features from which the point cloud is generated – trees, buildings and the ground when it is not obscured. The orthophoto mosaic is the final product that is based on the DSM, in which all geometric distortion has been removed from individual images (orthographically corrected) and a seamless GIS-ready mosaic is calculated.

Figure 32. *UAS products of a mangrove area created from 85 overlapping stereo images taken at different perspectives and processed using photogrammetry software*

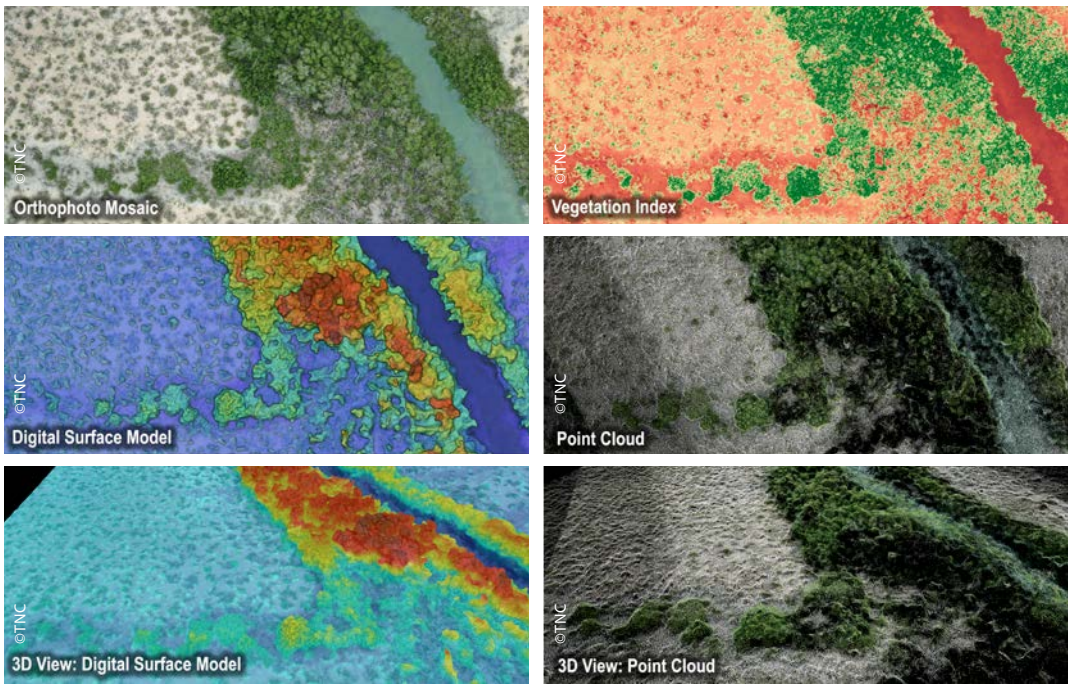

Notes: The resulting orthophoto mosaic was computed to a 1.3 cm pixel based on 4.9 million points generated in the point cloud. The vegetation index shown is the VARI method that estimates presence of vegetation based only on the visible range of the spectrum (i.e. RGB).

Table 10. *Options for postprocessing UAS data into photogrammetric products*

SOFTWARE	OS	PRICE*
COLMAP	Windows, MacOS, Linux	Free – 3D models only
Meshroom	Windows, Linux	Free – 3D models only
openMVG	Windows, MacOS, Linux, Android, iOS (code only)	Free – 3D models only
Regard3D	Windows, MacOS, Linux	Free – 3D models only
VisualSFM	Windows, MacOS, Linux	Free – 3D models only
WebODM	Windows, MacOS, Linux	Free or USD 57 for installer
WebODM Lightning	Cloud-based	Pay as you go, from USD 35/month
MapsMadeEasy	Cloud-based	Pay as you go, from USD 5/month
Photomodeler	Windows	From USD 59/month
Mapware	Cloud-based	From USD 99/month
Agisoft Metashape	Windows, MacOS, Linux	From USD 550 (academic)
PIX4Dmapper	Windows, MacOS, Cloud	From USD 260/month
Simactive Correlator3D	Windows	From USD 295/month
3DFlow Zephyr	Windows	From USD 300/month
SpexiGeo	Cloud-based	From USD 300/month or by credit
DroneDeploy	Cloud-based	From USD 329/month
Autodesk ReCap	Windows	USD 360/year
iWitnessPro	Windows	USD 2 495
Bentley ContextCapture	Windows	From USD 3 647
RealityCapture	Windows	By credit or USD 3 750 unlimited
Skyline – PhotoMesh	Windows or Linux	Call for price
TBC photogrammetry	Windows	Call for price
Mapper UgCS	Windows, MacOS, or Linux	USD 50/month or USD 500/ perpetual
ArcGIS Drone2Map	Windows	Call for price
Site Scan for ArcGIS	Windows	Call for price

*Prices as of December 2023.
Source: Authors' elaborations.

There are desktop and cloud-based options available for photogrammetry software. Desktop software provides the user with more control of the output and the ability to customize more parameters. However, it requires a robust workstation to process the huge amount of data that is generated. This option is best for remote areas with slow internet access. Cloud-based options have a simpler interface, can produce results faster (provided that there is a fast internet connection) and enable team collaboration through web-sharing of products.

Some of the widely used photogrammetric software packages are listed in **Table 10** with their system operating requirements and pricing. Several free options are available, however they might not create an orthophoto mosaic. The more expensive options offer trial periods for users to experiment with and test the software. It is up to the users to evaluate the workflow and orthophoto mosaic generation process to determine which one best meets their needs based on budget, accuracy requirement and skill level.

Of the low-cost options, WebODM (Open Drone Map) is a popular open-source drone mapping app that has been improving over the years as it is maintained by a large community of software developers. The software allows for creation of diverse types of maps from JPEG and TIFF images and processes multispectral images to calculate different vegetation indexes. WebODM Lightning is a cloud-based version and offers a Pay As You Go option as well as a Pro option for USD 35/month for unlimited maps and 100 GB of cloud space.

The postprocessing workflow starts with the orientation and alignment of all images using the exchangeable image file format (EXIF) header, geo-tagged image information and advanced bundle block adjustment. Next, an algorithm searches for and matches millions of points (i.e. key points) between overlapping images and calculates each point's 3D coordinates. The resulting dense point cloud is then used to create a 3D polygonal mesh model and DSM. Finally, the software uses the DSM to project every pixel and generate the orthophoto mosaic which is a planimetrically correct image with all geometric distortions removed. The geometric correction Root Mean Square Error (RMSE) is reported in both horizonal and vertical dimensions. A rayCloud feature can be used to visually assess the quality of the reconstruction showing the GPS-derived position of the cameras (**Figure 33**).

The collection of UAS stereo images from both vertical and varying oblique angles can be used to create a realistic 3D model of a mangrove forest which can be useful for estimating above-ground

Figure 33. *The rayCloud camera positions showing the location where each stereo image was taken*

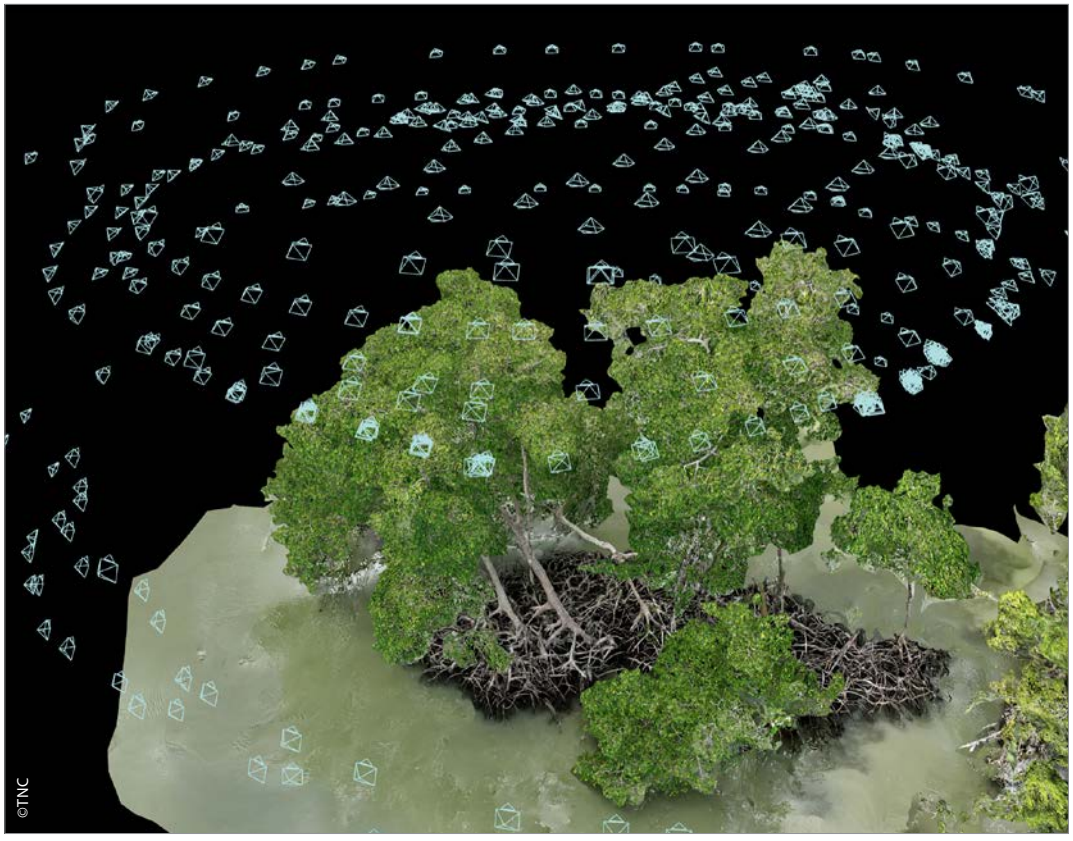

Notes: Using photogrammetry software, data can be assessed and interpreted using the rays connecting the 3D point cloud to the original input images.

Figure 34. *Comparison of the original image of a mangrove and a 3D point cloud[35] generated from stereo images using Agisoft Metashape photogrammetry software*

biomass and carbon storage (**Figure 34**). When acquiring these data, it is important to avoid having the sky in the images which can confuse the photogrammetric algorithm. Point clouds may have spurious artefacts that can be manually cleaned up using tools available in certain software (e.g. Metashape, Pix4D). Without high precision geometric correction (either RTK or PPK), geometric accuracy of the resulting orthophoto mosaic using the onboard GPS is typically between 3 cm to 6 cm horizontal (depending on the UAS model used). When conducting change detection between images collected at different times, it is important to align the pixels using RTK or PPK methods or by using GCPs based on accuracy requirements (usually centimetre level). If the processing of the orthophoto mosaic fails, it is typically the result of low key point generation between overlapping images. This can be due to insufficient overlap, a homogeneous environment or poor image quality, such as image blur (due to slow shutter speed). Following data processing, a quality report is typically generated by the software providing product details including output GSD, total area mapped, median shutter speed, geometric accuracy (i.e. RMSE), points generated in the point cloud, and the percent of images that are aligned (i.e. good stereo coverage vs poor coverage). For sharing data, point clouds and DSMs can be uploaded to OpenTopography.org and orthophoto mosaics to OpenAerialMap.org.

[35] https://tnc.app.box.com/s/3zv56y84042wdjrnya37yusk1532mt54

©TNC

3. MANGROVE MAPPING TECHNIQUES

3.1 VISUAL INTERPRETATION METHOD

The simplest method of mapping mangrove forests is to digitize the boundaries using head-up manual techniques based on visual interpretation of high spatial resolution imagery (< 5 m pixel) coupled with fieldwork and local knowledge. In order to successfully recognize a mangrove forest, the image analyst must consider a variety of image interpretation elements such as the forest canopy's tone and colour, size, shape, texture, location and situation. Mangroves require specific biophysical conditions to establish and grow (e.g. elevation, salinity, nutrient requirements) so recognizing where these conditions are likely to occur is critical for successfully identifying and mapping their location. This method is labour-intensive, highly subjective to the digitizer and subject to human error. As such, field accuracy assessments and review through local knowledge are important. Having imagery with sufficient spatial resolution and access to infrared bands also facilitates the recognition of mangrove presence or absence.

There are free GIS resources that can digitize polygon features using a georeferenced image base map (**Figure 35**). Open-source solutions, such as Quantum GIS[36] (QGIS) software, provide open access to stream-archived high resolution image basemaps maps, such as those available in Google Earth and Microsoft Bing aerial imagery.

Figure 35. *Example of mangrove digitization in QGIS with multiple basemaps*

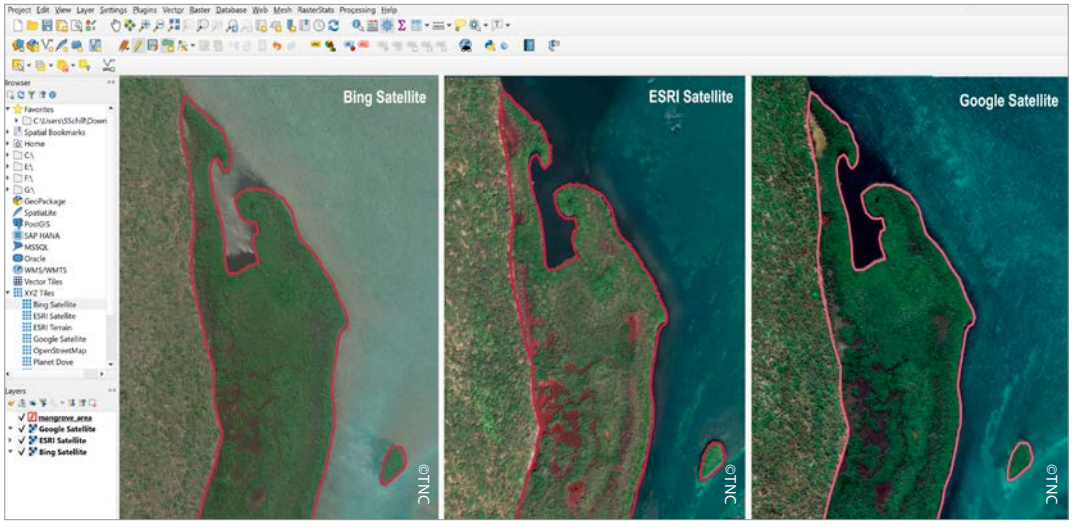

Notes: Mangrove extent can be digitized using open-source GIS software such as QGIS that permits users to stream high resolution satellite image basemaps for free. Figure 35 shows three satellite basemaps of different satellites and collection periods pulled from satellite archives. It is important to check each basemap to determine the optimal imagery to digitize from.

[36] www.qgis.org/en/site
[37] https://livingatlas.arcgis.com/wayback/
[38] www.planet.com/stories

In the desktop version of Google Earth, historical imagery going back to the early 2000s is available using the *Timeline* tool. Using Google Earth, polygons can be digitized in KML format, then imported into GIS for further analysis (**Figure 36** and **Figure 37**).

Other sources for older imagery include Esri's World Imagery Wayback[37] tool and Planet's Stories[38] with which users can build custom image change animations for anywhere in the world going back to 2015.

Figure 36. *Tracking the impacts of marina development on a mangrove forest in Playa de Maimon, Dominican Republic using the timeline tool in Google Earth*

Figure 37. *Tracking the change in mangrove forests at the mouth of the Barracote River in Bajo Yuna National Park, Dominican Republic using the timeline tool in Google Earth*

3.2. AUTOMATED CLASSIFICATION METHOD

Automated methods for mapping mangroves require specialized image processing software that uses pixel and object-based classification algorithms. Pixel-based means each pixel is assigned to a class while object-based uses groups of pixels that have similar spectral values and are classified together (**Figure 38**). These methods can be much less labour-intensive than manual digitization, but require quality imagery, adequate field data and technical expertise. Classifications can be informed and improved using additional GIS data layers on related ecosystem components (e.g. soil, elevation) and field data. When collecting field data, GPS-referenced terrestrial and/or aerial UAS images or videos of habitats can help identify different types of mangroves and the transition boundaries to other habitat types. UAS images and videos along strategically placed transects can be particularly useful in spatially documenting complex mangrove growth patterns and distinguishing mangroves from neighbouring (often spectrally similar) forest types. Spatial patterns of mangroves vary greatly between regions and even between neighbouring countries, so field data and local knowledge are crucial for informing localized mangrove classifications.

Automated pixel-based classification can be performed using QGIS which runs on Linux, Unix, Mac OSX, Windows and Android operating systems. The latest stable version and the required packages and plugins should be downloaded and used.[39] There are numerous tutorials[40] on how to classify imagery using open-source software. Prior to conducting the classification, the user will need to determine which and how many classes there will be. This decision should be determined by the research question, available data and resources. In a *supervised* classification, the user selects representative *training data* from the image for each class on which the classification is based. These training data should represent the full variation that exists within each class. They are also

Figure 38. *Segmenting a satellite image means creating objects around pixels that have similar spectral properties and reflectance values*

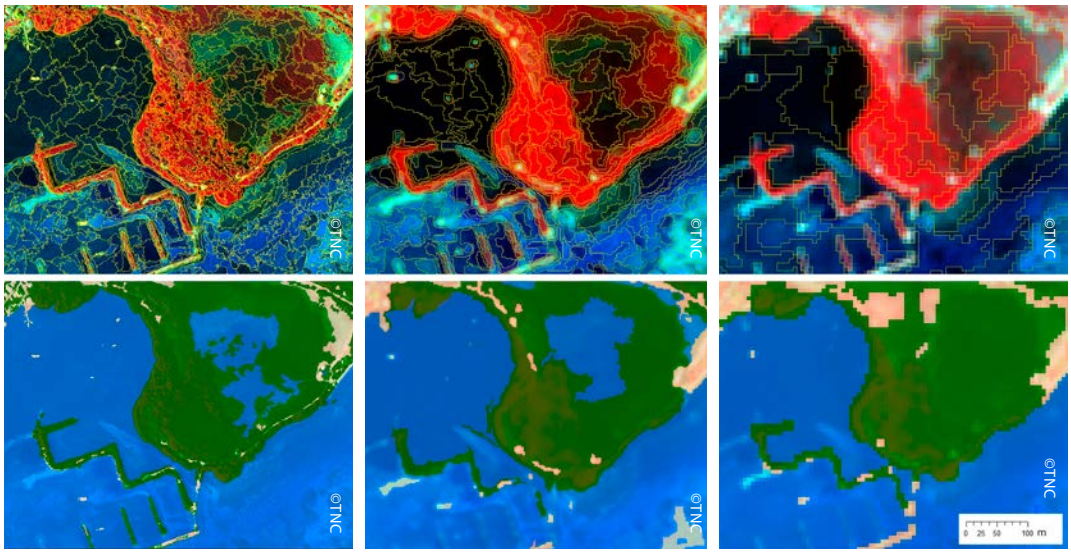

Notes: The scale of the objects can be specified to make them larger or smaller, depending on the mapping objecive. Object-based classification means it is the objects, not the individual pixels, that are being classified. These results show the same scale of objects applied to three different satellite images with different spatial resolutions over mangroves in Ashton Lagoon, Saint Vincent and the Grenadines (from left to right): SkySat (0.5 m), PlanetScope SuperDove (4 m) and Sentinel-2 (10 m). Beneath are the results of a simple three class classification applied to the objects. As the pixel size increases, the segments become coarser and the detail of the classification becomes less clear.

[39] https://plugins.qgis.org/
[40] https://servirglobal.net/Portals/0/Documents/Articles/ChangeDetectionTraining/Module3_LC_Classification_Accuracy_Assessment.pdf

used in the classification algorithm to learn the spectral patterns for each class and establish the rules upon which each pixel will be assigned to a class. *Unsupervised* classification does not require training data and automatically assigns pixels to a statistically defined spectral cluster based on their shared spectral signatures. It is then up to the user to determine what each of the clusters represents in terms of land cover class.

There are various image classification algorithms and each one has its advantages. The popular Random Forest algorithm mines the input data, then builds and operates on complex decision trees to assign each pixel to a class. Support Machine Vector works best with highly complex imagery and K-Nearest Neighbors (KNN) performs well with noisy training data. Finally, Convolution Neural Network and Deep Learning methods, which are quickly emerging, utilize libraries of specimen training labels of mangrove variations and assign classes based on recognized learned patterns, both spectral and contextual. QGIS has several classification plugins such as the Semi-Automatic Classification plugin[41] and other Deep Learning plugins[42] that can be used to classify imagery. In addition, the Orfeo ToolBox[43] (OTB) is an open-source software library for processing imagery and operates within the QGIS interface. A user can perform pixel-based or object-based classification using the OTB. Whatever classification method is used, it is important to refine outputs with manual corrections and conduct an accuracy assessment (in field or expert review) when available resources permit.

[41] https://plugins.qgis.org/plugins/SemiAutomaticClassificationPlugin/
[42] https://plugins.qgis.org/plugins/tags/deep-learning/
[43] www.orfeo-toolbox.org

3.3 REMOTE SENSING-DERIVED INDICATORS AND METHODS FOR FEATURE EXTRACTION

3.3.1 Vegetation indices

The spectral resolution of a remote sensing system dictates the segments of the electromagnetic spectrum that are recorded in spectral bands, such as red, green, blue, NIR and SWIR. These individual spectral bands can be used as inputs in vegetation indices (VIs) to highlight a particular property of vegetation. VIs are derived using the reflectance properties of vegetation and each one is designed to accentuate a particular vegetation property. Some of the more common VIs that are used to reliably extract vegetation pixels from non-vegetation pixels include the Normalized Difference Vegetation Index (NDVI), the Ratio Vegetation Index (RVI), the Enhanced Vegetation Index (EVI) and the Soil-Adjusted Vegetation Index (SAVI). VIs based on RGB bands include the Triangular Greenness Index (TGI), the Visible Atmospherically Resistant Index (VARI) and the Excess Green Index (ExGI) (**Table 11**). TGI is more effective in separating the vegetation from water than VARI and ExGI slightly outperformed other indices in discriminating vegetation cover.

Specialized VIs have been developed to distinguish mangroves from non-mangrove vegetation (Ali and Nayyar, 2020). These include the Combined Mangrove Recognition Index (CMRI), the Normalized Difference Mangrove Index (NDMI), the Landsat 8 Mangrove Index (L8MI) and the Mangrove Vegetation Index (MVI). CMRI distinguishes mangroves using NDVI and the Normalized Difference Water Index (NDWI) that are negatively correlated and are used to help separate mangroves from other vegetation.

Table 11. *Common vegetation indices and their corresponding formulas*

VEGETATION INDEX	FORMULA
Normalized Difference Vegetation Index (NDVI)	(NIR – Red)/(NIR + Red)
Ratio Vegetation Index (RVI)	NIR/Red
Enhanced Vegetation Index (EVI)	2.5*((NIR – Red)/(NIR +6 * Red-7.5*Blue+1))
Soil-Adjusted Vegetation Index (SAVI)	((NIR – R)/(NIR + R + L)) * (1 + L) *soil brightness correction factor (L) defined as 0.*
Triangular Greenness Index (TGI)	GREEN-(0.39*RED)-(0.61*BLUE)
Visible Atmospherically Resistant Index (VARI)	$\frac{\text{GREEN-RED}}{\text{GREEN+RED-BLUE}}$
Excess Green Index (ExGI)	2 * GREEN – (RED + BLUE)
Combined Mangrove Recognition Index (CMRI)	NDVI – NDWI *where NDWI = (Green – NIR)/(Green + NIR)*
Normalized Difference Mangrove Index (NDMI)	(SWIR2 – Green)/(SWIR2 + Green)
Landsat 8 Mangrove Index (L8MI)	L8MI1 = [ASST1 >T21] and SAVI > T1 L8MI2 = [ASST2 > T22] and SAVI > T1
Mangrove Vegetation Index (MVI)	|NIR – Green|/|SWIR – Green|

Sources: Ali, A. & Nayyar, Z.A. 2020. Extraction of mangrove forest through Landsat 8 Mangrove Index (L8MI). *Arabian Journal of Geosciences*, 13(21): 1–12; Baloloy, A.B., Blanco, A.C., Ana, R.R.C.S. & Nadaoka, K. 2020. Development and application of a new mangrove vegetation index (MVI) for rapid and accurate mangrove mapping. *ISPRS Journal of Photogrammetry and Remote Sensing*, 166: 95–117; Barr, J.R., Green, M.C., DeMaso, S.J. & Hardy, T.B. 2018. Detectability and visibility biases associated with using a consumer-grade unmanned aircraft to survey nesting colonial waterbirds. *Journal of Field Ornithology*, 2018, 89: 242–257; Boon, M.A., Drijfhout, A.P. & Tesfamichael, S. 2017. Comparison of a fixed wing and multirotor UAV for environmental mapping applications: A case study. *The International Archives of the Photogrammetry, Remote Sensing and Spatial Information Sciences*, 2017, XLII-2/W6, 47–54; Gupta, K., Mukhopadhyay, A., Giri, S., Chanda, A., Majumdar, S.D., Samanta, S., Mitra, D., Samal, R.N., Pattnaik, A.K. & Hazra, S. 2018. An index for discrimination of mangroves from non-mangroves using LANDSAT 8 OLI imagery. *MethodsX*, 5: 1129–1139; Huete, R.A. 1988. A soil-adjusted vegetation index (SAVI). Remote Sensing Environment, 25(3): 295–309; Jordan, C.F. 1969. Derivation of leaf-area index from quality of light on the forest floor. *Ecology*, 50(4): 663–666; McFeeters, S.K. 1996. The use of the Normalized Difference Water Index (NDWI) in the delineation of open water features. *International Journal of Remote Sensing*, 17(7): 1425–1432; Ramsey III, E.W. & Jensen, J.R. 1996. Remote sensing of mangrove wetlands: relating canopy spectra to site-specific data; Rouse, J.W. Jr., Hasas, R.H., Schell, J.A. & Deering, D.W. 1973. *Monitoring the vernal advancement and retrogradation (green wave effect) of natural vegetation*. Remote Sensing Center, Texas A&M University, College Station; Shi, T., Liu, J., Hu, Z., Liu, H., Wang, J. & Wu, G. 2016. New spectral metrics for mangrove forest identification. *Remote Sensing Letters*, 7(9): 885–894.

NDMI extracts mangrove forest pixels with some inclusion of barren land pixels. NDMI takes advantage of the decreased reflectance of SWIR in mangrove forests and the increase in reflectance of the green band in mangrove forests that naturally grow denser. This index has shown success in identifying forest disturbance and recovery in terms of water stress. MVI discriminates the distinct greenness and moisture of mangroves from other vegetation utilizing three Sentinel-2 bands (Green, NIR and SWIR1) with high accuracy. The NIR-Green relationship captures the difference of greenness between mangrove forests and other trees, while the SWIR-Green relationship identifies the distinct moisture of mangroves without the need for additional water indices. In comparison with other vegetation indices, MVI values are high for mangrove vegetation only and can be utilized as a single input for index-based mangrove mapping (Ali and Nayyar, 2020).

3.3.2 Change detection using Normalized Difference Vegetation Index

It is important to monitor changes in mangrove biomass to recognize where mangroves are under stress and where mangroves are growing. Such information can guide restoration planning and mitigation of threats.

Biomass can be monitored through change analyses of various vegetation indices, most commonly NDVI. NDVI is a normalized ratio of red and NIR spectral reflectance and is one of the most widely used vegetation indices. NDVI is determined by the degree of absorption by chlorophyll in the red wavelengths, which is proportional to leaf chlorophyll density, and by the reflectance of NIR radiation, which is proportional to green leaf density and serves as a proxy of vegetation productivity. Therefore, NDVI can be used as a surrogate to help evaluate the health status of mangroves. **Figure 39** shows how NDVI can be used to monitor the recovery of mangroves following a hurricane.

Figure 39. *Using a DJI M300RTK multirotor UAS with a Micasense RedEdge MX to capture and compute NDVI to track mangrove recovery following a hurricane*

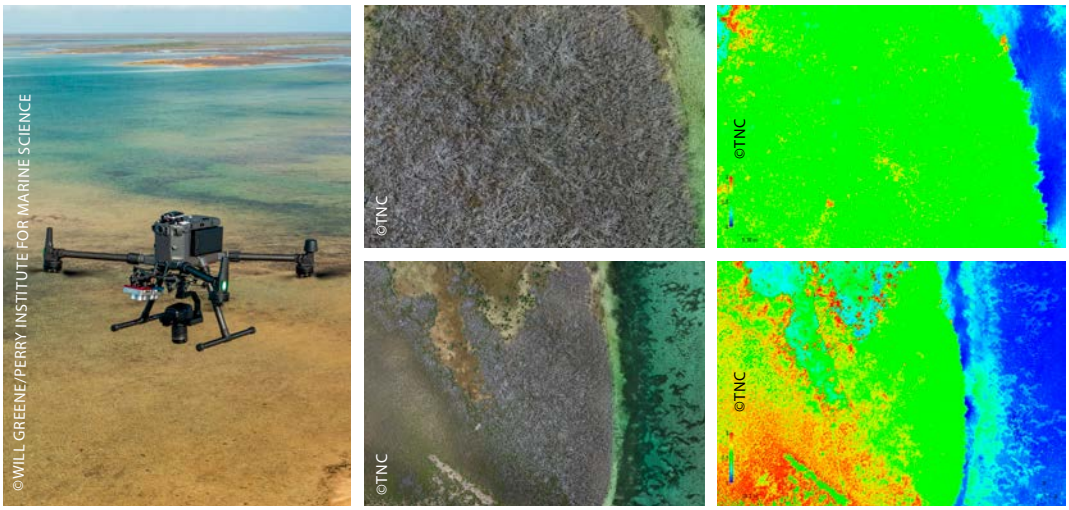

Left: A DJI M300RTK multirotor UAS with a dual-sensor payload consisting of a DJI P1 full frame camera (RGB) and a Micasense RedEdge MX Dual (10-band multispectral system). This setup allows for pixel-aligned outputs with centimetre-level accuracy and coverage up of to 81 ha on a single battery. Flown at 120 m, it provides 1.5 cm RGB and 8 cm calibrated multispectral imagery. ***Centre:*** Hurricane-damaged red mangroves in the Bahamas depicted with this system. ***Right:*** Computed NDVI values provide spatial investigations into mangrove recovery. The red and orange hues indicate regrowth while the greens and blues signal no photosynthesizing activity. The top half shows the ability of the system to pick up individual surviving plants, while the bottom shows broader spatial mortality patterns that are difficult to distinguish with visual data alone.

Figure 40. *TNC's Blue Carbon Explorer showing an example of NDVI change analysis in eastern Grand Bahama between 2015 and 2021 using Planet NICFI Dove imagery*

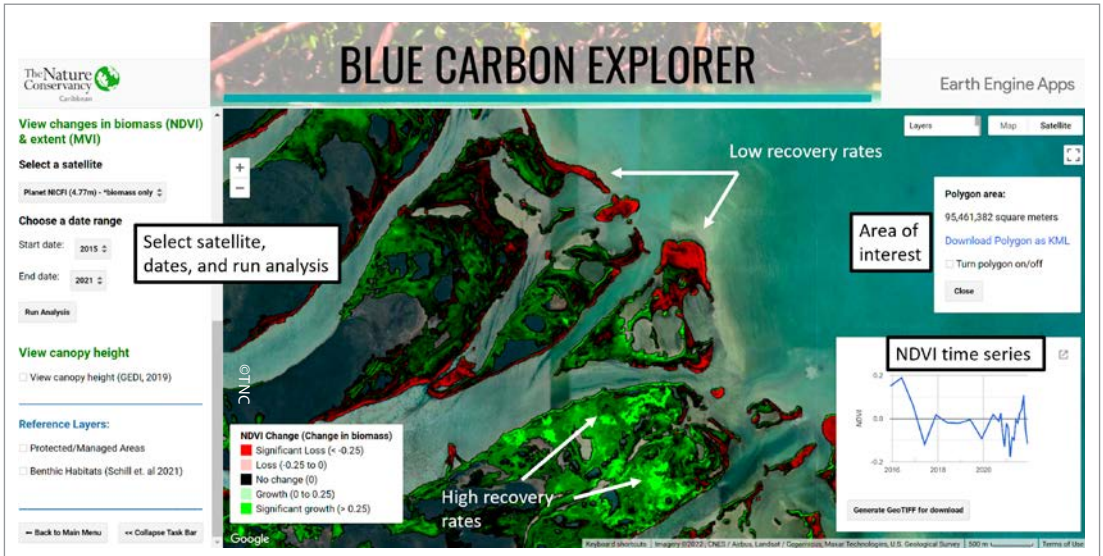

Notes: Hurricane Dorian ravaged mangroves in Grand Bahama and Abaco Island in the Bahamas in 2019. Using the Blue Carbon Explorer, these results show levels of recovery based on NDVI (areas in red indicate loss and green indicate recovery) and temporally through an NDVI time series chart. These types of data can be used to detect where reforestation efforts are needed.

Change in biomass can be monitored by analysing differences in NDVI across time periods, both spatially through change maps and temporally through NDVI time series (as shown in TNC's Blue Carbon Explorer) (**Figure 40**). This type of analysis requires a mangrove spatial footprint (vector layer) to which NDVI analysis can be clipped, showing growth and loss of biomass within the footprint of a mangrove area. The varying levels of NDVI values can be used to investigate changes in mangrove health, biomass, extent, and seasonal change.

Figure 41. *Examples of using natural colour (RGB) UAS imagery to calculate VARI to inform mangrove change detection in Bajo Yuna National Park, Dominican Republic*

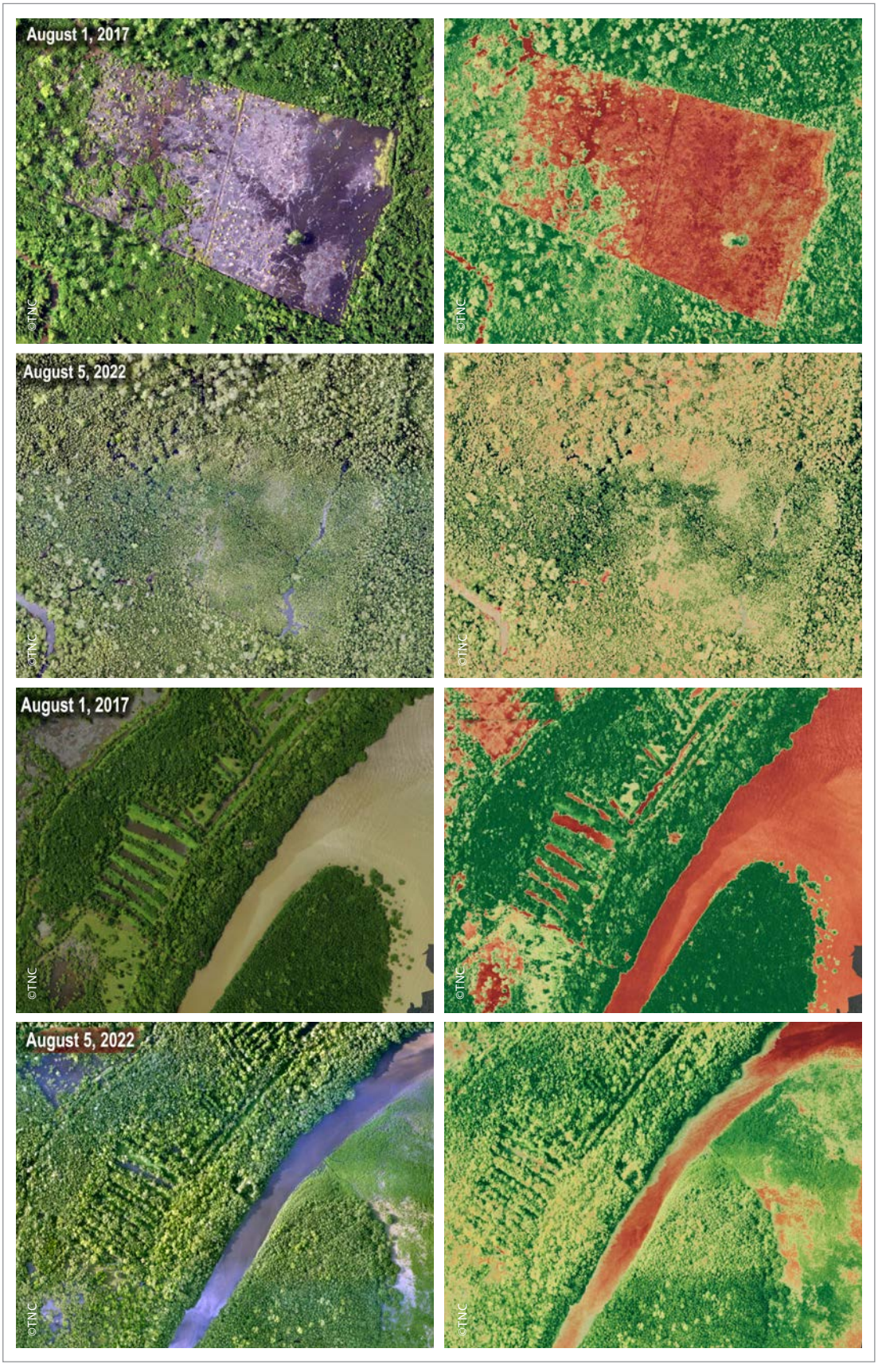

Analysis of NDVI change can highlight areas and the timing of die-off events that allow for further investigation of events such as hurricanes or deforestation with resultant mangrove loss. A study completed on Abaco, the Bahamas, showed little evidence of a relationship between NDVI and hurricanes or drought events, but found that leaf-eating herbivores likely facilitated the spread of disease, contributing to the dieback (Rossi *et al.*, 2020). These indices can also be used to track the recovery of restoration actions or natural expansion in areas such as river deltas (**Figure 41**). Seasonality in mangrove biomass is apparent in NDVI, EVI and NDWI analyses, where greenness is negatively correlated with litterfall (Pastor-Guzman, Dash and Atkinson, 2018). As such, it is recommended to compare NDVI using an annual average to understand long-term trends, or before and after specific events for spot damage assessments.

3.3.3 Change detection using other indices

Beyond NDVI, EVI has also been found to be useful in detecting changes in mangrove cover both seasonally and long term, particularly in large ecosystems (Berlanga-Robles and Ruiz-Luna, 2020). The Modified Soil-Adjusted Vegetation Index (MSAVI) and Normalized Difference Moisture Index (NDMA) can also be used as proxies for plant biomass (**Table 12**). In an analysis of NDVI, EVI, MSAVI and NDMA by Aljahdali, Munawar and Khan (2021), MSAVI performed best in capturing various trend patterns related to greenness to vegetation, and NDMI better identified forest disturbance and recovery in terms of water stress.

Vegetation health can be assessed at a larger scale via analyses of various environmental indicators, such as the Mangrove Quality Index (MQI) developed by Faridah-Hanum *et al.* (2019) which considers contributing components of a mangrove forest, including the soil, surrounding marine ecosystem, hydrology and the socio-economic variables. While field measurements such as DBH, canopy closure and canopy density are extremely valuable for monitoring mangrove health and biomass at the site level, MQI can be used to scale up monitoring efforts while reducing human resources, time and cost (Faridah-Hanum *et al.*, 2019). Analysis of environmental indicators or pressures can also help identify drivers of change. Maina *et al.* (2021) found that catchment erosion, human pressure, sea level and macroclimate are the main drivers of the present-day ecological condition of mangroves, and that NDVI was more sensitive to these drivers than vegetation condition index (VCI). Changes in area, or extent, of mangroves require derivation of the mangrove footprint (vector layer) at various points in time. This can be done using CMRI, L8MI, NDMI or MVI as already discussed.

Table 12. *Formulas for MSAVI and NDMA both useful for detecting changes in mangrove forests*

INDEX	FORMULAS
MSAVI	$(2 * NIR + 1 - sqrt((2 * NIR + 1)^2 - 8*(NIR - Red))/2$
NDMA	(NIR – SWIR1)/(NIR + SWIR1)

Source: Authors' elaborations.

©TNC

4. ONLINE RESOURCES FOR MANGROVE MAPPING

There are numerous published datasets for historical mangrove coverage, with the earliest starting in 2000. Table 13 provides a directory of online resources for mangrove maps and tools while Table 14 summarizes mangrove data covering habitat maps, biological characteristics such as mangrove height and biomass, as well as ecosystem services, such as coastal protection, tourism and blue carbon storage.

Table 13. *Directory of online resources for mangrove maps and tools*

APPLICATION	MAPS AND TOOLS	RESOLUTION (m)	GEOGRAPHIES	URLS
Ready-to-use maps	TNC Blue Carbon Explorer	1 and 4	TNC has mapped mangroves at regional and national scales at 1 m and 4 m resolution	https://BlueCarbon.tnc.org
	Global Mangrove Watch	~25 (0.8 arc seconds)	Global	www.globalmangrovewatch.org
	UNEP-WCMC Ocean Data Viewer	Various mangrove datasets	Global	https://data.unep-wcmc.org/
	WorldCover	10	Global	https://worldcover2021.esa.int/
Imagery sources	Planet NICFI	4.77	The four-band mosaics cover most tropical forested regions of the world	www.planet.com/nicfi
	EarthExplorer	Various datasets	USA & global datasets	https://earthexplorer.usgs.gov/
Analysis	QGIS	N/A	N/A	www.qgis.org/en/site
	Orfeo ToolBox	N/A	N/A	www.orfeo-toolbox.org
	Google Earth Engine	Various datasets	Global	https://earthengine.google.com/
Ecosystem service tools	Blue Carbon Explorer	4.77 (Planet NICFI), 10 (Sentinel-2), and 30 (Landsat-7 and Landsat-8)	Caribbean, Indonesia, and Papua New Guinea (as of April 2023)	https://BlueCarbon.tnc.org
	Mapping Ocean Wealth	Varies	Global	https://maps.oceanwealth.org/
	InVEST	Flexible, can be used at local, regional or global scales	Global	https://naturalcapitalproject.stanford.edu/software/invest

Adapted from: Worthington, T.A., Andradi-Brown, D.A., Bhargava, R., Buelow, C., Bunting, P., Duncan, C., Fatoyinbo, L., Friess, D.A., Goldberg, L., Hilarides, L. & Lagomasino, D. 2020. Harnessing big data to support the conservation and rehabilitation of mangrove forests globally. *One Earth*, 2(5): 429–443.

Table 14. *List of mangrove datasets*

DATASETS	DESCRIPTION	NOMINAL YEAR	RESOLUTION	MANGROVE EXTENT USED	DOWNLOAD OR VIEWER	REFERENCES
Mangrove extent and change	Composite extent map using remote-sensing and visual-interpretation approaches	1999–2003	–	–	https://data.unep-wcmc.org/datasets/5	Spalding, Kainumu and Collins (2010)
	First globally consistent remote-sensing-based map of mangrove extent	2000	30 m	–	https://data.unep-wcmc.org/datasets/4	Giri *et al.* (2011)
	Giri *et al.* (2011) dataset refined by the removal of areas above an elevation threshold	2000	–	Giri *et al.* (2011)		Tang *et al.* (2018)
	Global analyses of mangrove deforestation based on the Global Forest Cover dataset	Annual 2000–2012	30 m	–	http://faculty.salisbury.edu/sehamilton/mangroves	Hamilton and Casey (2016)
	Most current global analysis of extent captures both losses and gains over a 20-year period	1996, 2007–2010, 2015–2020	25 m	–	https://data.unep-wcmc.org/datasets/45	Bunting *et al.* (2018)
Mangrove biomass	Climate-driven model of potential mangrove AGB	–	–	Spalding, Kainumu and Collins (2010)		Hutchison *et al.* (2014)
Mangrove height and biomass	Canopy height maps based on a digital elevation model and LiDAR altimetry	2000	30 m	Giri *et al.* (2011)	https://doi.org/10.3334/ORNLDAAC/1665	Simard *et al.* (2019)
	Canopy height maps based on a digital elevation model; biomass derived from global allometric model	2000	–	Giri *et al.* (2011)		Tang *et al.* (2018)
Freshwater and sediment impact on mangrove condition	Changes in mangrove extent are modelled against human alteration to free-flowing rivers	–	–	Bunting *et al.* (2018)		Maynard *et al.* (2019)
Mangrove fragmentation	Global analyses of the change in fragmentation metrics over time	Annual 2000–2012	0.2° x 0.2°	Hamilton and Casey (2016)		Bryan-Brown *et al.* (2020)

Table 14. *List of mangrove datasets* (continued)

DATASETS	DESCRIPTION	NOMINAL YEAR	RESOLUTION	MANGROVE EXTENT USED	DOWNLOAD OR VIEWER	REFERENCES
Soil carbon	Covariates of climate and location data modelled against measurements of soil carbon	–	~10 km	Giri *et al.* (2011)		Jardine and Siikamäki (2014)
	Assessment of how soil carbon stocks vary across latitude, hemispheres and mangrove community composition	2014	–	Hamilton and Casey (2016)		Atwood *et al.* (2017)
	Fine-scale three-dimensional variation in soil-carbon density as assessed by machine-learning approaches	2000	30 m	Giri *et al.* (2011)	https://dataverse.harvard.edu/dataset.xhtml?persistentId=doi:10.7910/DVN/OCYUIT	Sanderman *et al.* (2018)
	Variation in soil carbon examined in relation to coastal environmental settings via climate-geophysical models	–	~25 km	Hamilton and Casey (2016)	Available from the corresponding author upon special request	Rovai *et al.* (2018)
	Mangrove soil-carbon stocks across different classifications of coastal environmental settings	–	30 m	Hamilton and Casey (2016)		Twilley, Chen and Hargis (1992)
Above-ground and below-ground carbon	Field measurements modelled against latitude for estimating total biomass carbon	–	–	WRI and IIED (1986)		Twilley, Chen and Hargis (1992)
	Mangrove AGB modelled against latitude; BGB assessed as a relative fraction of AGB	–	~9 km	Giri *et al.* (2011)		Siikamäki *et al.* (2012)
Total carbon	Annual assessment of total carbon stocks and losses from deforestation	Annual 2000–2012	30 m	Hamilton and Casey (2016)	https://dataverse.harvard.edu/dataverse/GMCSD	Hamilton and Friess (2018)
Mangrove tourism	Analysis of TripAdvisor website to identify mangrove attractions and their usage	Up to 2015	–	–	https://maps.oceanwealth.org	Spalding and Parrett (2019)
Coastal protection	Global valuation model of the role of mangroves in reducing annual coastal flood damages to people and property	2010	20 km	Giri *et al.* (2011)	https://osf.io/ecs4p/	Losada *et al.* (2018)
Conservation hotspots	Conservation hotspots identified by the intersection of threatened megafauna distributions with areas of high mangrove loss	2016	~20 km	Hamilton and Casey (2016)	https://megafauna.wetlands.app	Sievers *et al.* (2019)

Adapted from: Worthington, T.A., Andradi-Brown, D.A., Bhargava, R., Buelow, C., Bunting, P., Duncan, C., Fatoyinbo, L., Friess, D.A., Goldberg, L., Hilarides, L. & Lagomasino, D., 2020. Harnessing big data to support the conservation and rehabilitation of mangrove forests globally. *One Earth*, 2(5): 429–443.

4.1 EXISTING MANGROVE MAPS

4.1.1 Global Mangrove Watch

Global Mangrove Watch[44] (GMW) provides a free online tool (**Figure 42**) to visualize maps of mangroves worldwide (Bunting *et al.*, 2022; Spalding and Leal, 2022). The maps were developed from the baseline of mangrove extent determined from 2010 Landsat imagery with an overall accuracy of 95 percent (Bunting *et al.*, 2018) and has since been updated for 2022 using SAR data (Leal and Spalding, eds., 2022). The GMW website has a user-friendly interface with an interactive web map to view different data layers visualizing mangrove extent, net change over time, blue carbon storage and level of protection. In version 3.0, an additional map of restoration potential was also developed based on loss of mangroves between 1996 and 2020 (Leal and Spalding, eds., 2022). The map includes a restorability score that represents the feasibility of restoration and benefits to fisheries and carbon storage (Leal and Spalding, eds., 2022). Reports and data can be viewed and downloaded for mangroves globally or for individual countries. For each data layer, dropdown menus are available to customize date range. A Global Mangrove Watch leaflet which includes a listing of all available data layers in the GMW online platform is available in multiple languages at www.wetlands.org/publications/global-mangrove-watch-leaflet.

As the GMW maps are developed with coarser resolution (25-m) data that are better suited for global or regional analysis, there are limitations with regards to mapping mangroves at fine scales (Leal and Spalding, eds., 2022). Initial maps originally published in 2018 had increased error for areas with narrow and/or fragmented mangrove habitat (Bunting *et al.*, 2018). However, the most recent 2022 update, with a reported 95 percent accuracy (accuracy is variable by region), has improved mapping of mangroves in smaller areas especially for Small Island Developing States (SIDS) (Leal and Spalding, eds., 2022).

Figure 42. *The GMW online platform provides remote sensing data and tools for monitoring mangroves*

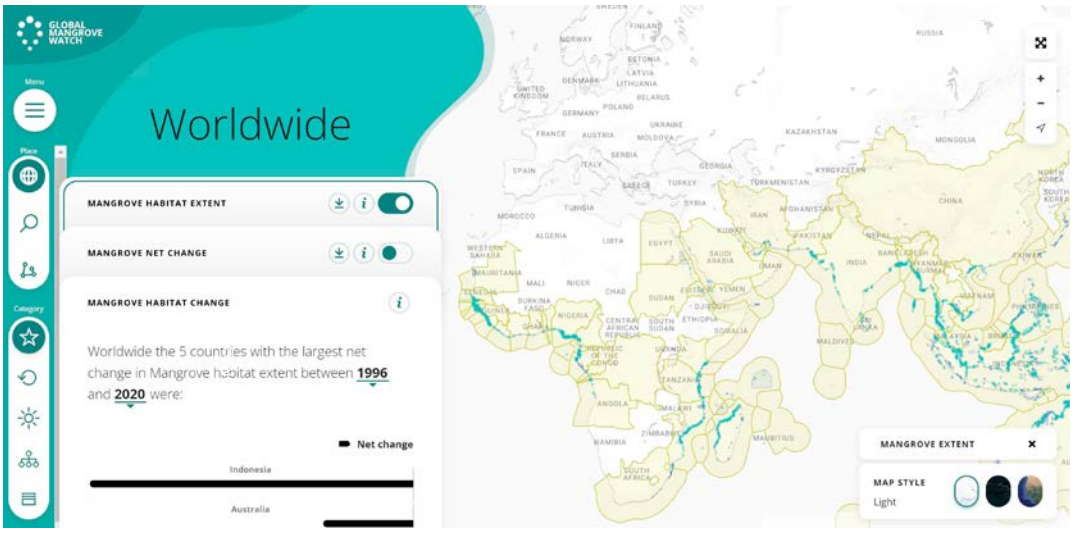

Source: Global Mangrove Alliance. 2023. Global Mangrove Watch. [Cited 1 April 2023]. www.globalmangrovewatch.org

[44] www.globalmangrovewatch.org

4.1.2 Ocean Data Viewer

The Ocean Data Viewer[45] hosted by the United Nations Environment Programme and the World Conservation Monitoring Centre provides access to a variety of global mangrove datasets including: the *World Atlas of Mangroves, version 3.1*; *Global Distribution of Modelled Mangrove Biomass, version 1*; *Global Biophysical Topology of Mangroves, version 2.2*; and the *USGS Global Distribution of Mangroves version 1.4*.

4.1.3 WorldCover 10-m mangrove class

The ESA in collaboration with a consortium of European research organizations, hosts *WorldCover* online,[46] a global map of land cover and forest types, which includes 11 different land classes including mangroves at 10-m resolution (**Figure 43**). The maps are updated continuously with versions now available for 2020 and 2021, using Sentinel-1 and Sentinel-2 data. The 2020 version has an estimated accuracy of 75 percent (Zanaga *et al.*, 2021), while the 2021 version has an accuracy of 76.1 percent (Zanaga *et al.*, 2022). Different algorithms were used to produce the forest cover maps, so any differences between years are attributable to difference in land cover and methods used. The dashboard not only provides options to view the forest cover maps, but also allows users to view the RGB and false-colour composites from Sentinel data. Data can be accessed and downloaded via the webmap viewer, Google Earth Engine or Terrascope with Python.

Figure 43. *The ESA* **WorldCover** *online portal that provides access to global 10-m data for land cover and forest types*

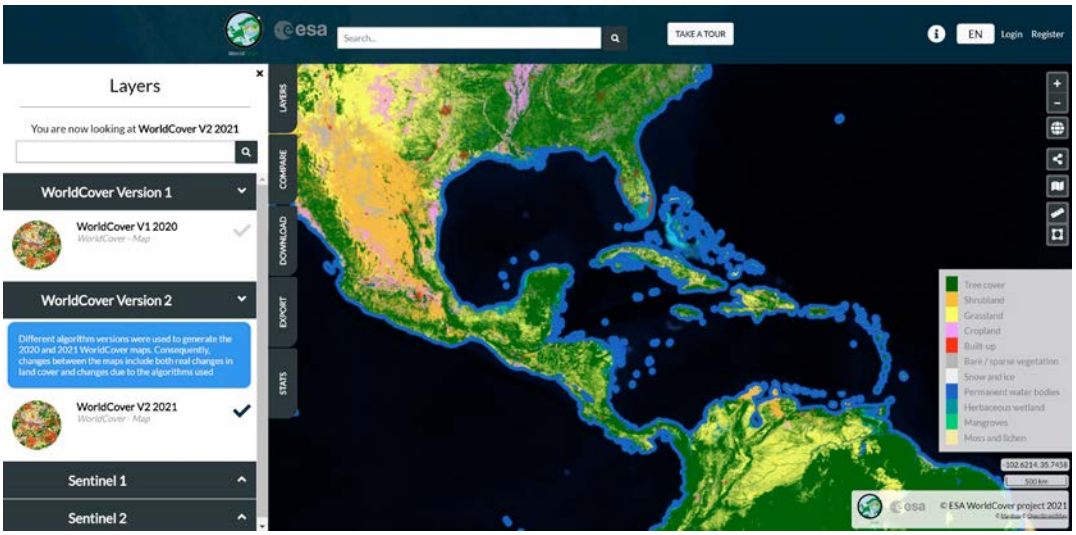

Source: ESA. 2021. WorldCover. [Cited 1 April 2023]. https://esa-worldcover.org/en

[45] https://data.unep-wcmc.org/
[46] https://esa-worldcover.org/

4.2 OPEN-SOURCE IMAGERY DATA, SOFTWARE AND TOOLS FOR MANGROVE MANAGERS

4.2.1 Imagery

Norway's International Climate & Forests Initiative – Planet access

Through Norway's International Climate & Forests Initiative[47] (NICFI), free access can be provided to Planet's high resolution, analysis-ready mosaics of the world's tropics in order to help reduce and reverse the loss of tropical forests, combat climate change, conserve biodiversity and facilitate sustainable development. Planet is a constellation of small satellites that can image the entire Earth on a daily basis. Now in its third generation, satellite sensors have been updated from 4-band multispectral imagery to 8-band imagery with the SuperDove constellation launched in 2020. Planet has a searchable database of basemaps and global mosaics that began in January 2016 and are available on a monthly or quarterly basis. A public application programming interface (API)[48] is available for use with a Python library and the command line interface, and an open-source code is available on GitHub.[49] For disaster areas,[50] Planet imagery will make available the entire archive to the public with an explorer account for a minimum of up to 30 days. Multiple training courses are available through Planet's University online courses[51] that offer guidance on using basemaps and how to integrate image workflows within various software, such as ArcGIS Pro, Google Earth Engine and QGIS. The NICFI satellite data program was specifically designed for monitoring changes in tropical forests to reduce deforestation. NICFI makes monthly imagery available from September 2020 to August 2022, and historical imagery collected every six months from 2015 to 2020.

United States Geological Survey EarthExplorer

The United States Geological Survey hosts EarthExplorer,[52] an online archive of remotely sensed imagery that is freely available to the public. The archive includes a wide range of satellite platforms from multispectral imagery, such as Landsat, and hyperspectral imagery, to the Hyperion sensor on the EO-1 satellite. Additional platforms include radar, aerial and UAS imagery, as well as additional spatial datasets such as digital elevation and vegetation monitoring using NDVI. The archive can be searched using a predefined area with a choice of platforms and datasets pooled from commercial and government entities, such as NASA and the National Oceanic and Atmospheric Administration.

4.2.2 Software

Quantum GIS

Quantum GIS (QGIS)[53] is a free and open-source geographic information system with a wide range of resources, tutorials and integrated toolsets that can be used for creating maps as well as analysing remotely sensed imagery. QGIS can be integrated with an online Planet account to allow for access to Planet's SkySat, PlanetScope and RapidEye imagery, through installation of the Planet plugin. Instructions on how to integrate QGIS with Planet's image search are available online through Planet University's online courses.[54]

Integrated Valuation of Ecosystem Services and Tradeoffs

Integrated Valuation of Ecosystem Services and Tradeoffs (InVEST)[55] is an open-source software that includes a suite of models for mapping ecosystem services, such as coastal blue carbon of mangrove and seagrass ecosystems. The model

[47] https://university.planet.com/page/nicfi
[48] https://developers.planet.com/open/
[49] https://github.com/planetlabs
[50] www.planet.com/disasterdata
[51] https://university.planet.com/
[52] https://earthexplorer.usgs.gov/
[53] www.qgis.org/en/site
[54] https://university.planet.com/
[55] https://naturalcapitalproject.stanford.edu/software/invest

can be analysed from local, regional to global scales with input of biophysical or economic information. The software works independently, but results must be viewed in GIS software, such as QGIS or ArcGIS. The software targets users with beginner to intermediate GIS skills. The InVEST Coastal Blue Carbon uses a bookkeeping approach that models three pools of carbon: AGB and BGB, dead litter and sediment. Detailed breakdown of the parameters and algorithms used in the model is hosted on the InVEST Coastal Blue Carbon model.[56] The user must provide the following inputs for the model: spatial information (mangrove footprint or extent) and biophysical information (amount of carbon storage and accumulation rate in all three carbon pools). The biophysical information should ideally be sourced from field or local data, but global data can be sourced from peer-reviewed literature and used as a proxy if local data are unavailable.

Open Foris

FAO's Open Foris[57] suite of tools is free open-source software and tools that facilitate flexible and efficient data collection, analysis and reporting. These include Collect Mobile[58] which is an Android app for field-based surveys, Collect Earth,[59] a Java-based tool that enables data collection through Google Earth, Collect Earth Online[60] that allows users to collect reference data using high resolution satellite images and big data analysis through the Google Earth Engine, Earth Map,[61] which permits the monitoring of land cover change in an easy, integrated and multitemporal manner, and SEPAL[62] that allows users to query and process satellite data quickly and efficiently, tailor their products for local needs, and produce sophisticated and relevant geospatial analyses quickly. SEPAL is a cloud computing-based platform that combines the Google Earth Engine and open-source software like the Orfeo Toolbox, Python, Jupyter, GDAL, R, R Studio Server, R Shiny Server, SNAP Toolkit and the Open Foris Geospatial Toolkit.

4.2.3 Tools

Orfeo ToolBox

The Orfeo ToolBox[63] is an open-source software library developed by the French Space Agency, National Center for Space Studies (CNES), for imagery processing in remote sensing. The library is based on C++, and can be accessed with QGIS, Python, the command line or Monteverdi. Features available with the Orfeo Toolbox include preprocessing imagery, such as radiometric and atmospheric corrections, feature extraction, change detection and image classification including supervised, machine-learning algorithms, and object-based image analysis.

The Blue Carbon Explorer

The Nature Conservancy, in collaboration with FAO and Planet, released the Blue Carbon Explorer in 2023 to allow users to explore blue carbon opportunities across the insular Caribbean, Indonesia and Papua New Guinea (**Figure 44**). This Google Earth Engine app aims to guide decision-making in terms of conservation by identifying mangroves that are degraded and in need of restoration, and mangroves that are healthy and in need of protection, as opportunities for blue carbon projects. The mangrove extent map for the Caribbean was developed in 2021 through hand-digitization, while the map for the Bahamas was refined in 2023 using automated detection from PlanetScope imagery and extensive field data and input from local experts. These maps

[56] http://releases.naturalcapitalproject.org/invest-userguide/latest/en/coastal_blue_carbon.html
[57] https://openforis.org/
[58] https://openforis.org/tools/collect-mobile/
[59] https://openforis.org/tools/collect-earth/
[60] https://openforis.org/tools/collect-earth-online/
[61] https://earthmap.org/login
[62] https://openforis.org/tools/sepal/
[63] www.orfeo-toolbox.org
[64] https://bluecarbon.tnc.org/

Figure 44. *The Blue Carbon Explorer's example of mangrove restoration prioritization in eastern Grand Bahama, 2015–2021*

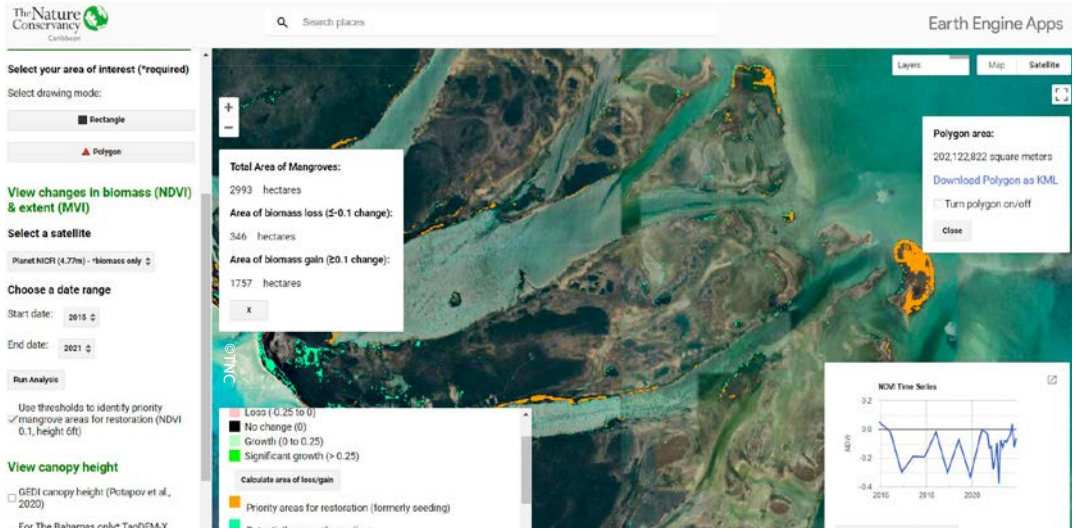

Note: This analysis based on Planet NICFI Dove imagery and TanDEM-X canopy height data (Simard *et al.*, 2023) was used by TNC and partners to support site selection for mangrove restoration on the islands of Grand Bahama and Abaco, Bahamas.

are being developed on a country-by-country basis for the insular Caribbean and will be added to the tool over time. For Indonesia and Papua New Guinea, the GMW mangrove extent is used in the tool. The tool not only shows where mangroves are, but also gives an estimation of what condition they are in. It allows users to assess changes in health or biomass of mangroves over time using NDVI change maps and time series. It also utilizes MVI to assess changes in the extent of mangroves over time. Canopy height from GEDI (Potapov *et al.*, 2020) and TanDEM-X (Simard *et al.*, 2023) can be overlaid, as well as protected areas and benthic habitats.

The Blue Carbon Explorer can also support prioritization of mangrove areas for restoration using NDVI thresholds and canopy height. This has been demonstrated by TNC and restoration partners in the Bahamas. Many of the mangroves on Grand Bahama and Abaco were devastated during Hurricane Dorian in 2019. With guidance from partners on the ground, TNC used the tool to prioritize mangrove areas for restoration that were not likely to recover naturally. Such areas comprised degraded areas of short, non-propagule-producing mangroves that were remote or isolated from taller and healthier propagule-producing mangroves. The resulting prioritization was reviewed with restoration partners on both islands, overlaid with current restoration sites and marine protected areas (MPAs) to select 10 000 ha of mangroves as priorities for restoration.

Mapping Ocean Wealth

TNC's Mapping Ocean Wealth[65] platform enables the sharing of ecosystem service data generated through many collaborative projects. The platform includes map viewers and data on potential blue carbon storage, mangrove tourism, and restoration sites based on area loss since 1996, using the extent of mangroves sourced from GMW (Worthington and Spalding, 2018) (**Figure 45**). Areas that were permanently lost due to erosion or urbanization were excluded from consideration for restoration. From the dropdown menu, restoration potential can be viewed globally or by country. The dashboard also has a layer for blue carbon which sums estimates of

[65] https://maps.oceanwealth.org/

Figure 45. *TNC's Mapping Ocean Wealth platform includes maps of mangrove restoration potential and blue carbon storage*

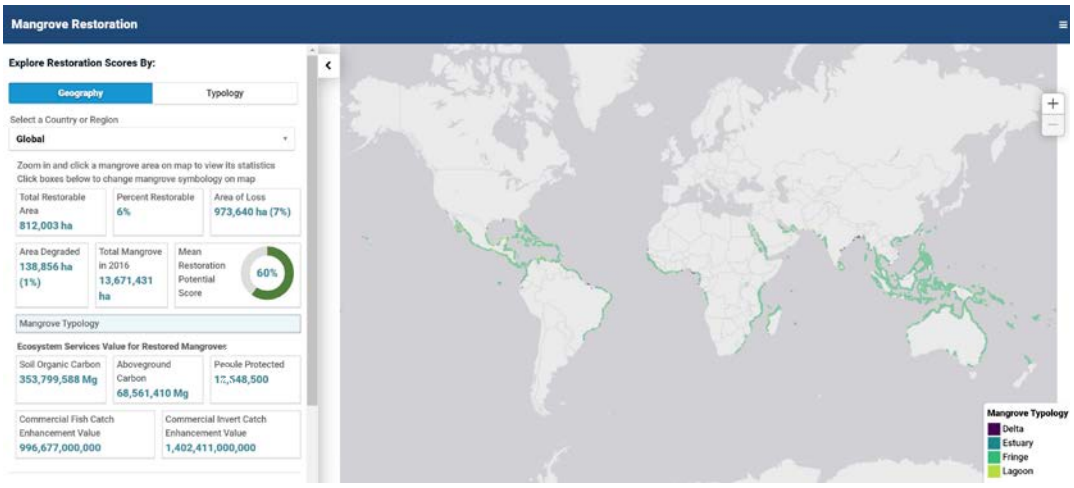

Source: Worthington, T. & Spalding, M. 2018. Mangrove restoration potential: A global map highlighting a critical opportunity. Apollo - University of Cambridge Repository. https://doi.org/10.17863/CAM.39153

AGB and soil carbon for mangroves using the GMW 2016 map. The AGB was estimated from a global dataset at 30-m resolution for the year 2000, which included maximum canopy height and individual tree height weighted in proportion to the basal area (Simard, 2019). The below-ground carbon was estimated from a machine-learning algorithm using mangrove forest extent in 2000, to map soil carbon at 30 m resolution (Sanderman *et al*., 2018).

Google Earth Engine

The Google Earth Engine Mangrove Mapping Methodology (GEEMMM) is a free tool developed for use within the Google Earth Engine (GEE) environment by non-specialists for coastal management (Yancho *et al*., 2020). The tool is freely available on GitHub,[66] and utilizes GEE's cloud computing capability to create multidate habitat maps that can be used in change detection. The tool is divided into three modules to define the region of interest, classification and accuracy assessment. The tool is also customizable for entering local datasets such as mangrove baseline extent DSMs or use of globally available datasets within GEE. GEEMMM provides access to the Landsat catalogue and will create a composite image based on time range of interest and cloud cover limit.

If higher resolution imagery is needed, the MVI Mapper is a fully automated tool for use in Google Earth Engine (Baloloy *et al*., 2020). MVI is an index developed to distinguish mangroves from other vegetation types with the use of green, NIR and SWIR bands.

The band combination helps to distinguish mangroves from other vegetation due to differences in the level of greenness and moisture content. The MVI Mapper in GEE gives access to atmospherically corrected Sentinel-2 (level-2A) imagery. The final outputs include RGB and false colour composites, and vegetation and mangrove raster format files. The MVI Mapper can also be used outside of the Google Earth Engine and offline, with Interactive Data Language (IDL®) software, available commercially. However, this method requires additional steps for sourcing and preprocessing of satellite imagery before applying the index in IDL.

[66] https://github.com/Blue-Ventures-Conservation/GEEMMM

©TNC

5. CONCLUSIONS AND FUTURE DIRECTIONS

As remote sensing technology continues to advance, it is expected that higher spatial and spectral resolution data with increased revisit times will become available. There will also be more integration with active sensors such as radar and LiDAR to better define mangrove extent and structure. The rise of big data and cloud computing will permit faster access to and processing of a vast amount of geospatial data that will lead to better understanding and mapping of mangrove patterns, conditions and change. Increased collaboration among mangrove networks will further promote awareness of the need to continue to prioritize, protect and restore mangroves.

Given that mangrove forests provide critical benefits to people, including food security, shoreline stabilization, flood reduction, carbon sequestration and biodiversity conservation, increased attention is needed on how we prioritize areas for restoration, facilitate improved mangrove management and enhance ecosystem services provided by mangroves. Enhanced remote sensing capabilities at finer scales are essential for accurately documenting and comprehending the spatial dynamics of mangrove changes, monitoring illegal deforestation activities, and evaluating the effectiveness of restoration initiatives. The methodologies outlined in this document play a crucial role in supporting national endeavors and pledges aimed at conserving, sustainably managing, and restoring mangrove ecosystems along with their diverse ecological and socio-economic benefits.

Remote sensing will especially play a critical role in serving the needs of SIDS, where information on the status of mangroves is often inadequate, as their decision-makers seek to better understand the distribution of mangroves and the important role they play in human well-being. Progress is still needed in providing data products that can support improved management at local scales, as well as in improving access to data and ensuring that such access is equitable (Worthington *et al*., 2020). The challenge will be to translate the growing body of information into policy and action that will result in on-the-ground conservation.

©TNC

REFERENCES

Aljahdali, M.O., Munawar, S. & Khan, W.R. 2021. Monitoring mangrove forest degradation and regeneration: Landsat time series analysis of moisture and vegetation indices at Rabigh Lagoon, Red Sea. *Forests*, 12(1): 52.

Alongi, D.M. 2020. Global significance of mangrove blue carbon in climate change mitigation (Version 1). *Science*, 2(3): 57.

Aslan, A. & Aljahdali, M.O. 2022. Characterizing global patterns of mangrove canopy height and aboveground biomass derived from SRTM data. *Forests*, 13(10): 1545.

Atwood, T.B., Connolly, R.M., Almahasheer, H., Carnell, P.E., Duarte, C.M., Ewers Lewis, C.J., Irigoien, X. *et al.* 2017. Global patterns in mangrove soil carbon stocks and losses. *Nature Climate Change*, 7: 523–528.

Avery, T.E. 1969. *Forester's guide to aerial photo interpretation*. No. 308. Washington, DC, US Department of Agriculture, Forest Service. https://naldc.nal.usda.gov/download/CAT87209514/PDF

Ayub, A.S., Nugroho, F., Suci, A.N.N. & Anggoro, A. 2021. Utilization of unmanned aerial vehicle (UAV) technology for mapping mangrove ecosystem. *Journal of Sylva Indonesiana*, 4(02): 70–77.

Baloloy, A.B., Blanco, A.C., Ana, R.R.C.S. & Nadaoka, K. 2020. Development and application of a new mangrove vegetation index (MVI) for rapid and accurate mangrove mapping. ISPRS *Journal of Photogrammetry and Remote Sensing*, 166: 95–117

Berlanga-Robles, C.A. & Ruiz-Luna, A. 2020. Assessing seasonal and long-term mangrove canopy variations in Sinaloa, northwest Mexico, based on time series of enhanced vegetation index (EVI) data. *Wetlands Ecology and Management*, 28(2): 229–249.

Bryan-Brown, D.N., Connolly, R.M., Richards, D.R., Adame, F., Friess, D.A. & Brown, C.J. 2020. Global trends in mangrove forest fragmentation. *Scientific Reports*, 10: 7117.

Bunting, P. Rosenqvist, A., Hilarides, L., Lucas, R.M., Thomas, T., Tadono, T., Worthington, T.A., Spalding, M., Murray, N.J. & Rebelo, L-M. 2022. Global Mangrove Extent Change 1996 – 2020: Global Mangrove Watch Version 3.0. *Remote Sensing*, 14(15): 3657.

Bunting, P., Rosenqvist, A., Lucas, R.M., Rebelo, L.M., Hilarides, L., Thomas, N., Hardy, A., Itoh, T., Shimada, M. & Finlayson, C.M. 2018. The Global Mangrove Watch - a new 2010 global baseline of mangrove extent. *Remote Sensing*, 10(10).

CBD (Convention on Biodiversity). 2022. Official CBD press release. Convention on Biological Diversity. 2022. www.cbd.int/article/cop15-cbd-press-release-final-19dec2022

Climate Champions. 2022. *The Mangrove Breakthrough: A call to action for a critical ecosystem*. Climate Champions.2022. https://climatechampions.unfccc.int/the-mangrove-breakthrough

Donato, D.C., Kauffman, J.B., Murdiyarso, D., Kurnianto, S., Stidham, M. & Kanninen, M. 2011. Mangroves among the most carbon-rich forests in the tropics. *Nature Geoscience*, 4(5): 293–7.

FAO. 2007. *The world´s mangroves 1980-2005*. FAO Forestry Paper 153. Rome, FAO. https://agris.fao.org/agris-search/search.do?recordID=XF2008433305

FAO. 2020a. *FAO Strategy on Mainstreaming Biodiversity across Agricultural Sectors*. Rome, FAO. doi.org/10.4060/ca7722en

FAO. 2020b. *Global Forest Resources Assessment*. Rome. [Cited 25 January 2023]. https://fra-data.fao.org.

FAO. 2021. *2021-23 Action plan for the implementation of the FAO strategy on mainstreaming biodiversity across agricultural sectors.* Rome, FAO. www.fao.org/3/cb5515en/cb5515en.pdf

FAO. 2023. *The world's mangroves 2000–2020.* Rome. https://doi.org/10.4060/cc7044en

Faridah-Hanum, I., Yusoff, F.M., Fitrianto, A., Ainuddin, N.A., Gandaseca, S., Zaiton, S., Norizah, K. *et al.* 2019. Development of a comprehensive mangrove quality index (MQI) in Matang Mangrove: Assessing mangrove ecosystem health. *Ecological Indicators*, 102: 103–117.

Friess, D.A., Rogers, K., Lovelock, C.E., Krauss, K.W., Hamilton, S.E., Lee, S.Y., Lucas, R. *et al.* 2019. The state of the world's mangrove forests: past, present, and future. *Annual Review of Environment and Resources*, 44: 89–115.

Giri, C., Ochieng, E., Tieszen, L.L., Zhu, Z., Singh, A., Loveland, T., Ma-sek, J. & Duke, N. 2011. Status and distribution of mangrove forests of the world using earth observation satellite data. *Global Ecology and Biogeography*, 20: 154–159.

Goldberg, L., Lagomasino, D., Thomas, N. & Fatoyinbo, T. 2020. Global declines in human-driven mangrove loss. *Global Change Biology*, 26(10): 5844–5855.

Hamilton, S.E. & Casey, D. 2016. Creation of a high spatio-temporal resolution global database of continuous mangrove forest cover for the 21st century (CGMFC-21). *Global Ecology and Biogeography*, 25: 729–738.

Hamilton, S.E. & Friess, D.A. 2018. Global carbon stocks and potential emissions due to mangrove deforestation from 2000 to 2012. *Nature Climate Change*, 8: 240–244.

Heenkenda, M.K., Joyce, K.E., Maier, S.W. & Bartolo, R. 2014. Mangrove species identification: Comparing WorldView-2 with aerial photographs. *Remote Sensing*, 6(7): 6064–6088.

Hutchison, J., Manica, A., Swetnam, R., Balmford, A. & Spalding, M. 2014. Predicting global patterns in mangrove forest biomass. *Conservation Letters*, 7: 233–240.

Jardine, S.L. & Siikamäki, J.V. 2014. A global predictive model of carbon in mangrove soils. *Environmental Research Letters*, 9: 104013.

Jensen, J.R. 1996. *Introductory digital image processing: a remote sensing perspective.* Second edition. Prentice-Hall Inc. www.scirp.org/(S(351jmbntvnsjt1aadkposzje))/reference/ReferencesPapers.aspx?ReferenceID=2028387

Jiang, Y., Zhang, L., Yan, M., Qi, J., Fu, T., Fan, S. & Chen, B. 2021. High-resolution mangrove forests classification with machine learning using worldview and UAV hyperspectral data. *Remote Sensing*, 13(8): 1529.

Joyce, K.E., Fickas, K.C. & Kalamandeen, M. 2023. The unique value proposition for using drones to map coastal ecosystems. *Cambridge Prisms: Coastal Futures*, 1: p.e6.

Klemas, V.V. 2015. Coastal and environmental remote sensing from unmanned aerial vehicles: An overview. *Journal of Coastal Research*, 31(5): 1260–1267.

Leal, M. & Spalding, M.D., eds. 2022. *The State of the World's Mangroves 2022.* Global Mangrove Alliance. www.mangrovealliance.org/wp-content/uploads/2022/09/The-State-of-the-Worlds-Mangroves-Report_2022.pdf

Losada, I.J., Menéndez, P., Espejo, A., Torres, S., Díaz-Simal, P., Abad, S., Beck, M.W. *et al.* 2018. *The global value of mangroves for risk reduction.* Technical Report. The Nature Conservancy. www.conservationgateway.org/ConservationPractices/Marine/crr/library/Documents/GlobalMangrovesRiskReductionTechnicalReport10.7291/V9DV1H2S.pdf

Lucas, R.M., Ellison, J.C., Mitchell, A., Donnelly, B., Finlayson, M. & Milne, A.K. 2002. Use of stereo aerial photography for quantifying changes in the extent and height of mangroves in tropical Australia. *Wetlands Ecology and Management*, 10(2): 159–173.

Maina, J.M., Bosire, J.O., Kairo, J.G., Bandeira, S.O., Mangora, M.M., Macamo, C., Ralison, H. & Majambo, G. 2021. Identifying global and local drivers of change in mangrove cover and the implications for management. *Global Ecology and Biogeography*, 30(10): 2057–2069.

Maynard, J., Tracey, D., Williams, G.J., Andradi-Brown, D.A., Grill, G., Thieme, M. & Ahmadia, G. 2019. *Mangrove cover change between 1996 and 2016 near river-ocean outlets: A global analysis to identify priority rivers for conservation.* Gland, Switzerland, World Wildlife Fund. https://doi.org/10.6084/m9.figshare.8094245.

Menéndez, P., Losada, I.J., Torres-Ortega, S., Narayan, S. & Beck, M.W. 2020. The global flood protection benefits of mangroves. *Scientific Reports*, 10: 4404.

Navarro, A., Young, M., Allan, B., Carnell, P., Macreadie, P. & Ierodiaconou, D. 2020. The application of unmanned aerial vehicles (UAVs) to estimate above-ground biomass of mangrove ecosystems. *Remote Sensing of Environment*, 242: 111747.

Pastor-Guzman, J., Dash, J. & Atkinson, P.M. 2018. Remote sensing of mangrove forest phenology and its environmental drivers. *Remote Sensing of Environment*, 205: 71–84.

Pham, T.D., Xia, J., Ha, N.T., Bui, D.T., Le, N.N. & Tekeuchi, W. 2019a. A review of remote sensing approaches for monitoring blue carbon ecosystems: Mangroves, seagrasses and salt marshes during 2010–2018. *Sensors*, 19(8): 1933.

Polidoro, B.A., Carpenter, K.E., Collins, L., Duke, N.C., Ellison, A.M., Ellison, J.C., Farnsworth, E.J. *et al.* 2010. The loss of species: mangrove extinction risk and geographic areas of global concern. *PLoS ONE*, 5.

Potapov, P., Li, X., Hernandez-Serna, A., Tyukavina, A., Hansen, M.C., Kommareddy, A., Pickens, A. *et al.* 2020. Mapping and monitoring global forest canopy height through integration of GEDI and Landsat data. *Remote Sensing of Environment*, 112165.

Rossi, R.E., Archer, S.K., Giri, C. & Layman, C.A. 2020. The role of multiple stressors in a dwarf red mangrove (Rhizophora mangle) dieback. *Estuarine, Coastal and Shelf Science*, 237: 106660.

Rovai, A.S., Twilley, R.R., Castan˜eda-Moya, E., Riul, P., Cifuentes-Jara, M., Manrow-Villalobos, M., Horta, P.A., Simonassi, J.C. *et al.* 2018. Global controls on carbon storage in mangrove soils. *Nature Climate Change*, 8: 534–538.

Ruzgienė, B., Bagdžiūnaitė, R. & Ruginytė, V. 2012. Scanning aerial photos using a non-professional scanner. *Geodesy and Cartography*, 38(3): 118–121.

Sanderman, J., Hengl, T., Fiske, G., Solvik, K., Adame, M.F., Benson, L., Bukoski, J.J. *et al.* 2018. A global map of mangrove forest soil carbon at 30 m spatial resolution. *Environmental Research Letters*, 13(5).

Sievers, M., Brown, C.J., Tulloch, V.J.D., Pearson, R.M., Haig, J.A., Turschwell, M.P. & Connolly, R.M. 2019. The role of vegetated coastal wetlands for marine megafauna conservation. *Trends in Ecology and Evolution*, 34: 807–817.

Siikamäki, J., Sanchirico, J.N. & Jardine, S.L. 2012. Global economic potential for reducing carbon dioxide emissions from mangrove loss. *Proceedings of the National Academy of Sciences of the United States of America*, 109: 14369–14374.

Simard, M., Fatoyinbo, T., Thomas, N., Stovall, A., Parra, A., Barenblitt, A., Bunting, P. *et al.* 2023. A New Global Mangrove Height Map. Manuscript in prepreparation.

Simard, M. 2019. Radar remote sensing of mangrove forests. In: A. Flores, K. Herndon, R. Thapa & E. Cherrington, eds. *NASA SAR Handbook: Comprehensive methodologies for forest monitoring and biomass estimation*. NASA 2019. DOI: 10.25966/33zm-x271

Simard, M., Fatoyinbo, T., Smetanka, C., Rivera-monroy, V.H., Castaneda, E., Thomas, N. & Van der stocken, T. 2019. *Global mangrove distribution, aboveground biomass, and canopy height*. Oak Ridge, Tennessee, USA, ORNL DAAC. doi.org/10.3334/ORNLDAAC/1665

Spalding, M. & Parrett, C.L. 2019. Global patterns in mangrove recreation and tourism. *Marine Policy*, 110: 103540.

Spalding, M.D., Kainumu, M. & Collins, L. 2010. *World Atlas of Mangroves.* UK, Earthscan. https://books.google.co.th/books/about/World_Atlas_of_Mangroves.html?id=wzSCkulW9SQC&redir_esc=y

Tang, W., Zheng, M., Zhao, X., Shi, J., Yang, J. & Trettin, C. 2018. Big geospatial data analytics for global mangrove biomass and carbon estimation. *Sustainability*, 10: 472.

Taureau, F., Robin, M., Proisy, C., Fromard, F., Imbert, D. & Debaine, F. 2019. Mapping the mangrove forest canopy using spectral unmixing of very high spatial resolution satellite images. *Remote Sensing*, 11(3): 367.

Tian, Y., Huang, H., Zhou, G., Zhang, Q., Tao, J., Zhang, Y. & Lin, J. 2021. Aboveground mangrove biomass estimation in Beibu Gulf using machine learning and UAV remote sensing. *Science of the Total Environment*, 781: 146816.

Twilley, R.R., Chen, R.H. & Hargis, T. 1992. Carbon sinks in mangroves and their implications to carbon budget of tropical coastal eco-systems. *Water, Air, & Soil Pollution*, 64: 265–288.

Waldron, A., Adams, V., Allan, J., Arnell, A., Asner, G., Atkinson, S., Baccini, A. *et al.* 2020. *Protecting 30% of the planet for nature: costs, benefits and economic implications*. University of Helsinki. doi:10.13140/RG.2.2.19950.64327

Waltham, N.J., Elliott, M., Lee, S.Y., Lovelock, C., Duarte, C.M., Buelow, C., Simenstad, C. *et al.* 2020. UN decade on ecosystem restoration 2021–2030—what chance for success in restoring coastal ecosystems? *Frontiers in Marine Science*: 71.

Ward, R.D., Friess, D.A., Day, R.H. & Mackenzie, R.A. 2016. Impacts of climate change on mangrove ecosystems: a region by region overview. *Ecosystem Health and Sustainability*, 2(4): e01211.

Worthington, T. & Spalding, M. 2018. *Mangrove restoration potential: A global map highlighting a critical opportunity.* Apollo - University of Cambridge Repository. https://doi.org/10.17863/CAM.39153

WRI (World Resources Institute) & IIED (International Institute for Environment and Development). 1986. *World Resources 1986. Pollutants and forest decline.* Washington, DC, WRI and London, UK, IIED. www.wri.org/research/world-resources-1986.

Yancho, J.M.M., Jones, T.G., Gandhi, S.R., Ferster, C., Lin, A. & Glass, L. 2020. The Google Earth Engine Mangrove Mapping Methodology (GEEMMM). *Remote Sensing*, 12(22): 1–35.

Zanaga, D., Van De Kerchove, R., De Keersmaecker, W., Souverijns, N., Brockmann, C., Quast, R., Wevers, J. *et al.* 2021. *ESA WorldCover 10 m 2020 v100.* Paris, France. European Space Agency. https://doi.org/10.5281/zenodo.5571936

Zanaga, D., Van De Kerchove, R., Daems, D., De Keersmaecker, W., Brockmann, C., Kirches, G., Wevers, J. *et al.* 2022. Paris, France, European Space Agency. *ESA WorldCover 10 m 2021 v200.* doi.org/10.5281/zenodo.7254221

Zimudzi, E., Sanders, I., Rollings, N. & Omlin, C.W. 2021. Remote sensing of mangroves using unmanned aerial vehicles: Current state and future directions. *Journal of Spatial Science*, 66(2): 195–212.

Zu Ermgassen, P.S., Mukherjee, N., Worthington, T.A., Acosta, A., da Rocha Araujo, A.R., Beitl, C.M., Castellanos-Galindo, G.A. *et al.* 2020. Fishers who rely on mangroves: Modelling and mapping the global intensity of mangrove-associated fisheries. *Estuarine, Coastal and Shelf Science*, 247: 106975.

APPENDIX
Case studies in mapping mangrove change

Four case studies that demonstrate the use of remote sensing for detecting mangrove change at fine scales are presented. High resolution satellite imagery and UAS data were used to map and monitor mangrove changes in the Dominican Republic, Grenada, Haiti and Saint Vincent and the Grenadines. These countries face similar, as well as different, threats to mangroves, ranging from aquaculture and coastal development, to harvesting of biomass for charcoal production. The need for monitoring mangroves is not only to understand where mangroves are being lost, but also where mangroves are expanding. The objectives of these projects were to establish a baseline for gauging future change and understanding the threats so that adaptive management plans can be designed and put in place to safeguard the mangroves.

CASE STUDY 1
PARQUE NACIONAL MANGLARES DEL BAJO YUNA, THE DOMINICAN REPUBLIC

The Parque Nacional Manglares Del Bajo Yuna is located in a karst estuarine wetland ecosystem at the western end of Samaná Bay, encompassing an area of 12 000 ha. Declared a Ramsar site, the park is one of the largest semi-closed bays in the Caribbean and supports various endemic species. The total mangrove extent measured using satellite imagery acquired in December 2017 was 3 456 ha. Field surveys were conducted in 2016 and 2017 collecting, *inter alia*, the following field parameters: 1) mangrove species composition; 2) canopy height; 3) DBH; and 4) species richness and percent cover (by species).

Quickbird imagery was used to map the mangrove extent in 2003 and WorldView-2 imagery was used for 2013 and WorldView-3 for 2017. An object-based image analysis approach was applied to delineate mangrove extent. This approach segments satellite imagery into landscape objects that have ecologically meaningful shapes, and classifies the objects across spatial, spectral and textural scales. These segments represent distinct patches of uniform mangrove habitat. Object-oriented methods yield accuracy improvements compared to conventional pixel-based image analysis techniques as the non-spectral attributes of the imagery such as texture, spatial and contextual information are integrated into the classification workflow. The software used for mapping in this study was eCognition (v. 9.1, Trimble Inc.). Image segmentation requires identifying the appropriate scale of segments that can adequately represent the features that are being mapped. After segmentation, statistics pertaining to the spectral and textural properties of the satellite imagery were used to identify all mangrove segments. Mangrove segments that were adjacent to each other were merged; the results were visually interpreted and manually cleaned to improve the final accuracy for both time periods.

WorldView-3 satellite imagery of Parque Nacional Manglares Del Bajo Yuna collected on 6 July 2017, was used to calculate NDVI values and compare them with the baseline dataset of 3 December 2013

both in terms of mangrove extent and biomass. A pixel-by-pixel NDVI comparison between the 2013 and 2017 NDVI datasets was performed and a difference threshold that represented a varying amount of change between the two NDVI images was computed. The five threshold classes above and below the no change class represent the magnitude of biomass change. The thresholds are based on standard deviations from the baseline map. Change (+5) represents the largest areas that have gained mangrove biomass, while Change (-5) indicates the largest loss of mangrove biomass. The classes in between are scaled respectively.

Results of the NDVI analysis indicated that biomass decreased in 96.32 ha of mangroves between 2013 and 2017 while biomass increased in 160.27 ha of mangroves particularly near the mouth of the Barracote River to the south where mangroves had expanded. Growth was also detected in the north in areas that had been cleared for aquaculture but were later abandoned. The results in **Figure A1.1** show the area extent for each magnitude of change in biomass based on the difference threshold.

Changes in mangrove cover since 2003 were also assessed. In the north, near the town of Sanchez, a total of 233 ha of mangroves had been removed within the national park boundary. Records show that this was largely due to the expansion of shrimp aquaculture and polluted water generated by the municipality's landfill. However, mangrove cover has increased by 206 ha since 2001 around the mouth of the Barracote River. This is a result of sediment deposition that has decreased water depth and facilitated the natural establishment of mangrove propagules across a wider area. **Figure A1.2** and **Figure A1.3** shows that this area has high mangrove biomass indicating a highly productive system.

FIGURE A1.1 *NDVI class magnitude of change in hectares*

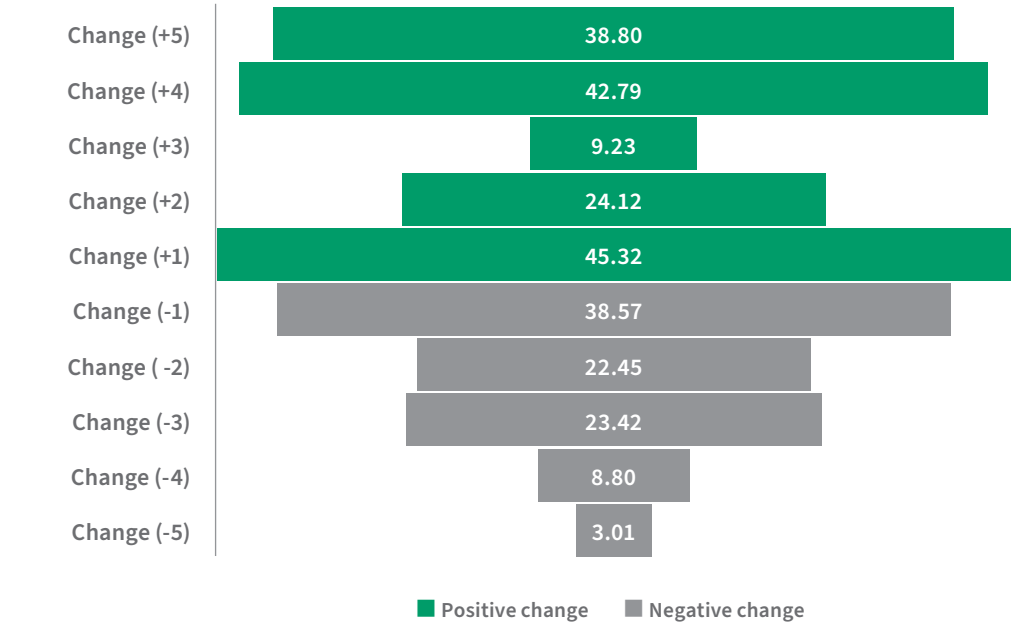

Source: TNC

FIGURE A1.2 *Mangrove change detection (2003 to 2017) in Parque Nacional Manglares Del Bajo Yuna, Dominican Republic, showing areas of mangrove loss and growth since 2003 using Quickbird and WorldView-2 satellite imagery*

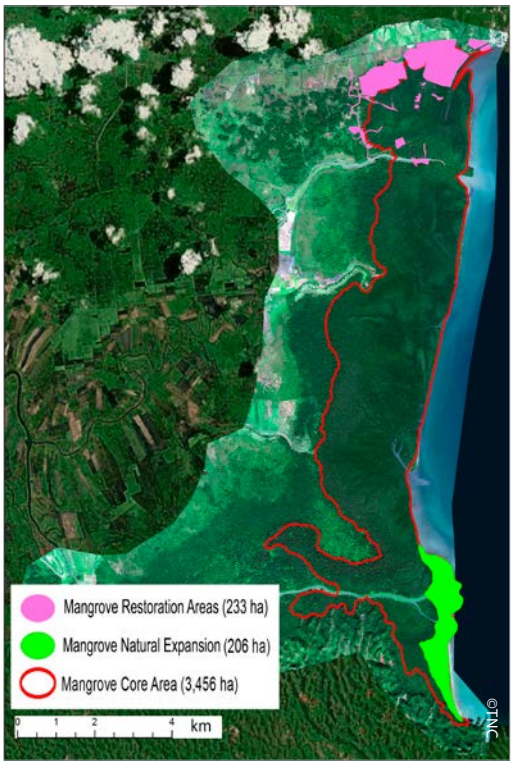

FIGURE A1.3 *Areas of change in mangrove biomass based on NDVI values in Parque Nacional Manglares Del Bajo Yuna between December 2013 and July 2017*

CASE STUDY 2

CARACOL AND FORT-LIBERTÉ, THREE BAYS NATIONAL PARK, HAITI

Three Bays National Park (3BNP) was designated by the Haitian Government in 2013. The MPA encompasses three bays: Limonade, Caracol and Fort-Liberté, as well as one of the largest inland brackishwater lagoons – the Important Bird Area of Lagon aux Boeufs – covering an area of 75 618 ha. 3BNP represents one of the largest protected areas of mangrove and coastal wetlands in Haiti and has a total mangrove area of 4 257.42 ha as measured from satellite imagery acquired in April 2014, representing about 20 percent of Haiti's remaining mangroves.

Field surveys were carried out in June and November 2015 as well as July 2017 to document existing conditions within the mangrove and coastal wetland habitats of 3BNP. The total mangrove area mapped within 3BNP using Quickbird 2002/2003 images equalled 4 146.27 ha. Using WorldView-2 2014 imagery, a total of 4 257.42 ha for a net increase of 111.15 ha was identified for the entire park. Total loss of mangrove areas detected from 2003 to 2014 was estimated to be 91.48 ha, mostly due to harvesting of mangrove wood for charcoal production. On the other hand, there was an expansion of 202.63 ha of mangroves into new areas as a result of ongoing reforestation initiatives that engaged communities located within the park to sow mangrove propagules in areas of die-off. These activities were also supported by the construction of mangrove nurseries and awareness-raising on the importance of mangroves, encouraging environmental stewardship.

Results of NDVI analysis indicated that a total of 57.47 ha of mangroves had been lost while a total of 101.1 ha of mangroves had established between 2014 and 2017 (**Figures A2.1**, **A2.2** and **A2.3**).

FIGURE A2.1 *Mangrove loss and expansion (ha) between 2014 and 2017 in 3BNP*

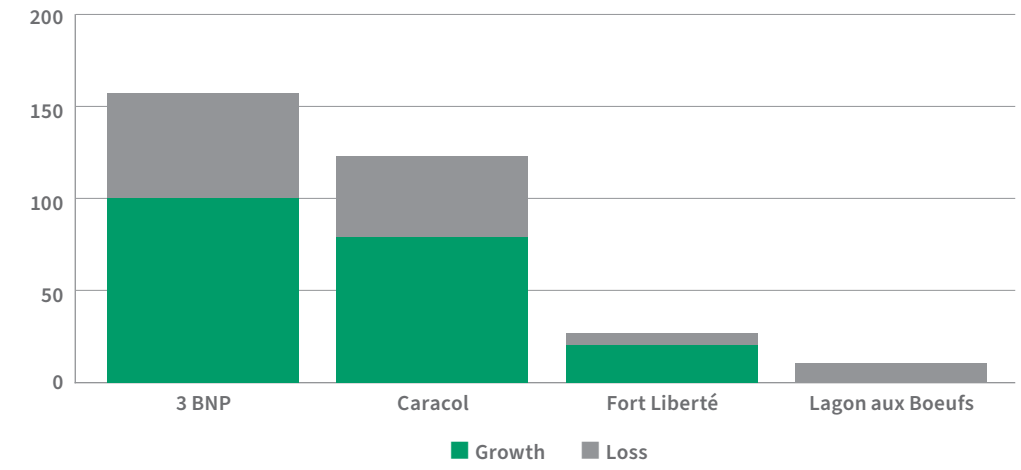

Source: TNC

FIGURE A2.2 *NDVI biomass change detection in Caracol Bay from 2014 to 2017*

FIGURE A2.3 *NDVI biomass change detection in Forte Liberté Bay and Lagon aux Bouefs from 2014 to 2017*

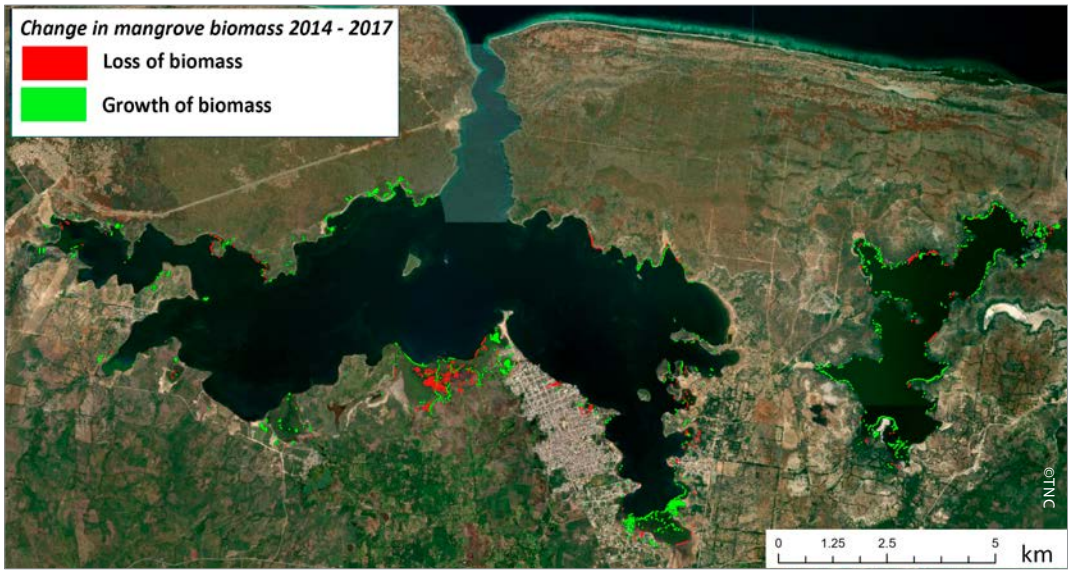

CASE STUDY 3

ASHTON LAGOON, UNION ISLAND, SAINT VINCENT AND THE GRENADINES

Ashton Lagoon is the largest lagoon in Saint Vincent and the Grenadines and home to the largest mangrove forest in the country. The lagoon harbours abundant seagrass beds, fringing, patch and barrier coral reefs, as well as an offshore island (Frigate) and mangrove wetlands that have been designated as an Important Bird Area by Birdlife International. Because of its rich ecological importance to the country, this area was formally designated a Conservation Area (under Schedule 11, Regulation 20, The Fisheries Act, 1986) in 1987. The total mangrove extent measured from drone imagery (acquired in December 2015) was 19.81 ha.

Field surveys were conducted in December 2015 and March 2016 to document the extent and density of mangroves. IKONOS imagery acquired in March 2009 and WorldView-2 imagery acquired in June 2012 revealed a total of 18.09 ha and 19.81 ha of mangroves, respectively. One major threat that negatively impacted the mangroves was a 300-berth marina project that started in 1994 and became

Figure A3.1 *NDVI difference between 2009 and 2012*

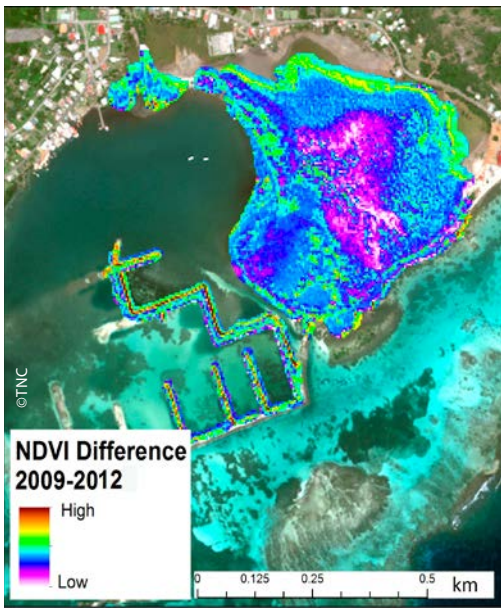

Notes: Changes in mangrove extent over three years, from 2009 to 2012. The dark blue and purple shades indicate mangrove die-off, while green, yellow and brown indicate mangrove growth. Note signs of die-off in the centre of the forest, largely due to an alteration of hydrology when an access road was built to the marina along the edge of the mangrove. Expansion of mangroves was detected along the causeways and to the north.

Figure A3.2 *Reduction and increase in mangrove biomass as modeled by remotely sensed NDVI values in Ashton Lagoon between 2009-2012*

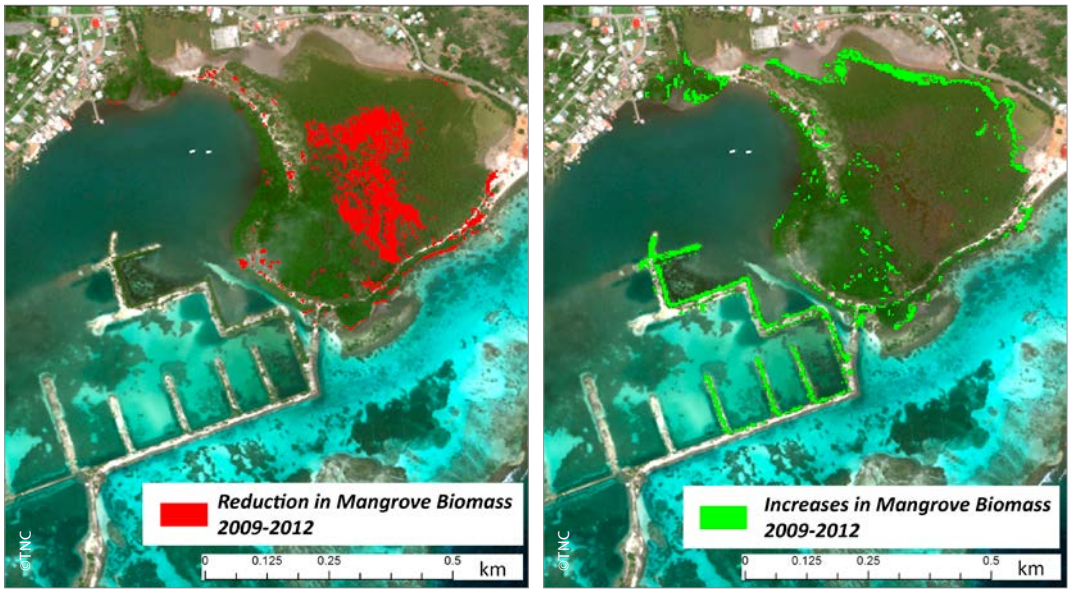

Left: Areas where mangrove biomass was reduced in Ashton Lagoon between 2009 and 2012 (3.01 ha).
Right: Areas where mangrove biomass increased over the same period (1.1 ha).

non-operational a year after. Nonetheless, massive dredging and causeway construction had already occurred and modified the natural hydrology in the bay, reducing nutrient inflow and stunting mangrove growth. Although a steady mangrove die-off can be seen in the central part of the wetland, mangrove growth continues along the abandoned causeways and there is a slow expansion to the north of the wetland.

Figure A3.3 *Aerial UAS image of Ashton Lagoon, Saint Vincent and the Grenadines taken from a DJI Phantom 4 Pro at an altitude of 120 m on 24 June 2017*

Figure A3.4 *A colour infrared orthophoto mosaic, the resulting DSM and computed NDVI values of Ashton Lagoon, Saint Vincent and the Grenadines*

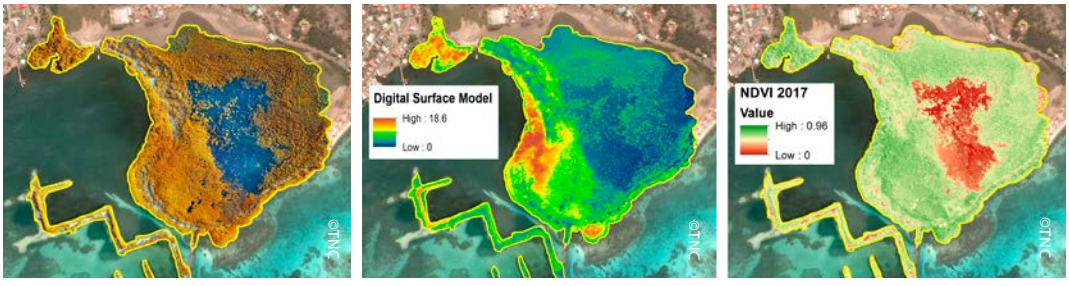

Left: A colour infrared orthophoto mosaic acquired by a Sony QX1 camera from a 3DR Solo drone on 24 June 2017 at a flying height of 120 m which yielded a pixel resolution of 2 cm. ***Centre:*** The resulting DSM. ***Right:*** The computed NDVI values which indicate mangrove biomass

CASE STUDY 4

TYRREL BAY, CARRIACOU, GRENADA

Tyrrel Bay is part of the Sandy Island Oyster Bed Marine Protected Area established in 2009 and comprises an area of 787 ha on the southwest coast of Carriacou, Grenada. The mangroves in Tyrrel Bay provide habitat for mangrove oysters that grow on the roots of the red mangroves. These mangroves also serve as nursery grounds for several species of fish and are used by local boats to secure their vessels during tropical storms. The total mangrove extent measured from satellite imagery acquired in November 2014 was 26.48 ha.

To calculate the mangrove spatial extent and biomass in Tyrrel Bay, the following datasets were used: IKONOS satellite imagery acquired on 2 November 2000; WorldView-2 satellite imagery acquired on 10 January 2010; WorldView-2 satellite imagery acquired on 12 November 2014; and UAS imagery acquired from 122 m (2-cm resolution) on 30 November 2015. The main threat to this mangrove area is the continued construction of a marina in Tyrrel Bay which began in 2003. Dredging to accommodate yachts has destroyed seagrass beds, reduced water quality and continues to negatively impact the mangrove ecosystem. Assessment results show that 13.8 percent of the mangroves were removed through clear-cutting and back-filling. In the north-eastern part of the mangrove forest, dwarf mangroves have slowly expanded into the mud flats with a total expansion of 2.57 ha. These dwarf mangroves have restricted growth and low biomass due to their locations at higher elevations with minimal tidal flushing and therefore limited nutrient inputs.

Figure A4.1 *The extent and change detection of mangroves in Tyrrell Bay, Carriacou, Grenada*

Left: WorldView-2 satellite imagery acquired on 10 January 2010. ***Centre:*** WorldView-2 image acquired on 12 November 2014. ***Right:*** The mangrove change detection map.

Figure A4.2 *Aerial view of Tyrrell Bay, Carriacou, Grenada*

FAO Forestry Division –
Natural Resources and Sustainable Production
https://www.fao.org/forestry/en/

Food and Agriculture Organization of the United Nations
Rome, Italy

ISBN 978-92-5-138796-2

9 789251 387962

CD0823EN/1/07.24